CHEMISTRY AND CATALYSIS OF COAL LIQUEFACTION: CATALYTIC AND THERMAL UPGRADING OF COAL-LIQUID AND HYDROGENATION OF CO TO PRODUCE FUELS. QUARTERLY PROGRESS REPORT, JANUARY-MARCH 1983

UTAH UNIV., SALT LAKE CITY. DEPT. OF MINING AND FUELS ENGINEERING

APR 1983

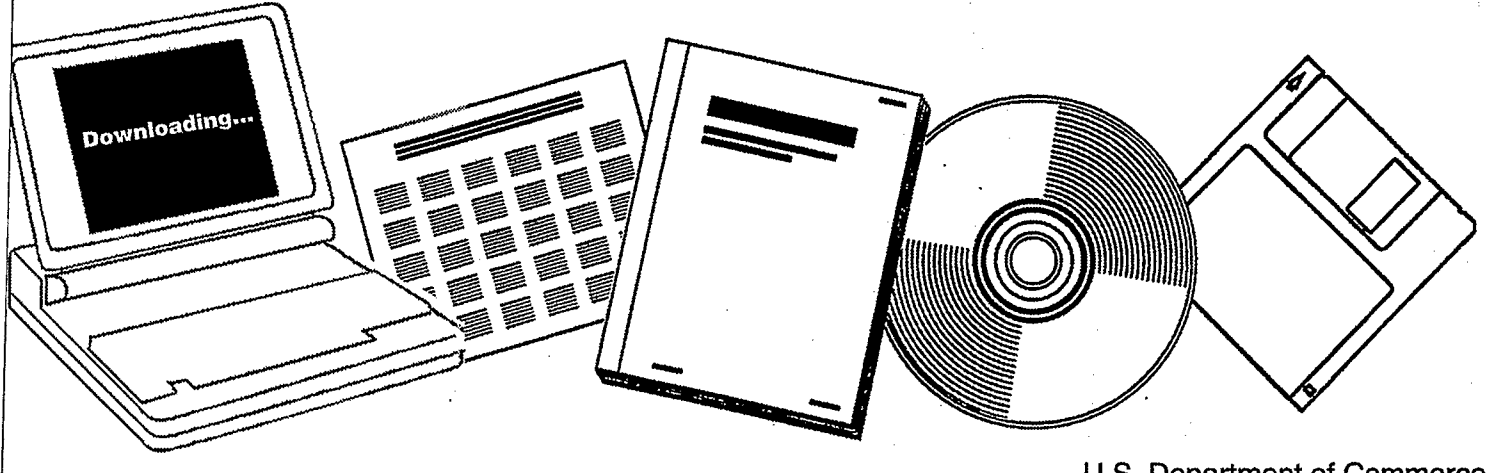

DOE/ET/14700-14
(DE83011316)
Distribution Category UC-90d

Chemistry and Catalysis of Coal Liquefaction Catalytic and Thermal Upgrading of Coal Liquid and Hydrogenation of CO to Produce Fuels

Quarterly Progress Report
for the Period Jan - Mar 1983

Dr. Wendell H. Wiser

University of Utah - Department of
Mining and Fuels Engineering
Salt Lake City, Utah 84112

Date Published - April 1983

Prepared for the United States Department
of Energy
Under Contract No. DE-AC22-79ET14700

CONTENTS

OBJECTIVE AND SCOPE OF WORK

I. The chemistry and Catalysis of Coal Liquefaction

Task 1 Chemical-Catalytic Studies

Coal will be reacted at subsoftening temperatures with selective reagents to break bridging linkages between clusters with minimal effect on residual organic clusters. The coal will be pretreated to increase surface area and then reacted at 25 to 350°C. Reagents and catalysts will be used which are selective so that the coal clusters are solubilized with as little further reaction as possible.

Task 2 Carbon-13 NMR Investigation of CDL and Coal

Carbon-13 NMR spectroscopy will be used to examine coal, coal derived liquids (CDL) and residues which have undergone subsoftening reactions in Task 1 and extraction. Improvements in NMR techniques, such as crosspolarization and magic angle spinning, will be applied. Model compounds will be included which are representative of structural units thought to be present in coal. Comparisons of spectra from native coals, CDL and residues will provide evidence for bondings which are broken by mild conditions.

Task 3 Catalysis and Mechanism of Coal Liquefaction

This fundamental study will gain an understanding of metal salt chemistry and catalysis in coal liquefaction through study of reactions known in organic chemistry. Zinc chloride and other catalytic materials will be tested as Friedel-Crafts catalysts and as redox catalysts using coals and selected model compounds. Zinc chloride, a weak Friedel-Crafts catalyst, will be used at conditions common to coal liquefaction to participate in well defined hydrogen transfer reactions. These experiments will be augmented by mechanistic studies of coal hydrogenation using high pressure thermogravimetric analysis and structural analysis. The results of these studies will be used to develop concepts of catalysis involved in coal liquefaction.

Task 4 Momentum Heat and Mass Transfer in CoCurrent Flow of Particle-Gas Systems for Coal Hydrogenation

A continuation of ongoing studies of heat and transport phenomena in cocurrent, co-gravity flow is planned for a one-year period. As time and development of existing work permits, the extension of this study to include a coiled reactor model will be undertaken. Mathematical models of coal hydrogenation systems will utilize correlations from these straight and coiled reactor configurations.

Task 5 The Fundamental Chemistry and Mechanism of Pyrolysis of Bituminous Coal

Previous work at the University of Utah indicates that coal pyrolysis, dissolution (in H-donor) and catalytic hydrogenation all have similar rates and activation energies. A few model compounds will be pyrolyzed in the range of 375 to 475°C. Activation energies, entropies and pro-

duct distributions will be determined. The reactions will assist in formulating the thermal reaction routes which also can occur during hydro-liquefaction.

II. Catalytic and Thermal Upgrading of Coal Liquids

Task 6 Catalytic Hydrogenation of CD Liquids and Related Polycyclic Aromatic Hydrocarbons

A variety of coal derived (CD) liquids will be hydrogenated with sulfided catalysts prepared in Task 10 from large pore, commercially available supports. The hydrogenation of these liquids will be systematically investigated as a function of catalyst structure and operating conditions. The effect of extent of hydrogenation will be the subject of study in subsequent tasks in which crackability and hydropyrolysis of the hydrogenated product will be determined. To provide an understanding of the chemistry involved, model polycyclic arenes will be utilized in hydrogenation studies. These studies and related model studies in Task 7 will be utilized to elucidate relationships between organic reactants and the structural-topographic characteristics of hydrogenation catalysts used in this work.

Task 7 Denitrogenation and Deoxygenation of CD Liquids and Related Nitrogen- and Oxygen-Containing Compounds

Removal of nitrogen and oxygen heteroatoms from CD liquids is an important upgrading step which must be accomplished to obtain fuels corresponding to those from petroleum sources. Using CD liquids as described in Task 6, exhaustive HDN and HDO will be sought through study of catalyst systems and operating conditions. As in Task 6, catalysts will be prepared in Task 10 and specificity for N- and O-removal will be optimized for the catalyst systems investigated. Model compounds will also be systematically hydrogenated using effective HDN/HDO catalysts. Kinetics and reaction pathways will be determined. A nonreductive denitrogenation system will be investigated using materials which undergo reversible nitridation. Conditions will be sought to cause minimal hydrogen consumption and little reaction of other reducible groups.

Task 8 Catalytic Cracking of Hydrogenated CD Liquids and Related Polycyclic Naphthenes and Naphthenoaromatics

Catalytic cracking of hydrogenated CD liquid feedstocks will be studied to evaluate this scheme as a means of upgrading CD liquids. Cracking kinetics and product distribution as a function of preceding hydrogenation will be evaluated to define upgrading combinations which require the minimal level of CD liquid aromatic saturation to achieve substantial heteroatom removal and high yields of cracked liquid products. Cracking catalysts to be considered for use in this task shall include conventional zeolite-containing catalysts and large-pore molecular sieve, CLS (cross-linked smectites) types under study at the University of Utah. Model compounds will be subjected to tests to develop a mechanistic understanding of the reactions of hydro CD liquids under catalytic cracking conditions.

Task 9 Hydropyrolysis (Thermal Hydrocracking) of CD Liquids

Heavy petroleum fractions can be thermally hydrocracked over a specific range of conditions to produce light liquid products without excessive hydrogenation occurring. This noncatalytic method will be applied to a variety of CD liquids and model compounds, as mentioned in Task 6, to determine the conditions necessary and the reactibility of these CD feedstocks with and without prior hydrogenation and to derive mechanism and reaction pathway information needed to gain an understanding of the hydropyrolysis reactions. Kinetics, coking tendencies and product compositions will be studied as a function of operating conditions.

Task 10 Systematic Structural-Activity Study of Supported Sulfide Catalysts for Coal Liquids Upgrading

This task will undertake catalyst preparation, characterization and measurement of activity and selectivity. The work proposed is a fundamental study of the relationship between the surface-structural properties of supported sulfide catalysts and their catalytic activities for various reactions desired. Catalysts will be prepared from commercially available. Supports composed of alumina, silica-alumina, silica-magnesia and silica-titania, modification of these supports to change acidity and to promote interaction with active catalytic components is planned. The active constituents will be selected from those which are effective in a sulfided state, including but not restricted to Mo, W, Ni and Co. The catalysts will be presulfided before testing. Catalyst characterization will consist of physico-chemical property measurements and surface property measurements. Activity and selectivity tests will also be conducted using model compounds singly and in combination.

Task 11 Basic Study of the Effects of Coke and Poisons on the Activity of Upgrading Catalysts

This task will begin in the second year of the contract after suitable catalysts have been identified from Tasks 6, 7 and/or 10. Two commercial catalysts or one commercial catalyst and one catalyst prepared in Task 10 will be selected for a two-part study, (1) simulated laboratory poisoning/coking and (2) testing of realistically aged catalysts. Kinetics of hydrogenation, hydrodesulfurization, hydrodenitrogenation and hydrocracking will be determined before and after one or more stages of simulated coking. Selected model compounds will be used to measure detailed kinetics of the above reactions and to determine quantitatively how kinetic parameters change with the extent and type of poisoning/coking simulated. Realistically aged catalysts will be obtained from coal liquids upgrading experiments from other tasks in this program or from other laboratories conducting long-term upgrading studies. Deactivation will be assessed based on specific kinetics determined and selective poisoning studies will be made to determine characteristics of active sites remaining.

Task 12 Diffusion of Polyaromatic Compounds in Amorphous Catalyst Supports

If diffusion of a reactant species to the active sites of the catalyst is slow in comparison to the intrinsic rate of the surface reaction, then only sites near the exterior of the catalyst particles will be utilized effectively. A systematic study of the effect of molecular size on the sorptive diffusion kinetics relative to pore geometry will

be made using specific, large diameter aromatic molecules. Diffusion studies with narrow boiling range fractions of representative coal liquid will also be included. Experimental parameters for diffusion kinetic runs shall include aromatic diffusion model compounds, solvent effects, catalyst sorption properties, temperature and pressure.

III. Hydrogenation of CO to Produce Fuels

Task 13 Catalyst Research and Development

Studies with iron catalysts will concentrate on promoters, the use of supports and the effects of carbiding and nitriding. Promising promoters fall into two classes: (1) nonreducible metal oxides, such as CaO, K_2O, Al_2O_3 and MgO, and (2) partially reducible metal oxides which can be classified as co-catalysts, such as oxides of Mn, Mo, Ce, La, V, Re and rare earths. Possible catalyst supports include zeolites, alumina, silica, magnesia and high area carbons. Methods of producing active supported iron catalysts for CO hydrogenation will be investigated, such as development of shape selective catalysts which can provide control of product distribution. In view of the importance of temperature, alternative reactor systems (to fixed bed) will be investigated to attain better temperature control. Conditions will be used which give predominately lower molecular weight liquids and gaseous products.

Task 14 Characterization of Catalysts and Mechanistic Studies

Catalysts which show large differences in selectivity in Task 13 will be characterized as to surface and bulk properties. Differences in properties may provide the key to understanding why one catalyst is superior to another and identify critical properties, essential in selective catalysts. Factors relating to the surface mechanism of CO hydrogenation will also be investigated. Experiments are proposed to determine which catalysts form "surface" (reactive) carbon and the ability of these catalysts to exchange C and O of isotopically labelled CO. Reactions of CO and H_2 at temperatures below that required for CO dissociation are of particular interest.

Task 15 Completion of Previously Funded Studies and Exploratory Investigations

This task is included to provide for the orderly completion of coal liquefaction research underway in the expiring University of Utah contract, EX-76-C-01-2006.

III Highlights to Date

Task 10 Stereochemical studies of naphthalene hydrogenation over several sulfided CoMo, NiMo and NiW catalysts have revealed unusually high trans/cis ratios in the decalin products. This result is quite different from the low ratios reported for hydrogenation over metal catalysts, and indicates a different site geometry for sulfided catalysts. The active site may consist of a cavity into which the molecule adsorbs, the hydrogen atoms being added from opposite sites, in contrast to the flat adsorption proposed for metal sites.

Task 12 It has been previously shown that at room temperature restrictive diffusion can significantly lower the effectiveness factor of a catalyst when the molecular size of the diffusing molecule is an appreciable fraction of the pore size of the catalyst. New results show that this restrictive diffusion effect decreases with increasing temperature, but may still be important under hydroprocessing conditions.

Papers and Presentations

"Chemical Structure of Heavy Oil from Coal Hydrogenation 1. Hydrogenation with Zinc Chloride Catalyst," S. Yokoyama, D.M. Bodily and W.H. Wiser, Fuel, 1983, 62, 4.

"Analysis of the n-Heptane Soluble Fraction of Coal Hydrogenolysis Products by HPLC," D.M. Bodily, J.W. Miller and M.J. England, Preprints, Fuel Chem. Div., Am. Chem. Soc., 1983, 28 (1), 168.

Task 1

Comparison of Catalyst for Coal Conversion at Subsoftening Conditions

Faculty Advisor: L.L. Anderson
Graduate Student: T.C. Miin

Introduction

Since the last report the direction of research has been shifted to studies of variables. In this report data on two variables are given. The variables are reaction time and concentration of catalyst. Only one catalyst, ZnI_2, which gives high yields, has been investigated.

Project Status

As indicated in Figure 1, three hours reaction time is sufficient to reasonably complete the conversion reactions. In Figure 2 one can observe that concentrations values for catalysts, greater than 1.3 grams of catalyst/ 1.0 gram of coal is sufficient to give maximum yields. A large excess of catalysts can only increase the gas production, whereas the total conversion yield stays the same.

If we calculate the optimum concentration of catalyst in molar equivalent, the optimum concentration of catalyst ZnI_2 is about 0.07 molar equivalent to 1 gram coal. This is the same concentration as the optimum concentration needed for intercalation done by H. Beall in Massachusetts.[1,2]

Future Work

It is still necessary to do more experiments to answer why the HSAB principle can predict the viability of catalysts for coal conversion under subsoftening conditions. (See previous reports.) At least one more catalyst in the high-yield category will be investigated to evaluate the variables of concentration and reaction time. The same procedures will be used for medium-yield and low-yield catalysts. The effect of solvent vehicles will also be studied. However, the conventional pressure variable will not be studied at this time.

References

1. Herbert Beall, Fuel, 58, 319 (1979).

2. ibid., 59, 140 (1980).

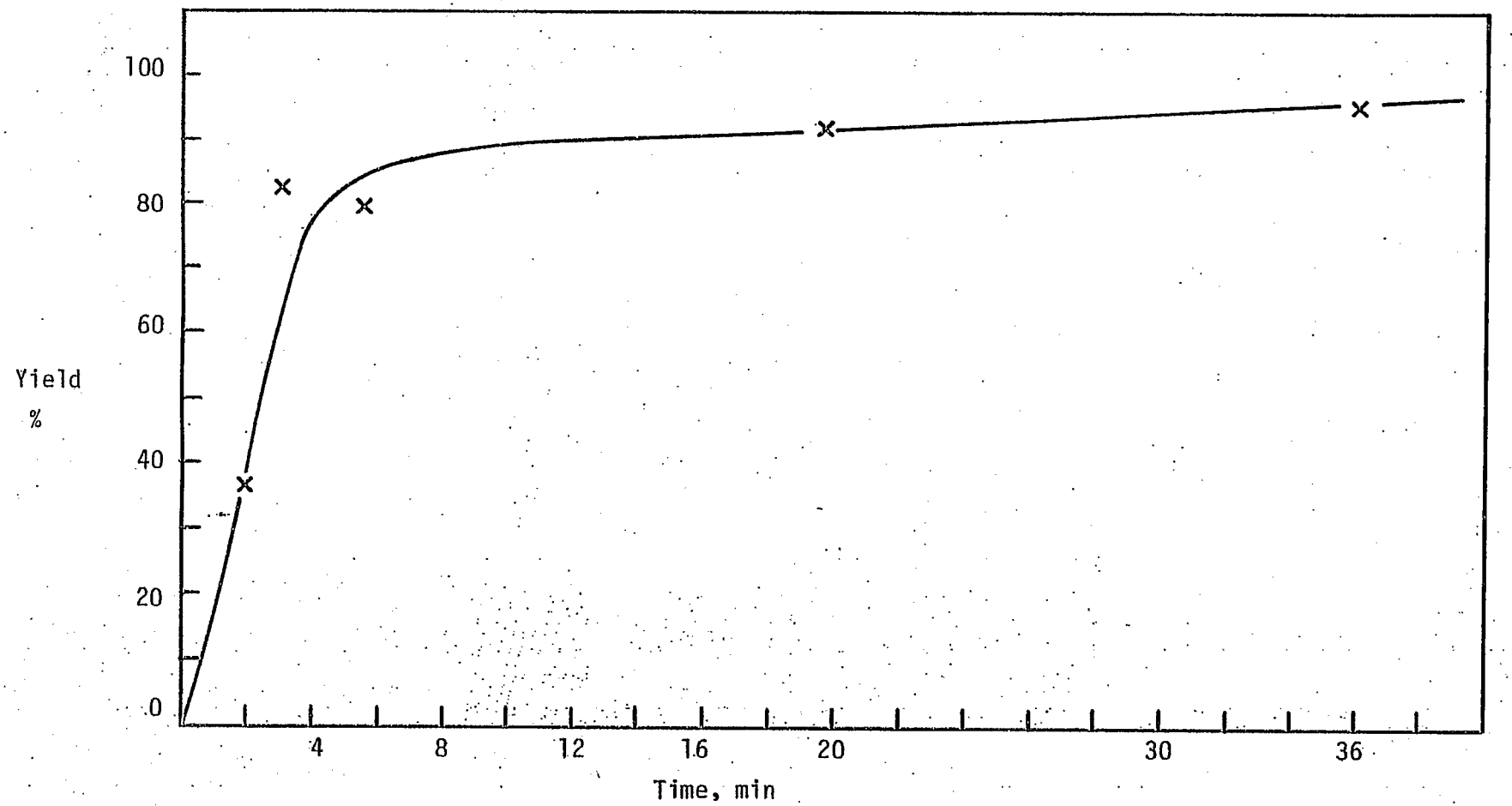

Figure 1. Time effect on yield (Catalyst: ZnI_2) (Con. Cat/coal = 1.32/1.00).

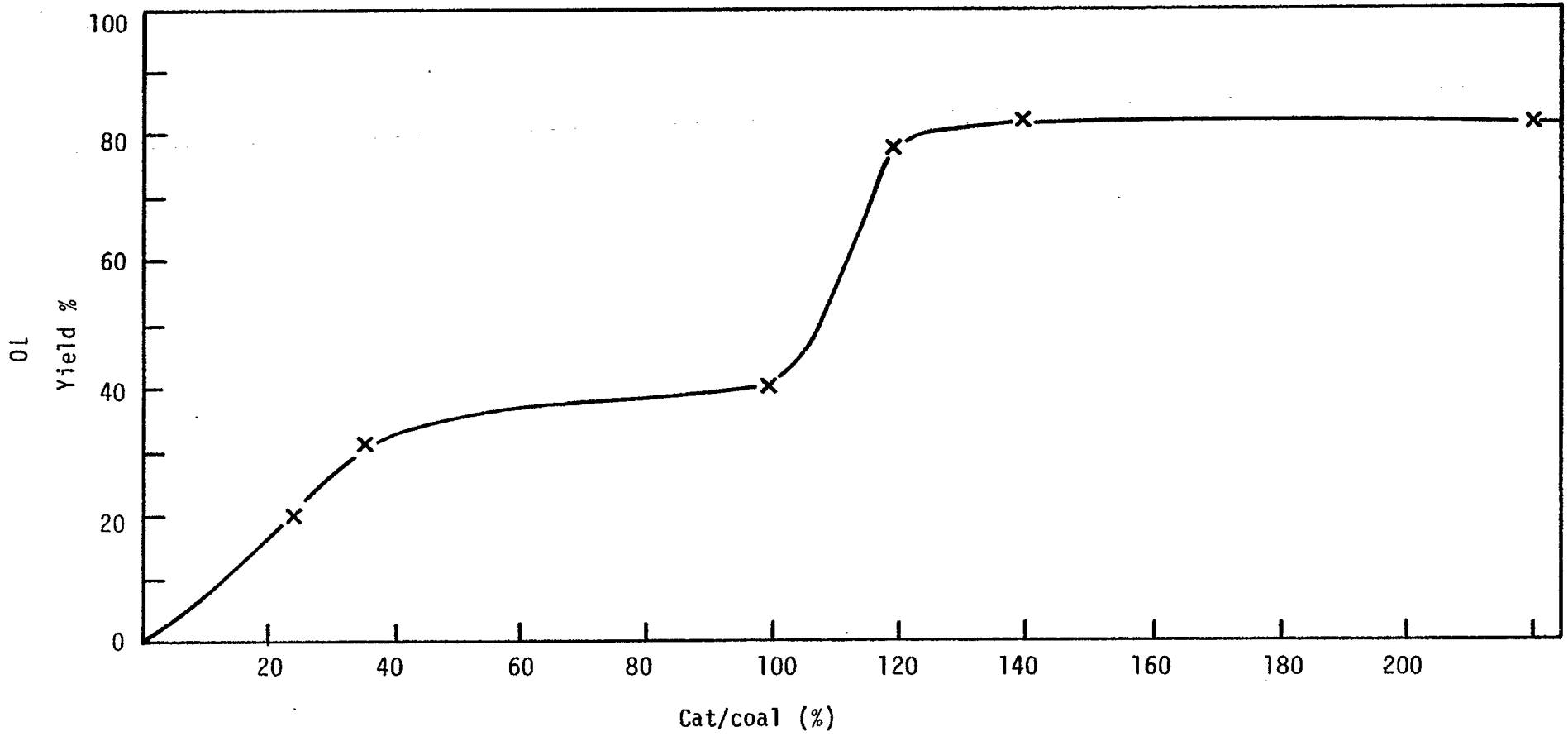

Figure 2. Cat. Concentration effect on yield (Cat ZnI_2) (R_X, time 3 hr).

Task 2

Carbon-13 NMR Investigation of CDL and Coal

Faculty Advisor: R.J. Pugmire
D.K. Dalling
W.R. Woolfenden

Introduction

Work has begun on a set of samples obtained from the Exxon Coal Data Bank. Progress on the project is still limited by the delay in a graduate student finishing his Ph.D. thesis. In the mean time, Dr. Warner Woolfenden continues to work part-time on the project.

Project Status

During the past quarter work was initiated on the Exxon Coal Data Bank samples, and 9 of the 25 samples were analyzed by standard CP/MAS and dipolar dephasing studies.

Employing T_2 values obtained for model compounds and 6 coals that were studied in some detail, we were able to calculate a number of structural parameters on each of the coals. In addition to the normal aromaticity values, we were able to calculate $f_a^{A,H}$, $f_a^{A,N}$, f_a^H, f_s^*, and H_{Ar} (fraction of aromatic carbon that is protonated, fraction of aromatic carbon that is nonprotonated, fraction of total carbon that is aromatic and protonated, relative fraction of carbon that is aliphatic methyl or aliphatic quaternary carbon, and fraction of protons located on aromatic rings, irrespectively). The data obtained so far indicates a high degree of variability in these parameters from the different coals. When the data is completed on all of the coals, we will attempt to correlate the findings with liquefaction data obtained by Exxon on these samples in conjunction with Dr. Neavel.

Task 3

Catalysis and Mechanism of Coal Liquefaction

The Effect of Zinc Chloride on the Softening Temperature and Hydrogenolysis Activity of Coal

Faculty Advisor: D.M. Bodily
Graduate Student: Tsejing Ray

Introduction

Metal halides such as $ZnCl_2$ are well-known to be active catalysts for coal hydrogenation. Zinc chloride has been shown to be a very effective catalyst for coal hydrogenation in the entrained-flow reactor developed at the University of Utah.[1,2] Bell and co-workders[3-5] have studied the reactions of model compounds with $ZnCl_2$ under conditions similar to those employed in coal hydrogenation. They observed cleavage of C-O and C-C bonds in the model compound and proposed that the active catalytic species is a Bronsted acid formed from $ZnCl_2$.

Shibaoka, Russell and Bodily[6] proposed a model to explain the liquefaction of coal, based on microscopic examination of the solid products from metal halide catalyzed coal hydrogenation. The model involves a competition between hydrogenation and carbonization reactions. The hydrogenation process starts at the surface of vitrinite particles and progresses toward the center. The vitrinite is converted to a plastic material of lower reflectance, which is the source of oils, asphaltenes and preasphaltenes. Concurrently, carbonization occurs in the center of the particles, resulting in vesiculation and a higher reflectance material. The partially carbonized material can be hydrogenated at later stages, but at a lower rate than the original coal.

Thermal and/or catalytic bond rupture occurs during the liquefaction process. The initial products of the bond cleavage reactions may be stabilized by hydrogen addition, resulting in cleavage of bridges between aromatic ring systems and in dealkylation of aromatic rings. If the initial products of the reaction are not stabilized, they may polymerize to form semicoke-like material. This primary semicoke may be isothropic or exhibit a fine-grained anisotropic mosiac texture, depending on the rank of coal. The plastic material formed by stabilization of the initial products may be further hydrogenated or, under hydrogen deficient conditions, may form secondary semicoke. The secondary semicoke is of medium to coarse-grained anisotropic mosiac texture. Bodily and Shibaoka[7] used this model to explain the nature of the residues from hydrogenation in the short-residence, entrained-flow hydrogenation reactor. The role of the $ZnCl_2$ catalyst is examined in this study.

Project Status

Samples of Clear Creek coal have been heat-treated at various temperatures in hydrogen and in nitrogen, with $ZnCl_2$ catalyst and without catalyst. Samples were heated to temperature in two minutes and then held at temperature for five minutes. The reacted samples were observed with an optical microscope under oil immersion conditions. Polished

grain mounts were prepared for observation. The samples are described in Table 1.

When 10% $ZnCl_2$ is impregnated on the coal, some reaction is observed after heating to 350°C. The samples are free-flowing and do not agglomerate, but a reaction is observed at the edge of vitrinite grains and along cracks. An example of such a reaction is shown in photo 1 for heating in nitrogen. The reaction is quite apparent in samples heated to 350°C in hydrogen (photo 2). The reaction extends farther into the grain from the edge. Upon heating to 380°C, the reaction extends further into the grain (photo 3). Only the center of the grains is unreacted. Oil from the sample dissolves in the immersion oil and produces interference patterns, which are visible in photo 3. Exinite is still visible after heating to 380°C. Trimacerite grains show some reaction at the edge, but not to the same extent as the vitrinites. Some rounding of corners occurs, but the particles mostly retain their original morphology.

Samples that are heated in either nitrogen or hydrogen without $ZnCl_2$ show little reaction even up to 400°C (photo 4). The original morphology is retained and their is no reacted zone at the edge of the grains.

Zinc chloride causes a reaction in the coal, even when heated in nitrogen. The reaction is promoted by hydrogen. In higher rank coals it promotes the agglomeration of the coal and the formation of anisotropic material at lwoer temperatures.

Future Work

The reactions of Clear Creek coal will be studied at temperatures up to 500°C. Additional samples of medium volatile bituminous coal will also be studied.

References

1. R.E. Wood and W.H. Wiser, Ind. Eng. Chem., Proc. Design Devel., 15, 144 (1976).

2. J.M. Lytle, R.E. Wood and W.H. Wiser, Fuel, 59, 471 (1980).

3. D.P. Mobley and A.T. Bell, Fuel, 58, 661 (1979).

4. N.D. Taylor and A.T. Bell, Fuel, 59, 499 (1980).

5. D.P. Mobley and A.T. Bell, Fuel, 59, 507 (1980).

6. M. Shibaoka, N.J. Russel and D.M. Bodily, Fuel, 61, 201 (1982).

7. D.M. Bodily and M. Shibaoka, Fuel, submitted.

Legend to Photos

Photo 1. Clear Creek coal impregnated with 10% $ZnCl_2$. Heat-treated at 350°C in 1000 psi nitrogen.

Photo 2. Clear Creek coal impregnated with 10% $ZnCl_2$. Hydrotreated at

350°C in 1000 psi hydrogen.

Photo 3. Clear Creek coal impregnated with $ZnCl_2$. Hydrotreated at 380°C in 1000 psi hydrogen.

Photo 4. Clear Creek coal. Hydrotreated at 400°C in 1000 psi hydrogen.

Table 1. Appearance of heat-treated Clear Creek coal samples.

$ZnCl_2$, %	Temperature, °C	Gas	Description
10	302	H_2	No major change in morphology. Exinites unreacted. Some crack formation.
10	350	N_2	No major change in morphology. Some indication of reaction at grain edge. (See Photo 1.)
0	350	H_2	Edges sharp. Exinites unreacted. No indication of reaction.
10	350	H_2	Vitrinites show definite reaction at the grain edge. Some rounding of edges, but no major change in morphology. Exinites still observed. (See Photo 2.)
10	380	H_2	Some grains show very definite reaction at surfaces of grains and along cracks. Oil from reacted zones dissolves in immersion oil to give interference colors. No major change in morphology. (See Photo 3.)
0	400	H_2	No change in morphology. Exinites unreacted. Some cracks. No evidence for reaction. (See Photo 4.)
0	400	N_2	No change in morphology. No evidence of reaction.

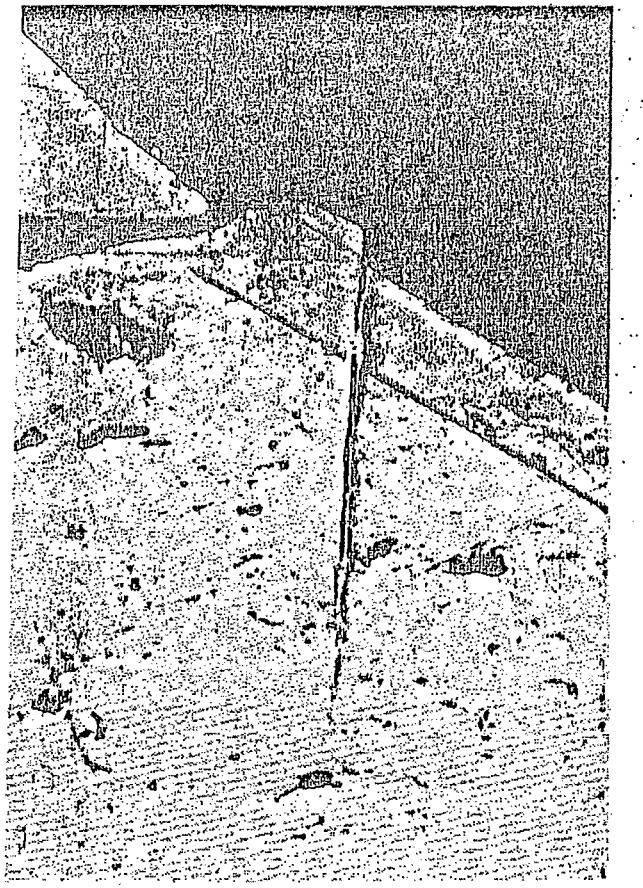

Photo 1

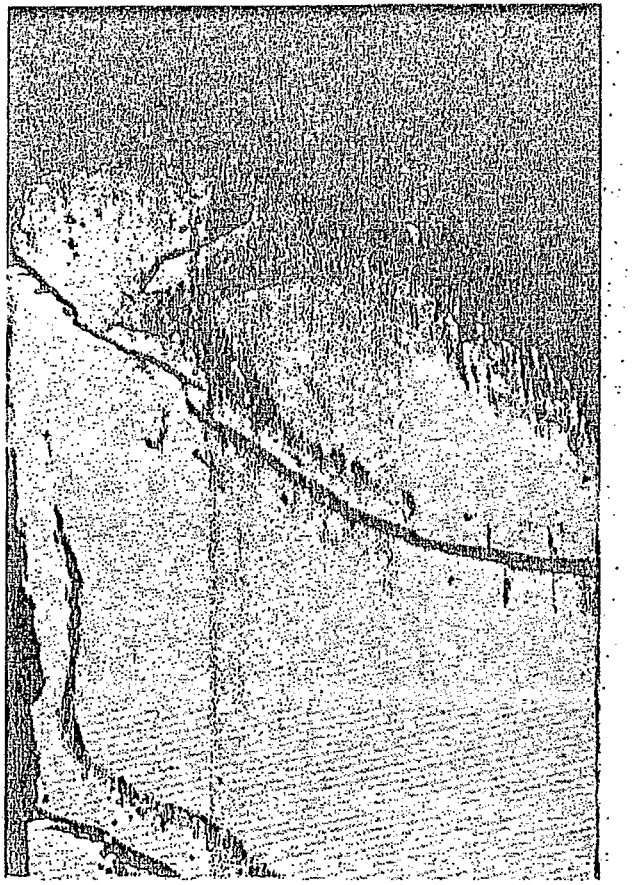

Photo 2

Photo 3

Photo 4

Task 5

The Mechanism of Pyrolysis of Bituminous Coal

Faculty Advisor: W.H. Wiser
Graduate Student: J.K. Shigley

Introduction

In the present state of knowledge concerning the fundamental chemistry of coal liquefaction in the temperature range 375-550°C, the liquefaction reactions are initiated by thermal rupture of bonds in the bridges joining configurations in the coal, yielding free radicals. The different approaches to liquefaction, except for Fischer-Tropsch variations, represent ways of stabilizing the free radicals to produce liquid-size molecules. The stabilization involving abstraction by the free radicals of hydrogen from the hydroaromatic structures of the coal is believed to be the predominant means of yielding liquid size molecules in the early stages of all coal liquefaction processes, except Fischer-Tropsch variations. The objective of this research is to understand the chemistry of this pyrolytic operation using model compounds which contain structures believed to be prominant in bituminous coals.

Project Status

Pyrolysis experiments for 9-benzyl-1,2,3,4-tetrahydrocarbazole (9-BTHC) have been completed at the temperatures of 410, 425 and 440°C. The compiled data for each temperature are shown in Tables 1, 2 and 3. The data for each reaction time are the average of at least two experiments and in some cases three. The relative product yields and the molar ratios of 9-benzylcarbazole/carbazole (9BC/CARB) for each temperature are shown in Tables 4, 5 and 6. The normalized product distributions vs. time for each temperature are plotted in Figures 1, 2 and 3. A plot of the 9BC/CARB molar ratio vs. time for all three temperatures is shown in Figure 4.

The normalized product distributions show some interesting trends with increasing temperature. The yields of 1,2,3,4-tetrahydrocarbazole (THC), carbazole and the apparent relationship between their production seems to vary with temperature. The lower the temperature the larger is the yield of THC absolutely and relative to the yield of carbazole. As the temperature is increased the molar ratio of THC/CARB approaches one and at high enough conversion is significantly less than one. At 410°C the THC yield is greater than carbazole, but appears to be leveling off in the same manner. The product distribution at 425°C shows the THC and carbazole yields crossing at about 16 minutes. THe 440°C distribution apparently shows the carbazole yield to be greater than the yield of THC at all times. This tendency of the THC and carbazole suggests that at lower conversions and temperatures the termally produced radicals are not being stabilized by intramolecular hydrogen transfer. If internal rearrangement was preferential, the carbazole would be a predominant product at all temperatures. This is logical because initially intramolecular rearrangement would yield dihydrocarbazole (DHC) and toluene. The DHC would rapidly dehydrogenate to form carbazole and most likely hydrogen. The data do not support an intramolecular rearrangement mechanism.

The 9BC/CARB molar ratio is at its highest value at low conversions and decreases at a rate apparently dependent on temperature. The higher the temperature the more rapid is the approach to the "final" value and the lower is this value. This tendency suggests that initially, especially at lower conversions, the thermally produced radicals are preferentially stabilized by abstraction of hydrogen (H·) from the hydroaromatic portion of a model compound molecule.

Kinetic analysis of the data has been performed using the integral technique of analysis.[1] The kinetic data are shown in Tables 7, 8 and 9 and are plotted in Figures 5, 6, 7, 8, 9 and 10. The data appear to be described better by first order kinetics at the higher temperatures (425 and 440°C). The data at 410 and 425°C were also analyzed using differential analysis to determine the overall reaction order. The results of these analyses are tabulated in Tables 10 and 11 and plotted in Figures 11 and 12. The differential analyses suggests that the overall reaction order at 410°C is 1.5 and 1.0 at 425°C.

In an attempt to better understand this apparent change in overall reaction order with temperature the data were analyzed assuming a parallel reaction pathways mechanism. One pathway was assumed to be first order and the other second order with respect to the model compound. Reaction constants for each pathway (1st and 2nd order pathways) were determined at five temperatures (375, 400, 410, 425 and 440°C). These constants were then utilized for the Arrhenius plot shown in Figure 13. The apparent activation energies from this analysis are 55.6 kcal/mole and 25.6 kcal/mole for the first and second order pathways, respectively. These activation energies support the idea that the first order pathway dominates at higher temperatures and the second order pathway is apparently favored at temperatures below 400°C. The activation energy for the first order pathway (55.6 kcal/mole) is remarkably similar to the bond dissociation energy for the nitrogen to benzyl carbon bond in 9-BTHC.

Gas chromatographic/mass spectrometric (GC/MS) analysis has been performed on a concentrated 9-BTHC pyrolysis product mixture. This analysis was performed in an attempt to determine the structures of unknown pyrolysis reaction products alluded to in the previous report.[2] The complexity of the analyses results has slowed progress in these structural determinations.

Initial experimentation on another model compound, 9-benzyloxy-1,10-propanophenanthrene (9-BOPP)[3] has begun. Progress on the pyrolysis of 9-BOPP has been minimal due to the difficulty encountered in finding a suitable solvent for its dissolution. The solvent utilized must dissolve 9-BOPP sufficiently for gas chromatographic calibration and analysis of pyrolysis reaction products without interfering with the analysis.

Future Work

The GC/MS data will be studied further in an attempt to discern the structures of some minor pyrolysis reaction products.

It will be decided if further pyrolysis experimentation of 9-BTHC is necessary to better understand its pyrolysis reaction mechanism and kinetics.

If more pyrolysis experiments are to be conducted they will most likely be performed at a lower temperature (i.e., 350°C).

Extensive experimentation will be conducted to find a suitable solvent for 9-BOPP. Once a solvent has been found pyrolysis experimentation on 9-BOPP will begin.

References

1. Octave Levenspiel, "Chemical Reaction Engineering," 2nd Ed., John Wiley & Sons, New York, New York, 1972.

2. W.H. Wiser et al., DOE Contract No. DE-AC22-79ET14700, Quarterly Progress Report, Salt Lake City, Utah, Oct-Dec 1982.

3. W.H. Wiser et al., DOE Contract No. E(49-18)-2006, Quarterly Progress Report, Salt Lake City, Utah, Jan-Mar 1979.

TABLE 1

PYROLYSIS OF 9-BENZYL-1,2,3,4-TETRAHYDROCARBAZOLE (9-BTHC)

TEMPERATURE: 683 K ($410^{o}C$)

Reaction Time, Min.	Initial Conc'n of 9-BTHC, $\frac{mmole}{cc}$	% Material Balance	Conversion of 9 BTHC ± SD
1.0	.0185	112.0	.1044 ± .006
3.0	.02118	99.60	.2927 ± .015
5.0	.02129	99.61	.3802 ± .03
8.0	.02217	97.01	.4934 ± .002
10.0	.01984	99.00	.5844 ± .018
15.0	.02272	203.2	.6921 ± .02
20.0	.02135	105.6	.7673 ± .015
30.0	.02053	102.4	.8490 ± .004

Notes:

1. % Material Balance = $\frac{N(THC)+N(CARB)+N(9BC)+N_A}{N_{Ao}} \times 100$

2. Conversion of 9 BTHC = $1 - \frac{N_A}{N_{Ao}}$

3. SD = Standard deviation between experiments where,

N_A = millimoles of 9 BTHC at t

N_{Ao} = millimoles of 9 BTHC at t = o

TABLE 2

PYROLYSIS OF 9-BENZYL-1,2,3,4-TETRAHYDROCARBAZOLE (9 BTHC)

TEMPERATURE: 698 K ($425^{o}C$)

Reaction Time, Min.	Initial Conc'n of 9-BTHC, $\frac{\text{mmole}}{\text{cc}}$	% Material Balance	Conversion of 9 BTHC ± SD
1.0	.01808	94.70	.2892±.02
3.0	.02107	98.75	.4342±.017
5.0	.02072	99.25	.6065±.028
8.0	.02043	101.80	.7688±.03
10.0	.01486	98.55	.8113±.015
15.0	.01919	92.98	.9086±.013
20.0	.01762	88.80	.9517±.011

Notes:

1. % Material Balance $= \left[\frac{N(THC)+N(CARB)+N(9BC)+N_A}{N_{Ao}}\right] \times 100$

2. Conversion of 9 BTHC $= 1 - \frac{N_A}{N_{Ao}}$

3. SD = Standard deviation between experiments where,

N_A = millimoles of 9 BTHC at t

N_{Ao} = millimoles of 9 BTHC at t = o

TABLE 3

PYROLYSIS OF 9-BENZYL-1,2,3,4-TETRAHYDROCARBAZOLE (9 BTHC)

TEMPERATURE: 713 K (440°C)

Reaction Time, Min.	Initial Conc'n of 9-BTHC, $\frac{\text{mmole}}{\text{cc}}$	% Material Balance	Conversion of 9 BTHC ± SD
1.0	.01957	99.52	.2775 ± .005
3.0	.01857	97.83	.7174 ± .01
5.0	.02099	95.73	.8538 ± .03
8.0	.02133	102.88	.9399 ± .001
10.0	.02045	99.75	.9416 ± .012
12.0	.02025	101.59	.9658 ± .003
15.0	.02042	96.42	.9787 ± .0005

Notes:

1. % Material Balance = $\frac{N(THC)+N(CARB)\ N(9BC)+N_A}{N_{Ao}}$ X 100

2. Conversion of 9 BTHC = $1 - \frac{N_A}{N_{Ao}}$

3. SD = Standard deviation between experiments where,

N_A = millimoles of 9 BTHC at t

N_{Ao} = millimoles of 9 BTHC at t = o

TABLE 4

PYROLYSIS OF 9-BENZYL-1,2,3,4-TETRAHYDROCARBAZOLE (9-BTHC)

TEMPERATURE: 683 K (410°C)

Reaction Time, Min.	Conversion of 9 BTHC SD	% Material Balance	Relative Yields (%, Normalized)				9BC/CARB Molar Ratio
			9-BTHC	9-BC	THC	CARB	
1.0	.1044 ± .006	112.0	79.87	15.67	1.80	2.66	9.14
3.0	.2927 ± .015	99.60	71.01	16.99	6.79	5.22	3.44
5.0	.3802 ± .03	99.61	62.79	18.99	11.67	6.55	2.90
8.0	.4934 ± .002	97.01	52.22	19.20	18.69	9.89	1.94
10.0	.5844 ± .018	99.0	42.04	20.57	23.16	14.23	1.45
15.0	.6921 ± .02	103.23	29.80	21.17	30.67	18.37	1.15
20.0	.7673 ± .015	105.6	22.05	21.02	34.51	22.42	.938
30.0	.8490 ± .004	102.4	14.71	20.64	37.79	26.87	.768

where,

9-BC = 9-Benzylcarbazole

THC = 1,2,3,4-Tetrahydrocarbazole

CARB = Carbazole

SD = Standard deviation between experiments

TABLE 5

PYROLYSIS OF 9-BENZYL-1,2,3,4-TETRAHYDROCARBAZOLE (9-BTHC)
TEMPERATURE: 698K (425°C)

Reaction Time, Min.	Conversion of 9 BTHC ± SD	% Material Balance	Relative Amounts (%, Normalized)				9BC/CARB Molar Ratio
			9-BTHC	9-BC	THC	CARB	
1.0	.2892 ± .02	94.70	78.07	11.39	2.29	2.99	3.81
3.0	.4342 ± .017	98.75	46.84	13.46	12.42	7.43	1.81
5.0	.6065 ± .028	99.25	28.62	11.96	17.10	12.62	.948
8.0	.7688 ± .03	101.80	14.85	12.09	20.65	15.88	.761
10.0	.8113 ± .015	98.55	11.76	10.85	20.18	18.52	.586
15.0	.9086 ± .013	92.98	6.11	8.35	21.90	20.87	.400
20.0	.9517 ± .011	88.80	3.41	8.13	21.37	22.85	.356

where,

9BC = 9-Benzylcarbazole

THC = 1,2,3,4-Tetrahydrocarbazole

CARB = Carbazole

SD = Standard Deviation between

TABLE 6

PYROLYSIS OF 9-BENZYL-1,2,3,4-TETRAHYDROCARBAZOLE (9-BTHC)

TEMPERATURE: 713 K (440°C)

Reaction Time, Min.	Conversion of 9 BTHC ± SD	% Material Balance	Relative Yields (%, Normalized)				9BC/CARB Molar Ratio
			9-BTHC	9-BC	THC	CARB	
1.0	.2775 ± .005	99.52	70.12	13.04	4.03	4.39	2.97
3.0	.7174 ± .01	97.83	22.21	12.11	17.82	18.12	.668
5.0	.8538 ± .03	95.73	9.45	8.76	19.51	21.39	.410
8.0	.9399 ± .001	102.88	3.49	6.83	20.34	24.50	.279
10.0	.9416 ± .012	99.75	3.33	7.10	19.82	24.96	.285
12.0	.9658 ± .003	101.6	2.00	5.79	19.79	26.32	.220
15.0	.9787 ± .0005	96.42	1.27	4.31	19.57	27.64	.156

where,

9BC = 9-Benzylcarbazole

THC = 1,2,3,4-Tetrahydrocarbazole

CARB = Carbazole

TABLE 7

Pyrolysis of 9-Benzyl-1,2,3,4-Tetrahydrocarbazole
Overall Reaction(s) Order Determination
Temperature: 683 K (410°C)

Reaction Time, Min	Kinetic Plots Ordinates	
	First Order $-\text{Ln}\ (1-X_A)$	Second Order $X_A/[C_{AO}(1-X_A)]$
1.0	0.1102	6.352
3.0	0.3465	19.66
5.0	0.4790	28.85
8.0	0.6801	44.05
10.0	0.8785	71.09
15.0	1.179	99.36
20.0	1.459	155.0
30.0	1.891	276.2

Least Squares Analysis

Plot	Y-Intercept	Slope	r^2
First Order $-\text{Ln}\ (1-X_A) = k_1 t$	0.1769	0.06096	0.9802
Second Order $\frac{X_A}{C_{AO}(1-X_A)} = k_2 t$	-17.64	9.148	0.9764

where, $k_1[=]\ \text{min}^{-1}$; $k_2[=]\frac{\text{cc}}{\text{mmole-min}}$

X_A = Conversion of 9-BTHC

C_{AO} = Initial concentration of 9-BTHC, mmole/cc

TABLE 8

Pyrolysis of 9-Benzyl-1,2,3,4-Tetrahydrocarbazole (9-BTHC)
Overall Reaction(s) Order Determination-Integral Technique
Temperature: 698 K (425°C)

Reaction Time, Min	Kinetic Plots Ordinates: First Order $-Ln\ (1-X_A)$	Kinetic Plots Ordinates: Second Order $X_A/[C_{A0}(1-X_A)]$
1.0	0.3416	22.54
3.0	0.5695	36.43
5.0	0.9327	74.39
8.0	1.464	162.7
10.0	1.668	289.3
15.0	2.392	517.7
20.0	3.043	1140.5

Least Squares Analysis

Plot	Y-Intercept	Slope	r^2
First Order $-Ln(1-X_A)=k_1t$	0.210	0.1442	0.9967
Second Order $\frac{X_A}{C_{A0}(1-X_A)}=k_2t$	-175.8	56.04	0.8924

where, k_1[=] min^{-1}; k_2[=] $\frac{cc}{mmole\text{-}min}$

X_A = Conversion of 9-BTHC

C_{A0} = Initial concentration of 9-BTHC, mmole/cc

TABLE 9

Pyrolysis of 9-Benzyl-1,2,3,4-Tetrahydrocarbazole (9-BTHC)
Overall Reaction(s) Order Determination-Integral Technique
Temperature: 713 K (440° C)

Reaction Time, Min	Kinetic Plots Ordinates	
	First Order $-\text{Ln}(1-X_A)$	Second Order $X_A/[C_{A0}(1-X_A)]$
1.0	0.3250	19.65
3.0	1.264	136.9
5.0	1.933	283.3
8.0	2.813	734.0
10.0	2.854	808.7
12.0	3.379	1404.2
15.0	3.850	2251.0

Least Squares Analysis

Plot	Y-Intercept	Slope	r^2
First Order $-\text{Ln}(1-X_A) = k_1 t$	0.4876	0.2408	0.9515
Second Order $\frac{X_A}{C_{A0}(1-X_A)} = k_2 t$	-362.8	151.43	0.9161

where, k_1[=] min^{-1}; k_2[=] $\frac{\text{cc}}{\text{mmole-min}}$

X_A = Conversion of 9-BTHC

C_{A0} = Initial concentration of 9-BTHC, mmole/cc

TABLE 10

PYROLYSIS OF 9-BENZYL-1,2,3,4-TETRAHYDROCARBAZOLE (9-BTHC)
Overall Reaction(s) Order Determination - Differential Technique
Temperature: 683 K ($410^{o}C$)

Reaction Time, Min.	C_A, $\frac{mmole}{cc}$	$-(\frac{\Delta C_A}{\Delta t})$	Ln $[-(\frac{\Delta C_A}{\Delta t})]$	Ln $[C_A]$
1.0	.01875			
		1.97×10^{-3}	-6.230	-4.088
3.0	.01481			
		9.15×10^{-4}	-6.997	-4.276
5.0	.01298			
		7.90×10^{-4}	-7.144	-4.440
8.0	.01061			
		9.55×10^{-4}	-6.954	-4.640
10.0	.0087			
		4.50×10^{-4}	-7.706	-4.883
15.0	.00645			
		3.15×10^{-4}	-8.062	-5.174
20.0	.00487			
		1.71×10^{-4}	-8.672	-5.517
30.0	.00316			

Linear Regression Analysis

$$\text{Ln}\left[-\left(\frac{\Delta C_A}{\Delta t}\right)\right] = \text{Ln}(k) + \eta \text{ Ln } C_A$$

y-intercept - Ln k = -.1186

slope = η = 1.543

r^2 = correlation coefficient = .9344

where,

C_A = Concentration of 9-BTHC, $\frac{mmole}{cc}$

TABLE 11

PYROLYSIS OF 9-BENZYL-1,2,3,4-TETRAHYDROCARBAZOLE (9-BTHC)

Overall Reaction(s) Order Determination - Differential Technique

Temperature: 698 K (425°C)

Reaction Time, Min.	C_A, $\frac{mmole}{cc}$	$-(\frac{\Delta C_A}{\Delta t})$	Ln $[-(\frac{\Delta C_A}{\Delta t})]$	Ln $[C_A]$
1.0	.01320			
		1.345×10^{-3}	-4.435	-6.6114
3.0	.01051			
		1.6015×10^{-3}	-4.721	-6.437
5.0	.007307			
		1.0047×10^{-3}	-5.150	-6.9031
8.0	.004293			
		3.945×10^{-4}	-5.547	-7.8379
10.0	.003504			
		3.614×10^{-4}	-5.952	-7.9255
15.0	.001697			
		1.6×10^{-4}	-6.648	-8.7403
20.0	.000897			

Linear Regression Analysis

$$\text{Ln}\left[-\left(\frac{\Delta C_A}{\Delta t}\right)\right] = \text{Ln } k + \eta \text{ Ln } C_A$$

y-intercept = Ln k = -1.632

slope = η = 1.068

r^2 = correlation coefficient = .9382

where,

C_A = Concentration of 9BTHC, $\frac{mmole}{cc}$

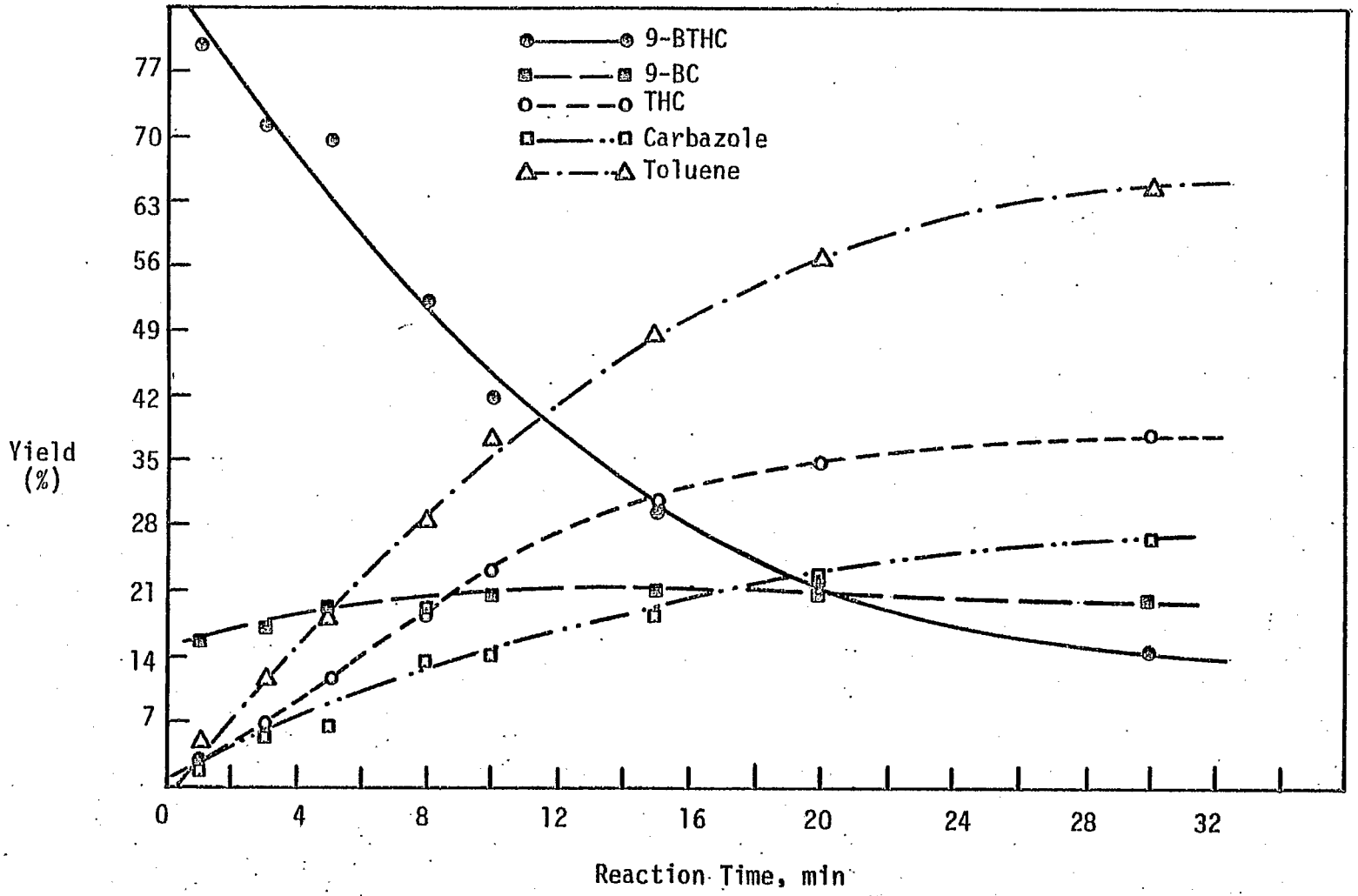

Figure 1. Normalized Product Distribution (%). Temperature: 683 K (410°C). Pyrolysis of 9-Benzyl-1,2,3,4-tetrahydrocarbazole (9-BTHC).

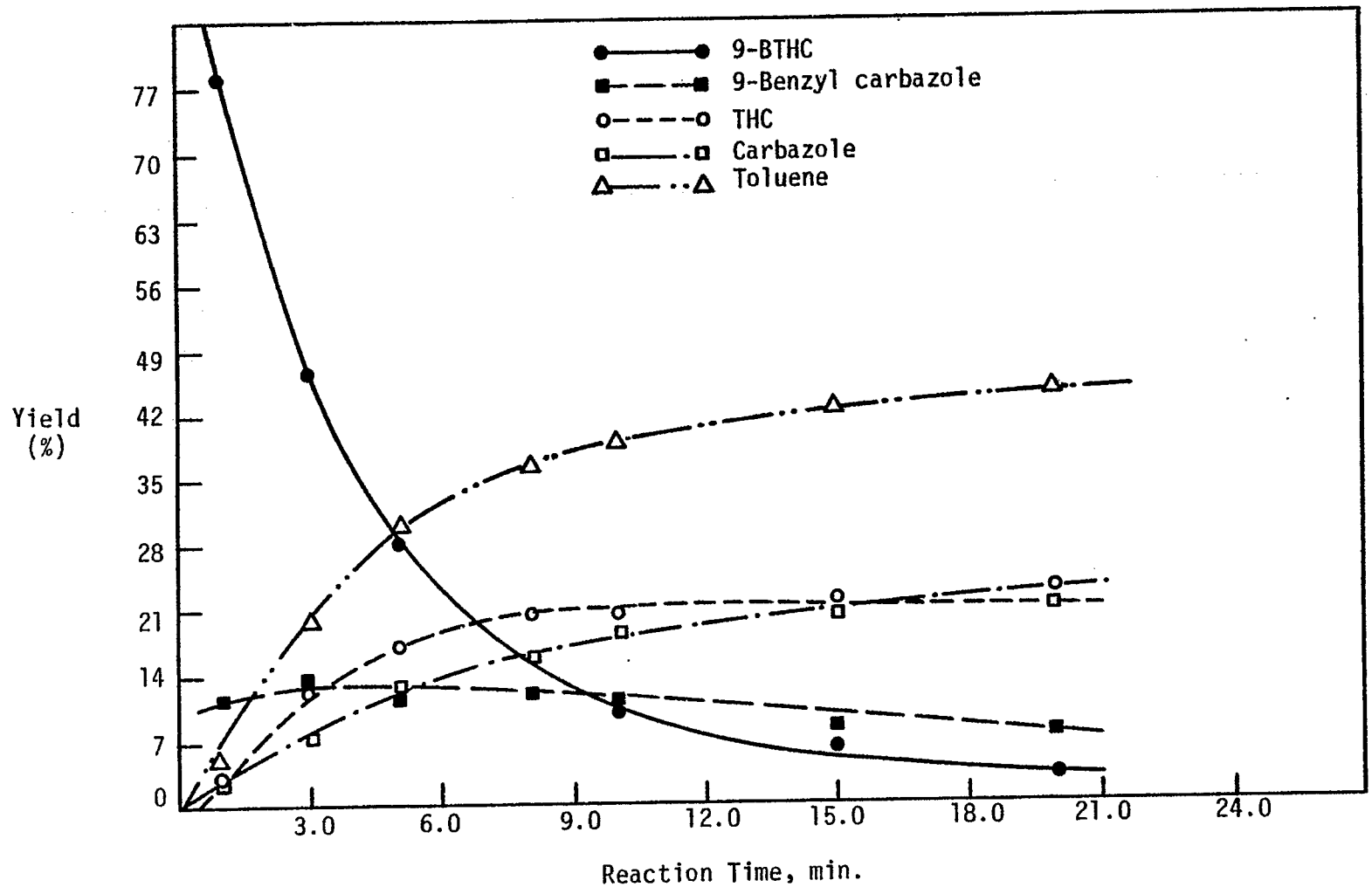

Figure 2. Normalized Product Distribution (%). Temperature 698 K(425^{o}C). Pyrolysis of 9-Benzyl-1,2,3,4-tetrahydrocarbazole (9-BTHC).

PYROLYSIS OF 9-BENZYL-1,2,3,4-TETRAHYDROCARBAZOLE (9-BTHC)

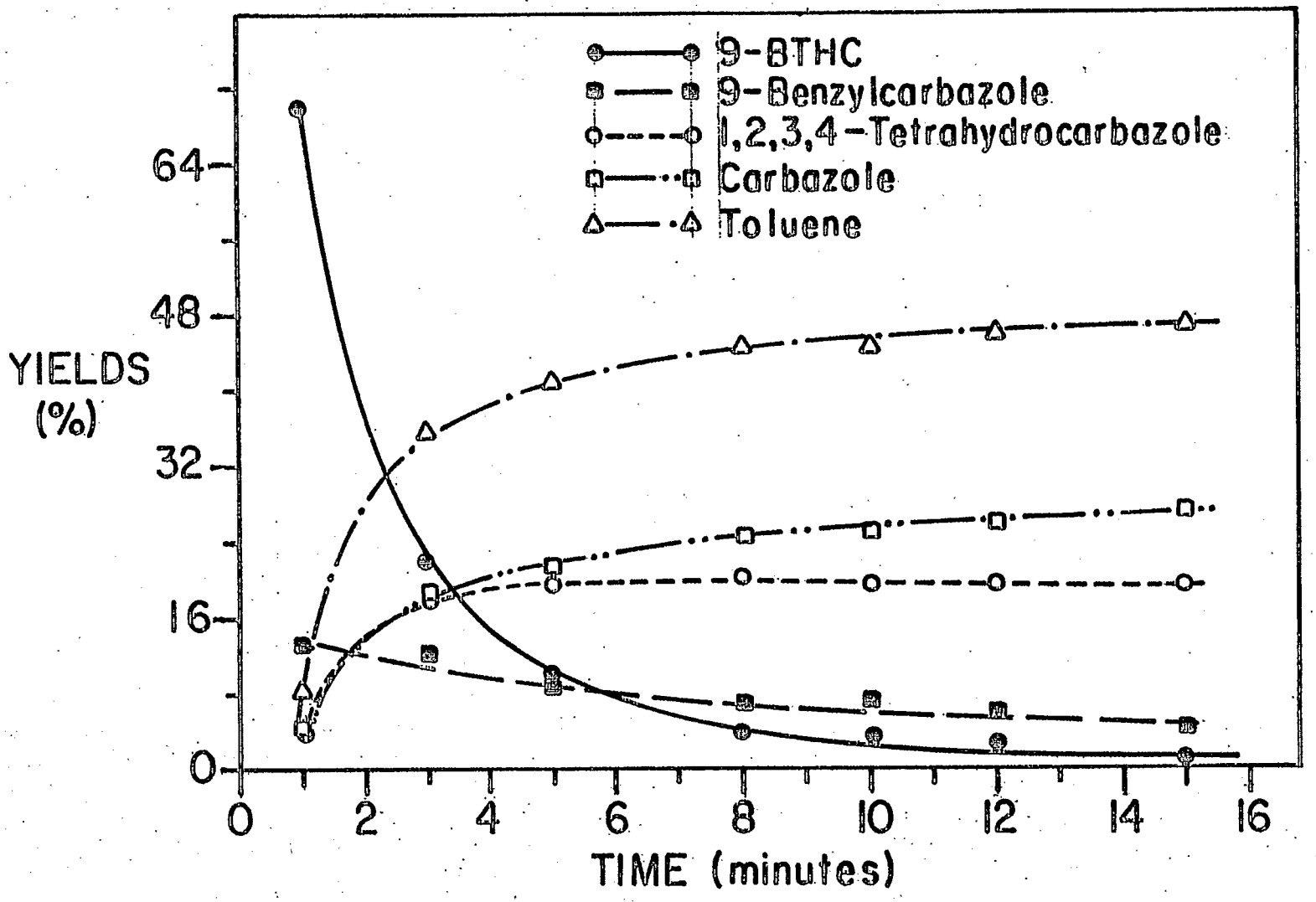

Normalized Product Distribution (%). Temperature: 713 K (440°C)

FIGURE 3

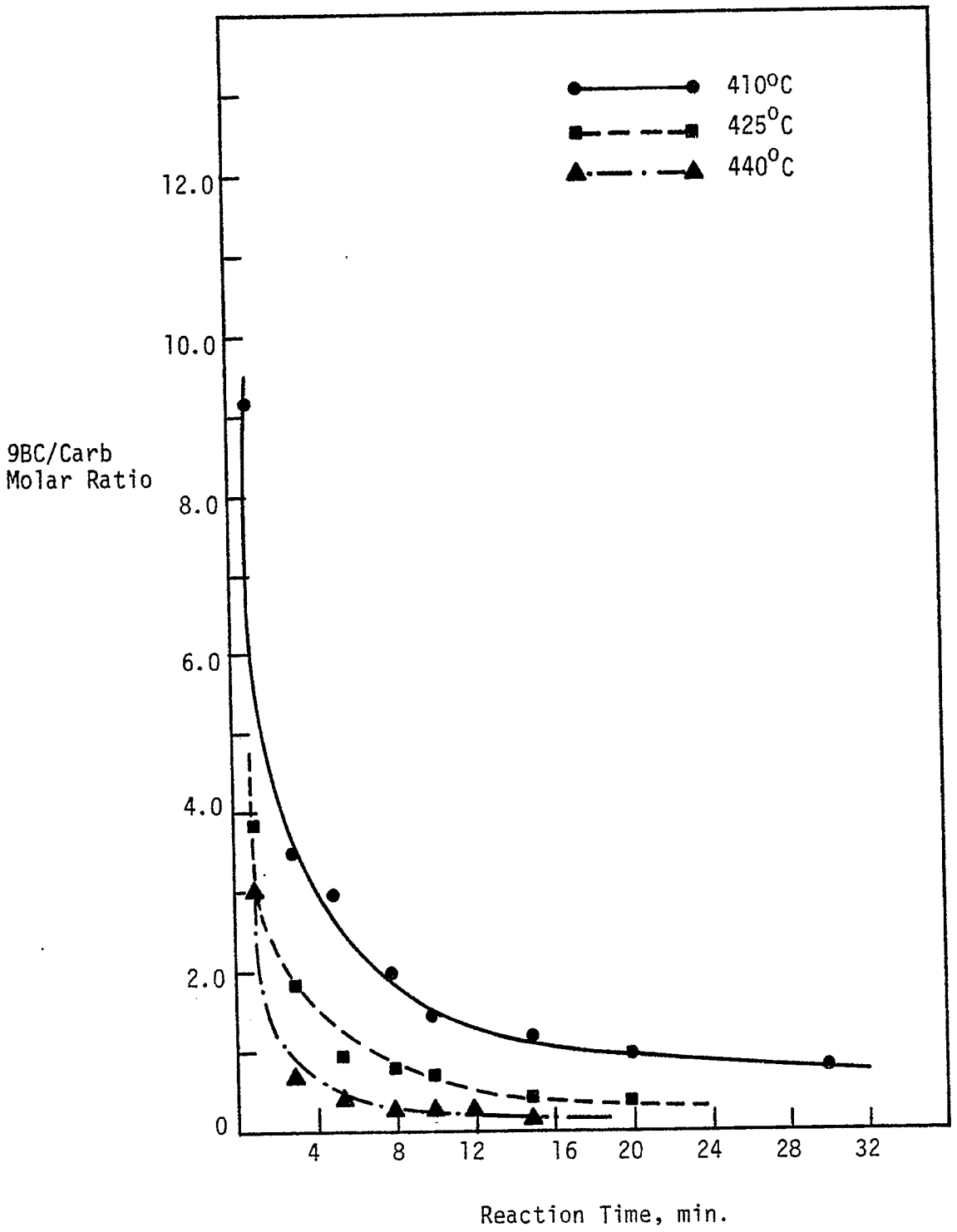

Figure 4. 9-Benzylcarbazole/Carbazole Molar Ratio vs. Time.

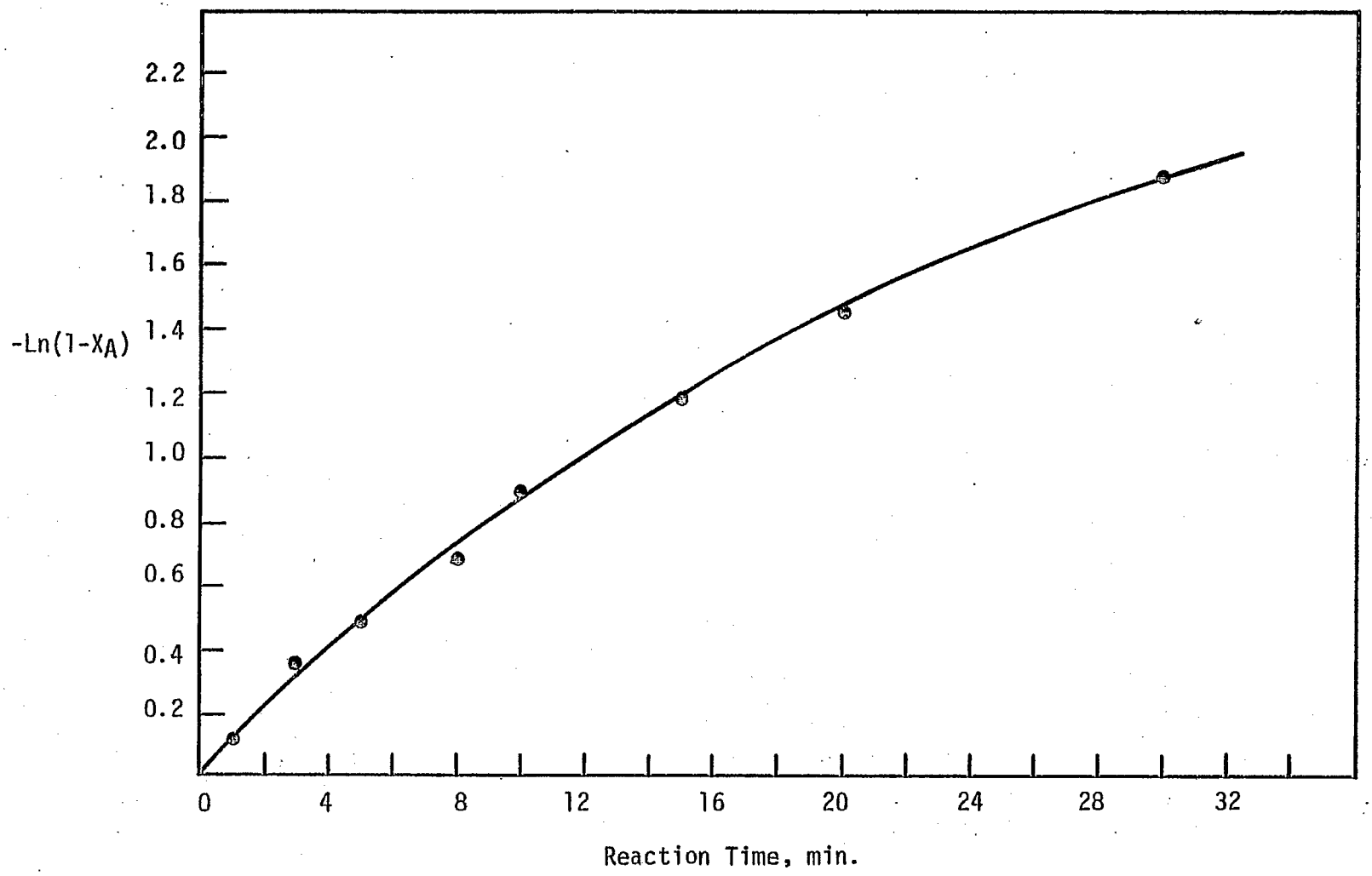

Figure 5. First Order Kinetics Plot. Temperature: 683 K (410°C). Pyrolysis of 9-Benzyl-1,2,3,4-tetrahydrocarbazole (9-BTHC).

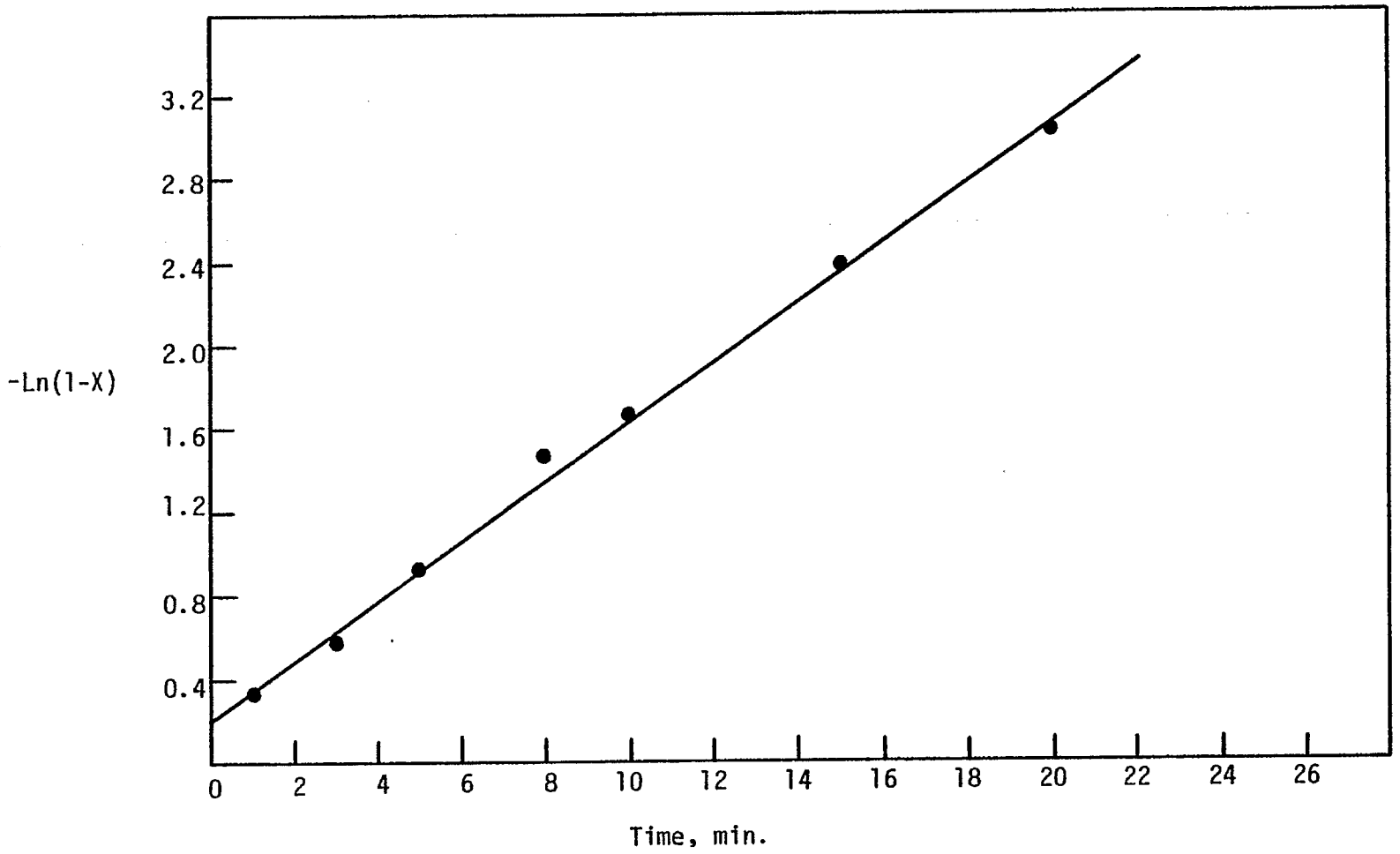

Figure 6. First Order Kinetics Plot. Temperature: 698 K (425°C). Pyrolysis of 9-Benzyl-1,2,3,4-tetrahydrocarbazole (9-BTHC).

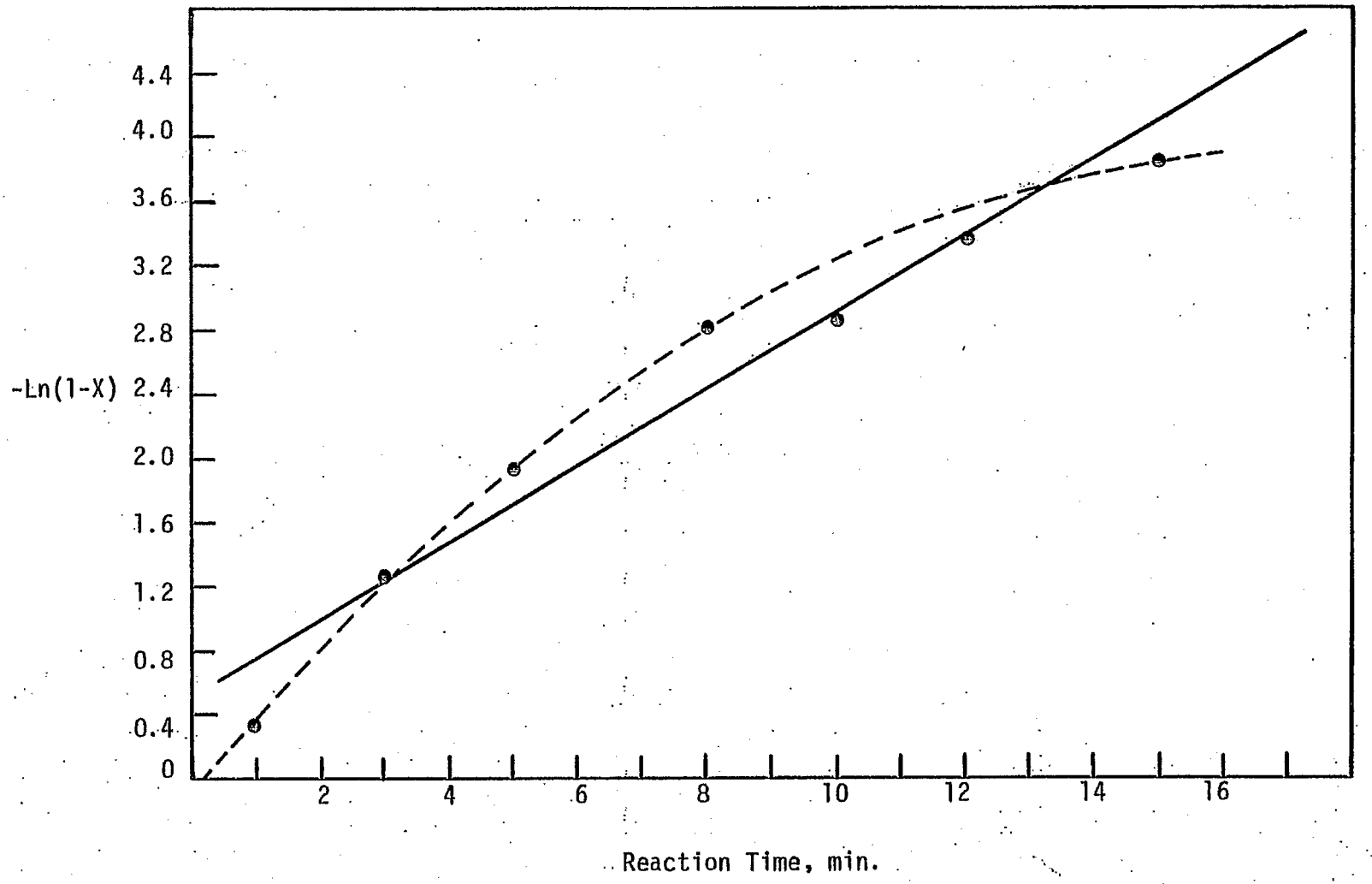

Figure 7. First Order Kinetics Plot. Temperature: 713 K (440°C). Pyrolysis of 9-Benzyl-1,2,3,4-tetrahydrocarbazole (9-BTHC).

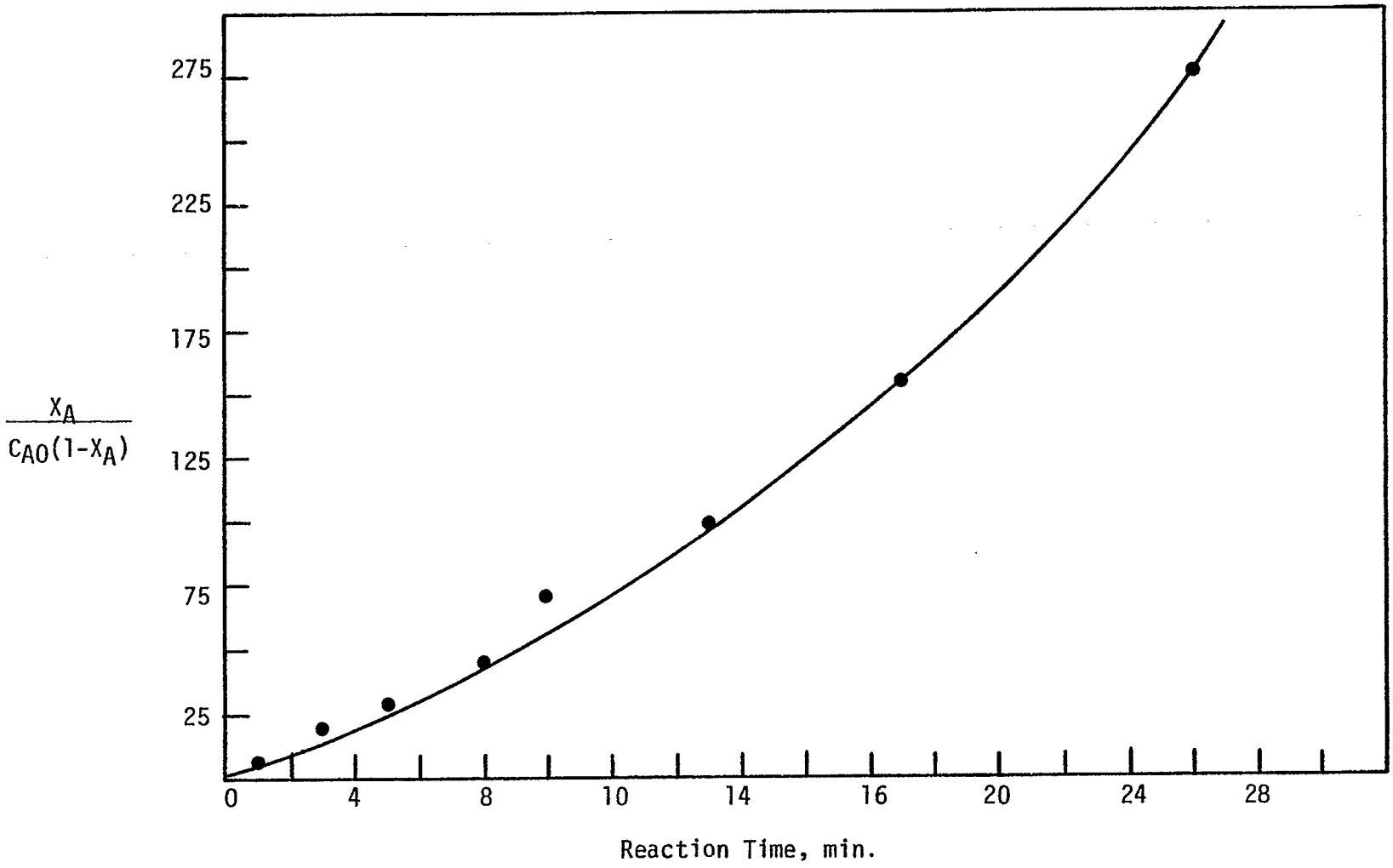

Figure 8. Second Order Kinetics Plot. Temperature: 683 K (410°C). Pyrolysis of 9-Benzyl-1,2,3,4-tetrahydrocarbazole (9-BTHC).

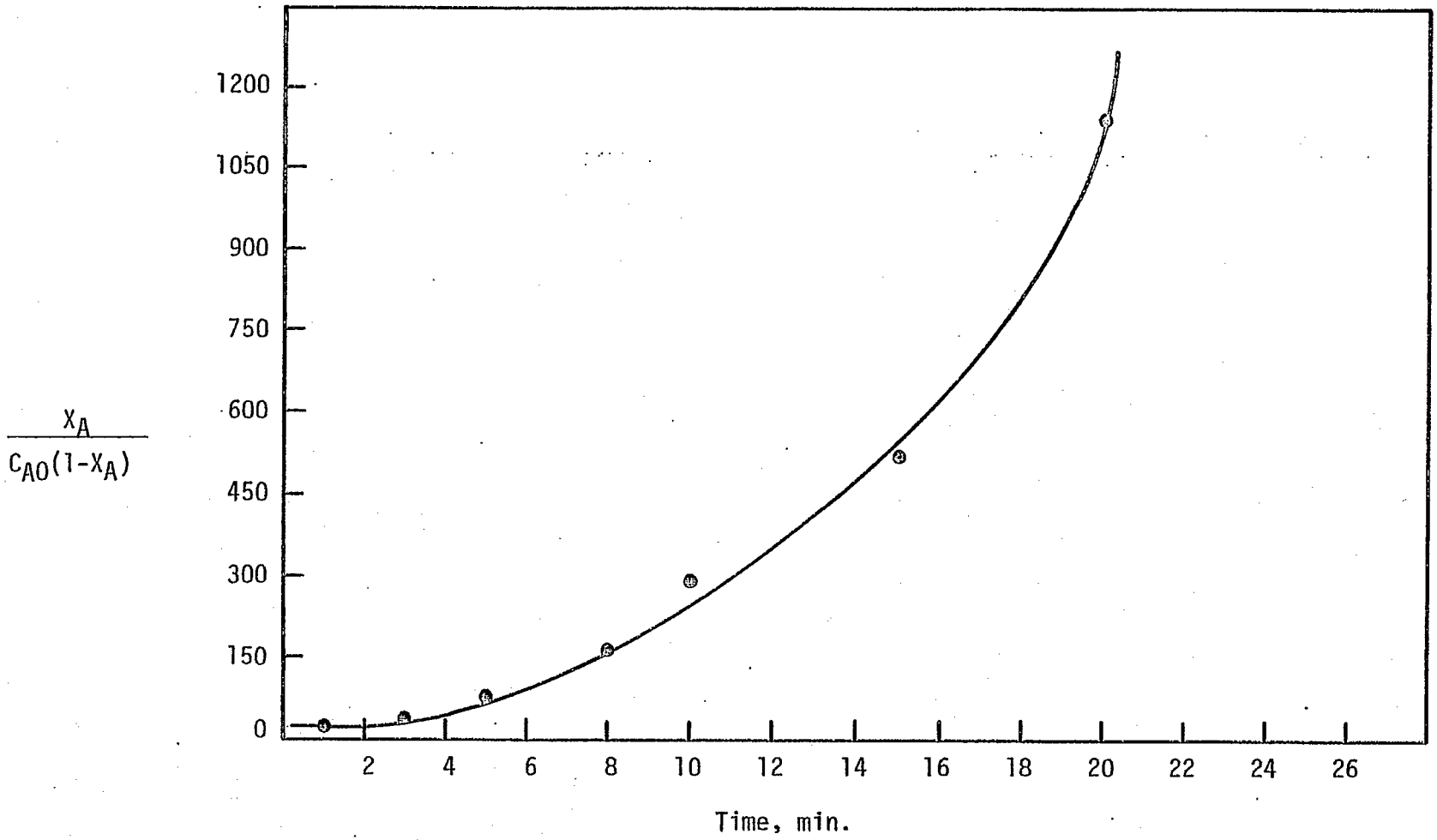

Figure 9. Second Order Kinetics Plot. Temperature: 698 K (425°C). Pyrolysis of 9-Benzyl-1,2,3,4-tetrahydrocarbazole (9-BTHC).

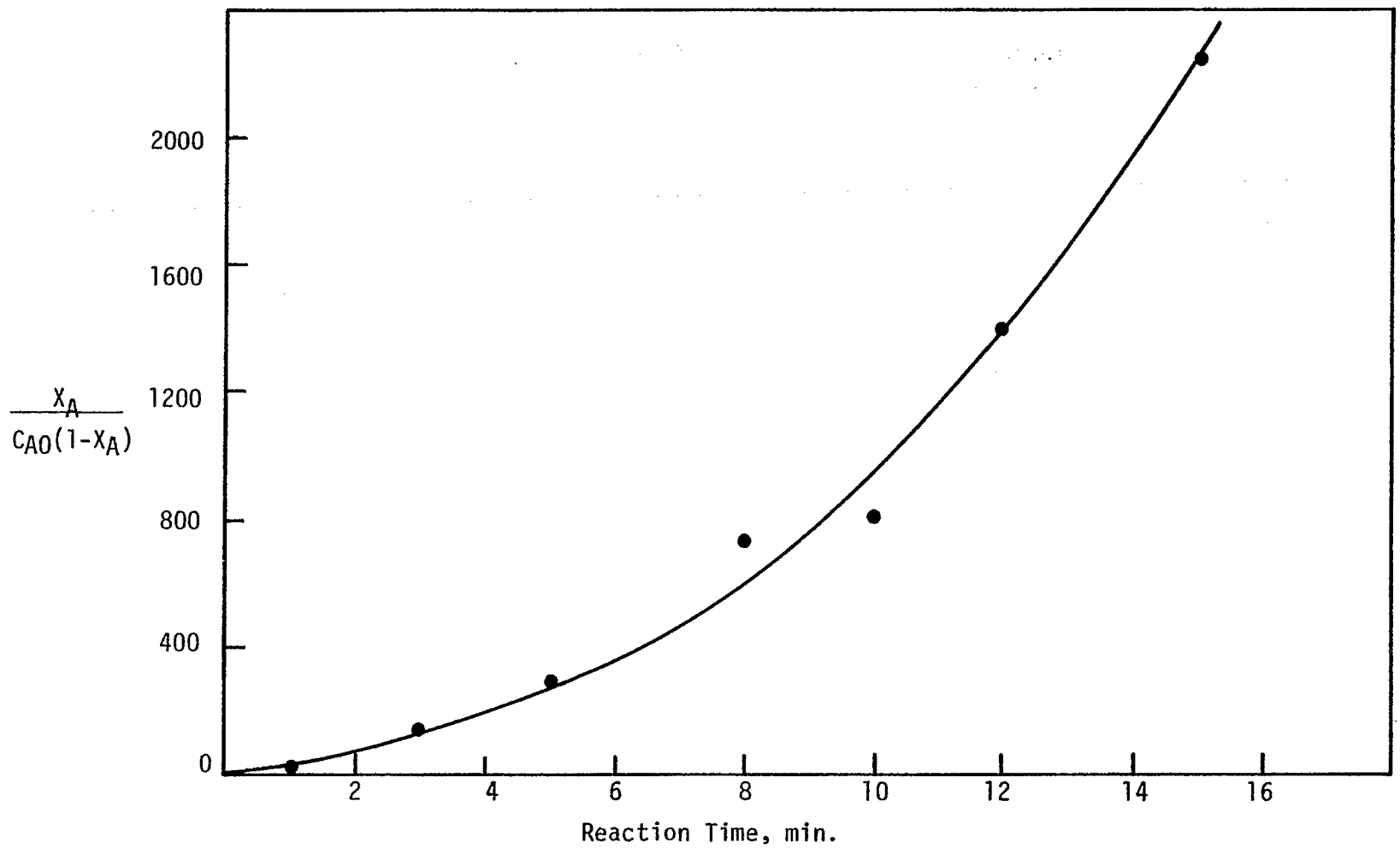

Figure 10. Second Order Kinetics Plot. Temperature: 713 K (440°C). Pyrolysis of 9-Benzyl-1,2,3,4-tetrahydrocarbazole (9-BTHC).

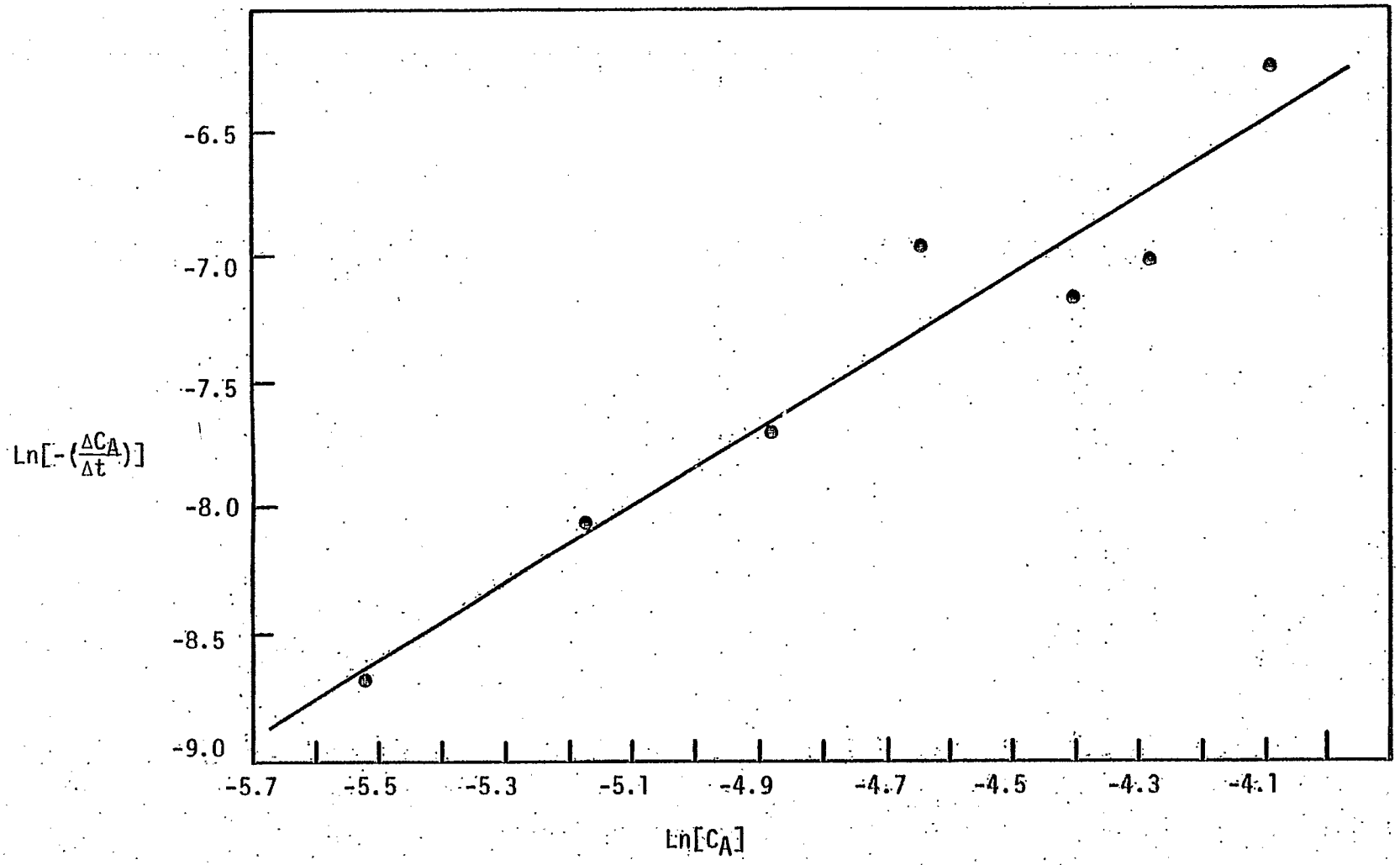

Figure 11. Differential Kinetics Analysis Plot. Temperature: 683 K (410°C). Pyrolysis of 9-Benzyl-1,2,3,4-tetrahydrocarbazole (9-BTHC).

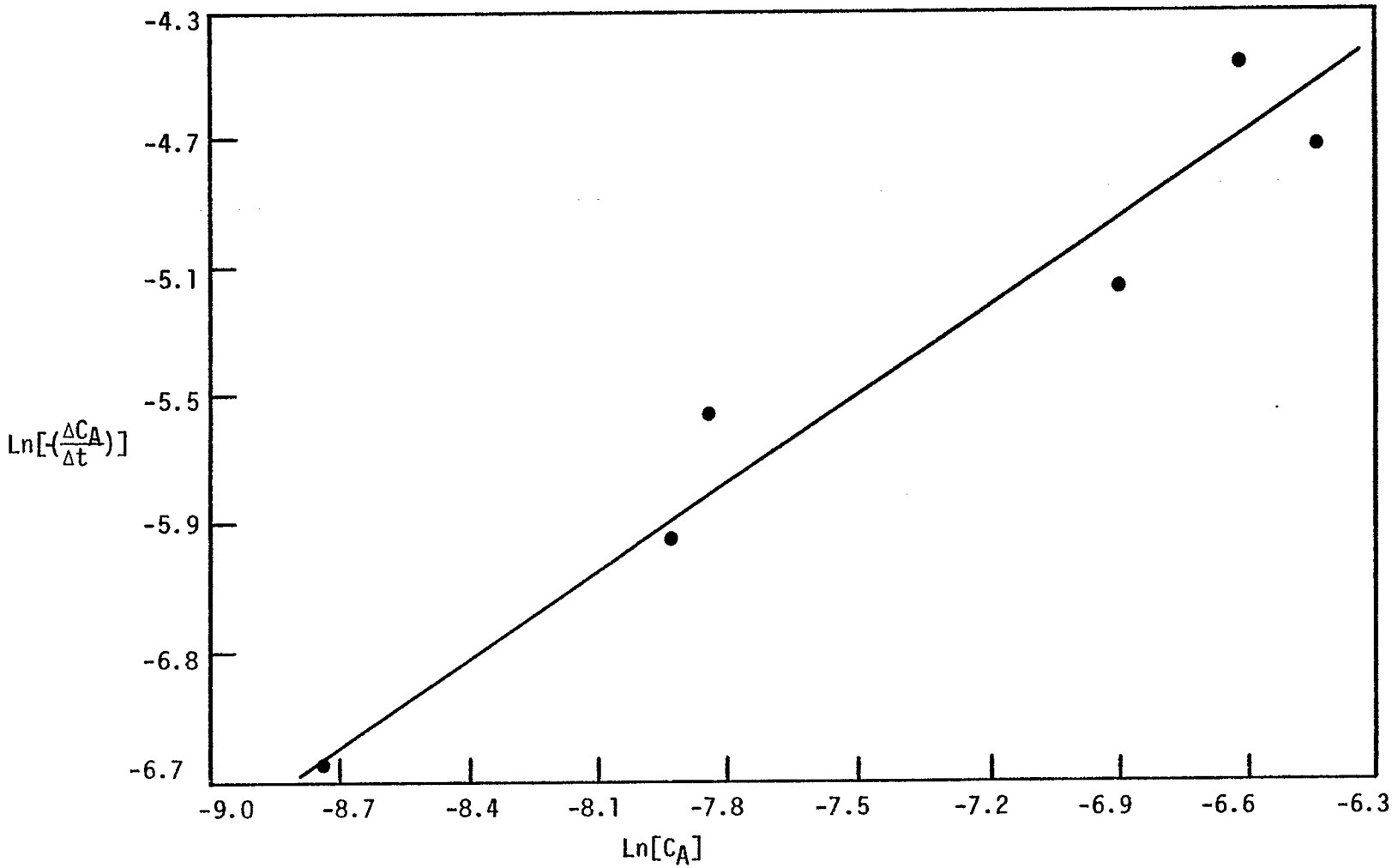

Figure 12. Differential Kinetics Analysis Plot. Temperature: 698 K (425°C). Pyrolysis of 9-Benzyl-1,2,3,4-tetrahydrocarbazole (9-BTHC).

FIGURE 13

PYROLYSIS OF 9-BENZYL-1,2,3,4-TETRAHYDROCARBAZOLE ARRHENIUS PLOT, LN K vs 1/T

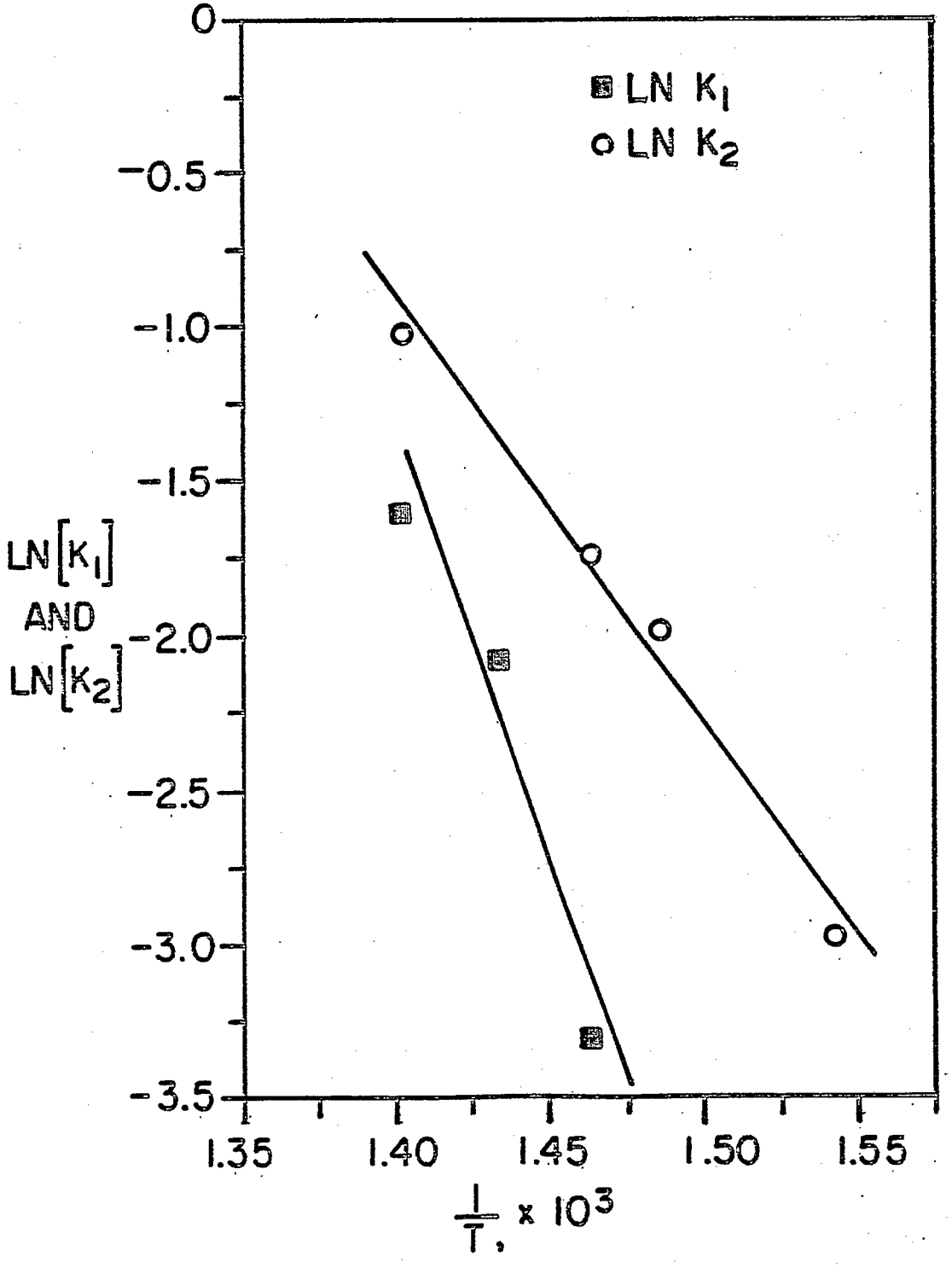

Task 6

Catalytic Hydrogenation of CD Liquids and Related Polycyclic Aromatic Hydrocarbons

Faculty Advisor: J. Shabtai
Research Associate: C. Russell

Introduction

The main objective of this research project is to develop a versatile process for controllable hydrotreating of highly aromatic coal liquids, viz., a process permitting production of naphthenic-aromatic feedstocks containing variable relative concentrations of hydroaromatic vs. aromatic ring structures. Such feedstocks, including the extreme case of a fully hydrogenated coal liquid, are suitable starting materials for catalytic cracking, as applied for preferential production of light liquid fuels. The overall objective of this project and of a parallel catalytic cracking study is, therefore, to develop and optimize a hydrotreating-catalytic cracking process sequence for conversion of coal liquids into conventional fuels.

The present project includes also a study of metal sulfide-catalyzed hydrogenation of model polycyclic arenes present in coal liquids, e.g., phenanthrene, pyrene, anthracene and triphenylene, as a function of catalyst type and experimental variables.[1] This part of the study provides basic information on the rate, mechanism and stereochemistry of hydrogenation of structurally distinct aromatic systems in the presence of sulfided catalysts.

Project Status

The study of the kinetics of ring hydrogenation of a selected coal liquid (SRC-II middle-heavy distillate), using a variety of newly synthesized Ni-Mo and Ni-W catalysts, is being continued.

Results obtained in the hydrogenation studies of polycyclic arenes, i.e., phenanthrene, anthracene, pyrene, chrysene, and triphenylene, are being summarized in the form of a series of papers, part of which will be shortly submitted for publication.

Future Work

The study of the hydrogenation-kinetics of a typical coal liquid (SRC-II middle-heavy distillate) will be continued.

Reference

1. J. Shabtai, C. Russell, L. Veluswami and A.G. Oblad, paper in preparation.

Task 7

Denitrogenation and Deoxygenation of CD Liquids and Related N- and O- Containing Compounds

Hydrodenitrogenation of Coal-Derived Liquids and Related N-Containing Compounds

Faculty Advisor: J. Shabtai
Graduate Student: J. Yeh

Introduction

The main objective of this research project is to develop effective catalyst systems and processing conditions for hydrodenitrogenation (HDN) of coal-derived liquids (CDL) in a wide range of nitrogen contents and structural type composition. This is of particular importance in view of the higher concentration of nitrogen-containing compounds in CDL as compared to that in petroleum feedstocks. For a better understanding of denitrogenation processes, the project includes systematic denitrogenation studies not only of CDL but also of related model N-containing compounds found in such liquids, e.g., phenanthridine, 1,10-phenanthroline, carbazoles, acridines, etc., as a funciton of catalyst type and experimental rate, mechanism and stereochemistry of HDN of structurally distinct N-containing aromatic systems in the presence of sulfided catalysts.

Project Status

The studies of hydrodenitrogenation kinetics of CDL fractions and of blends of CDL fractions with selected N-containing polycyclic compounds, e.g., isomeric, benzoquinolines, are being continued. Newly synthesized Co-Mo and Ni-Mo catalysts, possessing augmented C-N hydrogenolysis activity, are being used in these studies.

Future Work

HDN studies with CDL and model compounds will be continued.

Task 8

Catalytic Cracking of Hydrogenated Coal-Derived Liquids and Related Compounds

Faculty Advisor: J. Shabtai
A.G. Oblad
Graduate Student: John McCauley

Introduction

Hydrogenation followed by catalytic cracking provides a feasible process sequence for conversion of coal liquids into conventional fuels. Such a sequence has certain advantages in comparison with a hydrocracking-catalytic reforming scheme.

The present project is concerned with the following interrelated subjects: (1) systematic catalytic cracking studies of polycyclic naphthenes and naphthenoaromatics found in hydrogenated coal liquids and (2) systematic catalytic cracking studies of hydrotreated coal-derived liquids.

Project Status

Systematic catalytic cracking studies, using newly synthesized cross-linked smectite (CLS) molecular sieves,[1,2] are being continued. The cracking activities of Ce^{3+}- and La^{3+}- exchanged cross-linked montmorillonites (Ce-CLM and La-CLM, respectively) are being investigated in comparison with CeY-type zeolite, using large-size polycyclic naphthenes and naphthenoaromatics as feeds. Using dodecahydrotriphenylene (kinetic diameter = 11.7 Å) as feed, it is found that cracking rates with Ce-CLM and La-CLM catalysts are higher than the cracking rate with the CeY catalyst by at least two orders of magnitude. This clearly demonstrates the major advantage of CLS catalysts for cracking of large-size hydrocarbon molecules.

Future Work

The above indicated studies will be continued.

References

1. J. Shabtai, U.S. Patent 4,238,364 (1980).
2. J. Shabtai, R. Lazar and A.G. Oblad, Proc. 7th International Congress on Catalysis, Tokyo, Japan, 1980, pp 828-840.

Task 9

Hydropyrolysis (Thermal Hydrocracking) of CD Liquids

Faculty Advisor: J.S. Shabtai
A.G. Oblad
Graduate Student: Y. Wen

Introduction

This project is concerned with a systematic investigation of hydropyrolysis (thermal hydrocracking) as an alternative processing concept for upgrading of heavy coal-derived liquids (CDL) into light liquid products. The high efficiency and versatility of hydropyrolysis has been indicated in previous studies with heavy CDL feedstocks and with model compounds.[1-3] The present project is an extension of this previous work for the purpose of (a) further developing and enlarging the scope of the hydropyrolytic process, and (b) optimizing the operating conditions for different types of feedstocks, e.g., coal liquids from different liquefaction processes, partially hydrotreated coal liquids, and relevant model compounds. The project includes systematic studies of reaction kinetics, product composition, and coking tendencies, as a function of operating variables. The work with model compounds provides necessary data for further elucidation of mechanistic aspects of the hydropyrolysis process.

Project Status

The systematic studies of thermal hydrocracking reactions are being continued, using the following types of feedstocks:

(a) Naphthenoaromatic hydrocarbons (indan, 9,10-dihydroanthracene);

(b) N-containing pylycyclics (1,2,3,4-tetrahydroquinoline);

(c) Diaryl, diaralkyl and arylalkyl ethers (diphenyl ether, dibenzyl ether, phenyl cyclohexyl ether, anisole);

(d) Partially hydrotreated SRC-II distillates (carbon aromaticities in the range of 30 to 60%).

The above studies allow for examination of the feasibility of upgrading (viz., deoxygenation, denitrogenation, and molecular weight reduction) of coal-derived liquids by a combination of mild hydrotreatment and subsequent hydropyrolysis.

Future Work

The above indicated studies will be continued.

References

1. J. Shabtai, R. Ramakrishnan and A.G. Oblad, Advances in Chemistry, No. 183, Thermal Hydrocarbon Chemistry, Amer. Chem. Soc., 1979, pp 297-328.

2. R. Ramakrishnan, Ph.D. Thesis, University of Utah, Salt Lake City, Utah, 1978.

3. A.G. Oblad, J. Shabtai and R. Ramakrishnan, U.S. Patent, 4,298,457 (1981).

Task 10

Systematic Structural Activity Study of Supported Sulfided Catalysts for Coal Liquids Upgrading

Faculty Advisors: F.E. Massoth
J. Shabtai
Post-Doctoral Fellow: Y. Liu
N.K. Nag
Graduate Student: K. Baluswamy

Introduction

The objective of this research is to develop an insight into the basic properties of supported sulfide catalysts and to determine how these relate to coal liquids upgrading. The proposed program involves a fundamental study of the relationship between the surface-structural properties of various supported sulfide catalysts and their catalytic activities for various types of reactions. Thus, there are two clearly defined and closely related areas of investigation, viz., (1) catalyst characterization, especially of the sulfided and reaction states and (2) elucidation of the mode of interaction between catalyst surfaces and organic substrates of different types. The study of subject (1) will provide basic data on sulfided catalyst structure and functionality, and would allow the development of catalyst surface models. Subject (2), on the other hand, involves systematic studies of model reactions on sulfide catalysts, and the utilization of data obtained for development of molecular level surface reaction models correlating the geometry (and topography) of catalyst surfaces with the steric conformational structure of adsorbed organic reactants. The overall objective of the project is to provide fundamental data needed for design of specific and more effective catalysts for upgrading of coal liquids.

Atmospheric activity tests using model compounds representative of hydrodesulfurization (thiophene), hydrogenation (hexene) and cracking (isooctene) were employed to assay changes in the catalytic functions of various supported CoMo catalysts. It was found that hydrodesulfurization (HDS) and hydrogenation (HYD) activities were generally unaffected by the type of alumina used or by the cobalt salt used in the preparation; whereas, cracking (CKG) activity varied considerably. Increase in Co or Ni content at a fixed Mo content of 8% resulted in considerably higher promotion of HDS activity than HYD activity. Addition of additives at 1/2% level to the standard CoMo/Al_2O_3 catalyst generally increased HDS and CKG for acidic additives and decreased these functions for basic additives, HYD being unaffected. At 5% level, the additives decreased all functions, basic additives decreasing activities more severely. In a series of catalysts employing silica-alumina as the support, the HDS and hydrogenation functions decreased with increasing silica content, while cracking went through a maximum in activity. Catalysts prepared by supporting CoMo on TiO_2, SiO_2·MgO and carbon showed low activities, except for high cracking activity for the two former catalysts.

Oxide precursors of CoMo and Mo catalysts supported on various silica-aluminas evaluated by ESCA showed that support-active component interaction decreased with increase of silica in the support. It was also found that cobalt did not influence the Mo dispersion. On alumina, the Mo phase was found to be dispersed in essentially a monoatomic form.

Several catalysts, which were evaluated in the atmospheric pressure test unit, were subsequently tested at elevated pressure (34 atm) using dibenzothiophene (HDS), naphthalene (HYD) and indole (HDN). The high pressure runs were carried out sequentially in the order indicated to assess the separate catalytic functionalities. Repeat runs of HDS and HYD after HDN gave appreciably lower activities for HDS and HYD which was found to be due to strongly adsorbed residues containing nitrogen. The effect of increasing H_2S was to appreciably decrease HDS, moderately decrease HYD, and moderately increase HDN conversions.

Comparison of high pressure results for HDS of dibenzothiophene and HYD of naphthalene with atmospheric results for HDS of thiophene and HYD of hexene carried out in the same reactor showed good correlations, signifying that the low pressure tests reasonably reflect catalytic activity under high pressure test conditions, at least for the model compounds used.

Project Status

During this period further kinetic studies of the reactions of hydrodesulfurization (HDS), hydrogenation (HYD) and hydrodenitrogenation (HDN) at elevated pressure were carried out and rate equations developed. The effect of total pressure on the above reactions was examined. Several model compounds for testing catalyst activity for hydrodeoxygenation (HDO) were evaluated. Finally, stereochemical studies of naphthalene hydrogenation over several catalysts were undertaken.

In the elevated pressure (500 psi) tests for catalyst activity, the reactions of dibenzothiophene HDS, naphthalene HYD and indole HDN (defined here as the initial C-N bond breaking step) are run separately in the sequence indicated in order to determine the separate catalytic functionalities of various catalysts.[1] Preliminary analyses of the kinetics of these reactions have been reported.[2] Because of the limited data obtained in previous runs, it was decided to conduct a more detailed study of the kinetics of the different reactions. This was carried out on a commercial catalyst (Ketjen CoMo) with a wider range of liquid feed rates. The results are given in Figure 1 in terms of conversion versus liquid feed rate for each reaction. The total flow rate, pressure and temperature were held constant during these runs. The drop in conversion observed in Figure 1 with increasing reactant feed composition (liquid feed rate at constant total flow rate) indicates reaction inhibition in reactant and/or products, as has been discussed earlier.[2] Also, the concentration of H_2S has been shown to effect reactivities.[3]

The kinetics of the reactions were modelled with a general rate equation of the form,

$$r_i = \frac{k_i P_i}{(1+K_i P_i+K_p P_p+K_S P_S)^n} \qquad (1)$$

where r is the reaction rate, k the rate constant, P the partial pressure and K the dynamic adsorption constant, subscripts i referring to reactant, p to products and s to H_2S, and n is a constant (either 1 or 2). Because of the complexity of using this equation for analyzing conversion data from a fixed-bed reactor, a pseudo first-order treatment was used to analyze the results. In this treatment, the pseudo first-order rate constant, k', is calculated for each data point (different liquid feed rate) according to the equation,

$$k_i' = -S_V \ln(1-x_i) \tag{2}$$

where S_V is the space velocity (constant) and x is the conversion, and k_i' is given by,

$$\frac{1}{k_i'} = \frac{1}{k_i}(1+\Sigma K_j P_j)^n \tag{3}$$

In Equation (3), P_j is different for each data point, depending upon liquid feed composition and conversion. In principle, then, it is possible to calculate k_i and the various K_j's by a multilinear regression analysis of Equation (3).

Such an analysis has been carried out for the three reactions from the data of Figure 1. The following rate equations have been found to correlate the data satisfactorily:

$$\text{(HDS)} \quad r_T = \frac{k_T P_T}{(1+K_T P_T+K_S P_S)^2} \tag{4}$$

$$\text{(HYD)} \quad r_H = \frac{k_H P_A}{(1+K_A P_A^o+K_S P_S^o)^2} \tag{5}$$

$$\text{(HDN)} \quad r_N = \frac{k_N P_N P_S^o}{(1+K_N P_N^o+K_S P_S^o)^2} \tag{6}$$

In these equations, subscripts T stand for benzothiophene, A for naphthalene and N for indole, and the superscript ^{o} refers to feed composition. The pressure of H_2 has been included in k since it was constant in all runs. The inlet feed compositions have been used in Equations (5) and (6); this assumes an average adsorption constant for all products of the reaction. A P_S term is included in Equation (6) to account for the promotion effect of H_2S on HDN previously observed.[3] From the values of k and the different K's obtained from the analyses, predicted conversions at each liquid feed rate were calculated and are shown by the curves given in Figure 1. It can be seen that the predicted curves follow the experimental data quite well, indicating the validity of Equations (4) to (6) to describe the kinetics of the various reactions under the reaction conditions employed.

The effect of H_2S on conversions for the three reactions has also been analyzed with the above kinetics. The results are presented in Figures 2 and 3, where the curves are predicted from the kinetics and points are the experimental data obtained. Good agreement is again observed, showing the general applicibility of Equations (4) to (6) to changes in feed composition. Table 1 gives the parameter values obtained from these analyses and the run

conditions employed.

It has been observed previously that in a mixture of dibenzothiophene and naphthalene, the HYD conversion was appreciably lowered from that in naphthalene alone, while the HDS conversion was hardly affected. This means that dibenzothiophene adsorbs strongly on HYD sites but naphthalene does not adsorb on HDS sites. Using the above kinetic parameters, the adsorption constant for dibenzothiophene on HYD sites is estimated to be about 650 atm^{-1}. Comparing this value to its adsorption constant on HDS sites (28.4 atm^{-1}) indicates that dibenzothiophene adsorption is some 20 times greater on HYD than on HDS sites.

Catalyst tests have been carried out at one total pressure (34 atm). In order to evaluate the effect of H_2 pressure on conversions for the various reactions, a run was made at 17 atm total pressure on the commercial Ketjen CoMo catalyst. Comparison of conversions obtained at the two pressures but otherwise the same conditions is given below:

	Conversion, %	
Reaction	34 atm	17atm
HDS	65.3	64.0
HYD	59.0	37.0
HDN	49.5	33.0

As can be seen, lower pressure hardly affected HDS conversion but significantly decreased HYD and HDN conversions. This indicates that above at least 34 atm, the HDS sites are saturated by H_2 so no further conversion is achieved with higher pressure. But for HYD and HDN, increasing pressure evidently causes more H_2 adsorption and attendant increase in reaction. This interesting result needs confirmation at other pressures before a hydrogen function can be incorporated into the rate equations discussed above.

A model reaction to evaluate hydrodeoxygenation (HDO) activity of catalysts has been investigated. Furans seem to be suitable condidates at atmospheric pressure and dibenzofuran at elevated pressure. Preliminary runs indicated clean reactions to olefins or biphenyl without evidence of oxygenated intermediates. An interesting result was obtained on the effect of H_2S on the HDO of 3-methylfuran carried out at atmospheric pressure. Under identical reaction conditions, when the H_2S concentration was doubled, conversion increased from 26.2% to 31.2%, and when the concentration was halved from the original value, the conversion decreased to 25.2%. The promotion effect of H_2S is similar to that noted for HDN of indole and may mean that the same sites are involved in the two reactions. Further tests are needed to confirm this result.

Studies of the stereochemistry of reactions over sulfided catalysts have been started. The purpose of these studies is to gain insight into the geometry of the active sites by analyzing the course of stereospecific reactions. Initial studies have involved the hydrogenation of naphthalene at high pressures in an autoclave reactor.

Under the reaction conditions employed, naphthalene is first hydrogenated to tetralin, which is further converted to decalins. The latter reaction

presumably proceeds through the intermediate 9,10-octalin. The hydrogenation of this intermediate can give either trans-or cis-decalin, depending on the mode of addition of H_2 to the double bond. There are three possibilities for this addition:

(1) addition of two H atoms from the catalyst to the same side of the intermediate adsorbed flatwise, leading to cis-addition;

(2) addition of two H atoms to opposite sides of the intermediate adsorbed edgewise in a cavity in the catalyst, in which the H atoms come from different sites, leading to trans-addition; and

(3) a mechanism where the half-hydrogenated intermediate either flips over and adds the second H atom from the same catalyst site, or desorbs and migrates to another site not necessarily lying on the same plane for addition of the second H atom, leading to trans-addition.

The third mechanism can be ruled out from preliminary data showing that the trans/cis ratio remained unchanged for runs at different pressures and temperatures with NiMo and NiW catalysts supported on Al_2O_3; a different ratio would be expected if the third mechanism was operative. Therefore, the trans/cis ratio should be indicative of whether process (1) above (low ratio) or (2) above (high ratio) is occurring. For the results to be meaningful, interconversion between cis- and trans-decalin (isomerization of stereoisomers) should not occur under the reaction conditions. Separate experiments with mixtures of the two decalins showed no interconversion.

The results obtained for naphthalene hydrogenation with various catalysts are given in Table 2. Of significance, all trans/cis ratios were appreciable, indicating addition of H atoms from opposite sides. Studies with metal catalysts showed opposite results, i.e., low ratios,[4] which were taken as evidence for flatwise adsorption on metal sites. Evidently, the active HYD sites on sulfided catalysts are different, most likely consisting of cavities into which the molecule penetrates prior to being hydrogenated from each side of the cavity. In such a situation, two H atoms can come from the same side (leading to cis-decalin) as well as opposite sides, which can account for the lack of exclusive trans products. It is also observed from Table 2 that the trans/cis ratio varies with the catalyst, being lowest for Mo, intermediate for CoMo and highest for NiMo and NiW catalysts. This indicates that the promoter metals Co and Ni somehow influence the character of the adsorption site.

Future Work

Several NiW/Al_2O_3 catalysts of varying Ni content will be tested for HDS, HYD, HDN and HDO at elevated pressure. The effect of total pressure on the kinetics of the above reactions will be investigated. Stereochemical runs will continue using quinoline.

References

1. W.H. Wiser et al., DOE Contract No. DE-AC01-79ET14700, Quarterly Progress Report, Salt Lake City, Utah, April-June 1982.

2. ibid., Jan - Mar, 1982.

3. ibid., July - Sept, 1982.

4. A.W. Weitkamp, Adv. in Catal., 18, 1 (1968).

Table 1. Rate parameters from kinetic analyses of reactions at elevated pressure.

	HDS	HYD	HDN
Total P, atm	34	34	34
Temperature, ^{o}C	277	277	350
Total space velocity, mole/Hr·g cat	0.76	0.76	0.76
k_i, mole/hr·g cat·atm	3.7	2.7	33,700[a]
K_i, atm^{-1}	28.4	9.8	469
K_S, atm^{-1}	3.4	2.5	148

[a]Units are mole/hr·g cat·$atm.^2$

Table 2. Stereochemistry of the hydrogenation of naphthalene.[a]

Catalyst[b]	Conversion, %	Selectivity, %			Trans/Cis Ratio
		Tetralin	Trans-DHN	Cis-DHN	
Co(6)Mo(8)	99.5	91	6.5	2.5	2.6
Co(3)Mo(8)	98.0	92	5.7	2.2	2.6
Ni(6)Mo(8)	99.8	60	32	8	4.0
Ni(3)Mo(8)	99.0	68	26	6	4.3
Ni(6)W(16)	99.4	40	47	13	3.6
Ni(3)W(16)	99.7	37	50	13	3.9
Mo(8)	--[c]	99	0.55	0.45	1.2

[a]Conditions: 1% naphthalene in heptane, 300°C, 150 atm H_2, 2 h.

[b]Numbers are wt % supported on Al_2O_3.

[c]Feed was tetralin.

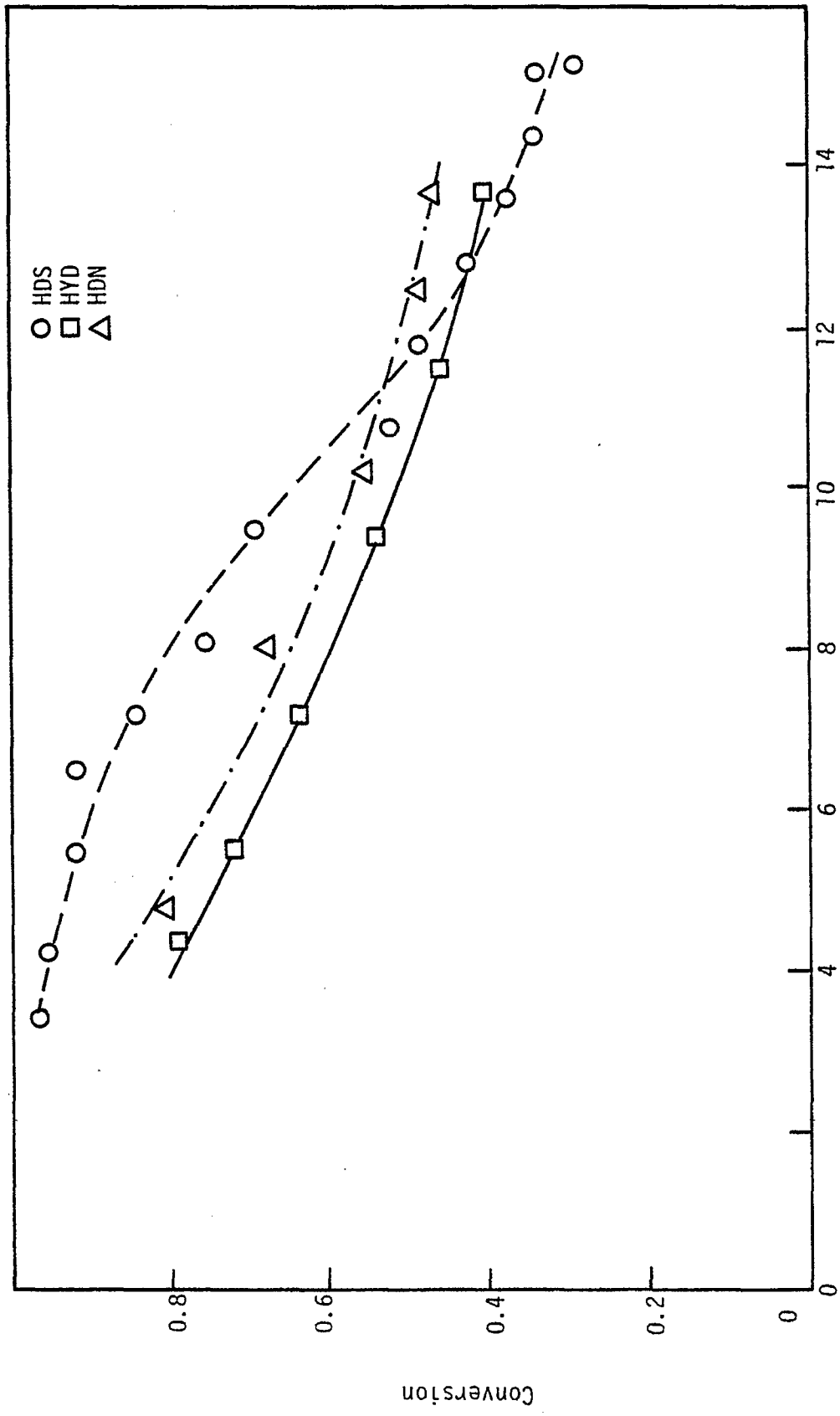

Figure 1. Effect of liquid feed rate on conversion for HDS, HYD and HDN.

FIGURE 2

DATA FIT TO KINETIC EQUATIONS

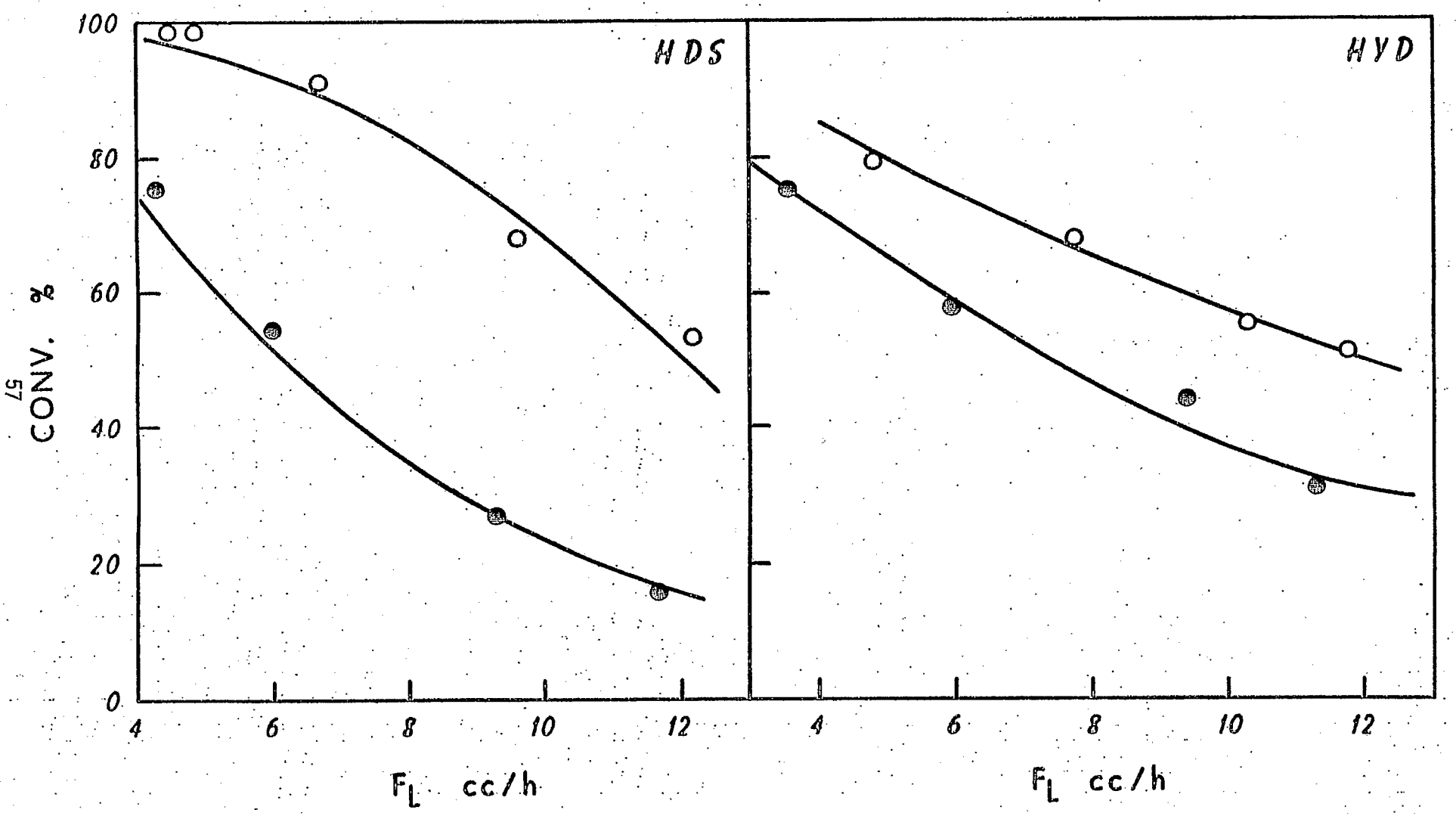

(O = Stand. run, ● = Excess CS_2)

FIGURE 3

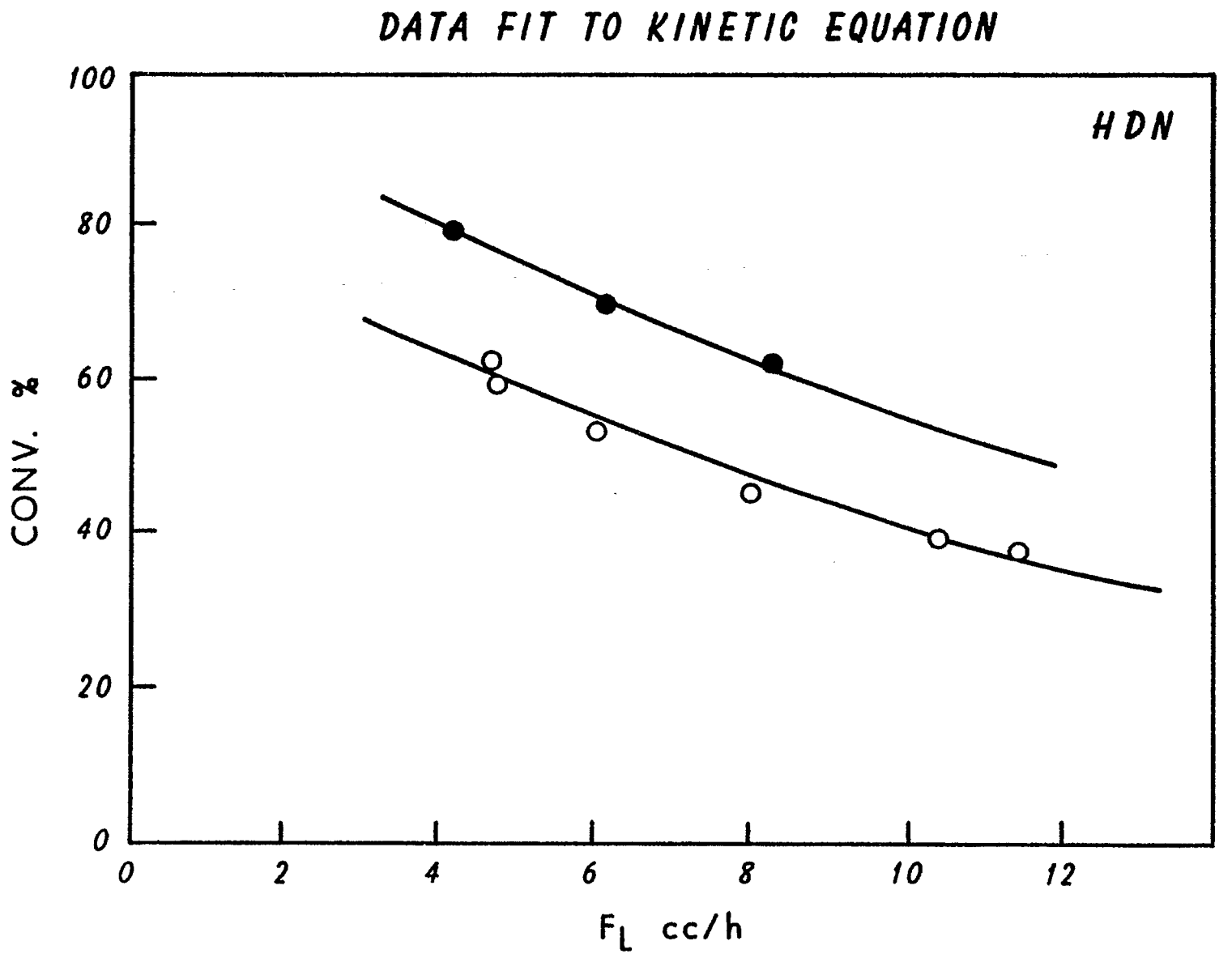

(○ = Stand. run, ● = Excess CS_2)

Task 11

Basic Study of the Effects of Poisons on the Activity of Upgrading Catalysts

Faculty Advisor: F.E. Massoth
Post-Doctoral Fellow: J. Miciukiewicz

Introduction

The importance of cobalt-molybdena catalysts for hydrotreating and hydrodesulfurization of petroleum feedstocks is well-known. These catalysts are also being studied for hydrodesulfurization and liquefaction of coal slurries and coal-derived liquids. However, such complex feedstocks result in rapid deactivation of the catalysts. To gain an insight into the deactivation mechanism, the detailed kinetics of reactions of model compounds representative of heteroatom hydrogenolysis and hydrogenation are compared before and after addition of various poisons and coke precursors. The studies are carried out using a constant stirred microbalance reactor, which enables simultaneous measurement of catalyst weight change and activity. Supplementary studies are made to gain additional insight into the effect of poisons on the active catalyst sites. Finally, catalysts aged in an actual coal pilot plant run are studied to compare with laboratory studies.

Previous work on this project has shown that catalyst poisoning by pyridine or coke results in loss of active sites for benzothiophene HDS, but that the remaining unpoisoned sites retain their original activity. Pyridine appeared to be site selective in poisoning effect whereas coke was nonspecific. Furthermore, at least two HDS sites were indicated from the pyridine poisoning studies.

Poisoning of a commercial $CoMo/Al_2O_3$ catalyst by several nitrogen containing compounds gave the following order of deactivation of hexene hydrogenation (HYD): quinoline > pyridine = 3,5-lutidine > indole > aniline. Thiophene hydrodesulfurization (HDS) was deactivated more than hexene hydrogenation, but was less sensitive to the type of poison adsorbed. Poisoning with 2,6-lutidine gave opposite results, hydrogenation being deactivated more than HDS, showing that steric and inductive effects are important in the effect of specific poisons on catalyst deactivation. Adsorption of 2,6-lutidine at low concentrations resulted in an increase in HDS activity rather than the decrease expected, while at the same time hexene HYD decreased.

Project Status

To determine if the unusual promotion of HDS activity at low concentrations of adsorbed 2,6-lutidine (2,6-dimethylpyridine) observed previously[1] with the commercial American Cyanamid (1442A) catalyst was a general phenomenon or specific to this catalyst, poisoning studies were repeated with a laboratory-prepared catalyst containing CoMo on a pure γ-Al_2O_3 support. The results of these runs are given in Figure 1 in terms of relative HDS activity versus amount of poison added to the catalyst. Deactivation of

HDS was considerably more prounounced than found previously with the commercial catalyst (see Figure 1 of Reference 1) for both poisons. Significantly, the positive promotion effect of 2,6-lutidine observed earlier with the commercial catalyst in the range up to 0.03 mmol/g was not obtained with the laboratory catalyst. However, the fact that the deactivation curve of 2,6-lutidine starts at 0.01 mmol/g rather than at zero, may indicate possible promotion of HDS activity at lower concentrations. Unfortunately, it was not possible to investigate this lower region due to experimental limitations. Further, a much smaller difference in deactivation responses of the two N-poisons with the laboratory catalyst was obtained than that obtained previously with the commercial catalyst. We conclude that the commercial catalyst must contain an impurity not present in the laboratory catalyst which is responsible for its lower deactivation response and unusual promotional activity at low concentrations of 2,6-lutidine.

Studies have begun on the kinetics of HDS and HYD for the commercial catalyst and spent samples of the same catalyst which had been used in a PDU run in the H-coal process. These samples were from the PDU-9 run and were supplied by Sandia Laboratories. The object of these studies is to assess catalyst deactivation of HDS and HYD due to coal processing time. In particular, it is desired to determine whether HDS and HYD activities deactivate to the same extent due to coke and metals on the catalyst and how the deactivation affects the kinetic parameters. Furthermore, by comparing the kinetics of the spent catalyst and regenerated catalysts (in which the coke is burned off but the metals remain), it should be possible to assess the deactivating effect of each of these contaminants separately.

Runs were carried out on the fresh catalyst (American Cyanimid 1442A) for thiophene HDS and 1-hexene HYD using particle sizes of 20-40 mesh. A specially constructed, stirred flow microbalance reactor was used to simultaneously obtain catalyst weight changes and activities. Details of the apparatus are given elsewhere.[2] The reactor operates as a constant stirred tank reactor; consequently, rate data are obtained directly. A Pt wire-screen bucket containing the catalyst was suspended in the reactor by means of thin quartz rods attached to the microbalance (Cahn R.G.). A squirrel-cage stirrer, magnetically operated from below the reactor, provided for gas mixing and gas-catalyst contact. Gas feed mixtures were made up by metering with calibrated rotometers. Thiophene or hexene was added by saturating a separate H_2 stream. Effluent gas samples were analyzed by gas chromatography for thiophene or hexene conversion. A catalyst charge of 500 mg was used. Presulfiding was accomplished in situ by exposing the oxidized catalyst to a 9% H_2S/H_2 mixture at 400°C for 2 hr, followed by a 2hr He purge. After presulfiding, the catalyst was exposed to a thiophene/H_2 stream at 350°C for an overnight period to assure attainment of a lined out activity, since preliminary runs had shown a gradual decrease in catalyst activity over several hours. Hexene hydrogenation followed the thiophene HDS run using the same charge of catalyst. Blank experiments were carried out without any catalyst in the sample bucket and also with sulfided γ-Al_2O_3, using both thiophene and hexene as feed. Thiophene and hexene showed no reaction in either case.

A series of runs for each reactant was carried out by varying partial pressures of the reactant and H_2S. The data were analyzed by nonlinear least squares analysis of the following general rate expression,

$$r_i = \frac{k_i p_i p_H}{(1+K_i p_i+K_s p_s)^n} \qquad (1)$$

where r is the reaction rate, k the rate constant, p the partial pressure and K the adsorption constant, subscript i referring to reactant and s to H_2S; n is a constant, being 1 or 2.

The results of the thiophene runs are given in Table 1. There was no catalyst aging during these runs as evidenced by the consistency of repeat runs at a standard set of conditions and the constancy in catalyst weight. The data fit for n=2 is slightly better in the 95% confidence intervals of the parameters. The absorption constant for thiophene is about four times larger than that for H_2S, but both are needed to adequately describe the kinetics.

Thiophene HDS forms n-butenes as primary products, which subsquently undergo hydrogenation to butene. The kinetics of this HYD step were also determined, with the results given in Table 1. The value of K_s obtained is negative, which is not physically meaningful. Besides, the value of K_B is small and has little effect on the reaction rate. Consequently, a simple first order rate constant best describes this HYD reaction.

The kinetic analyses for hexene HYD (run in the absence of thiophene) are presented in Table 2. The 95% confidence intervals of the parameters are rather large, especially for K_{HX}, indicating appreciable random error in the data. Catalyst weight was observed to gradually increase during those runs, presumably due to coking, which probably explains the high error. In any case, the adsorption parameters are small, and a simple first order reaction for HYD is again indicated within the accuracy of the data.

Future Work

Kinetic studies will continue on aged and aged-regenerated samples from the H-coal process.

References

1. W.H. Wiser et al., DOE Contract No. DE-AC01-79ET14700, Quarterly Progress Report, Salt Lake City, Utah, Oct-Dec 1982.

2. R. Ramachandran, Ph.D. Dissertation, University of Utah, Salt Lake City, Utah, 1980.

Table 1. Kinetic parameters for thiophene runs with Cyanamid catalyst.

Thiophene HDS	n=1	n=2
SSQ/DF[a] x 10^4	3.5	3.4
k_T, $cm^3/min\ g\ atm^2$	247 ± 18	233 ± 13
K_T, atm^{-1}	41 ± 11	16 ± 4
K_S, atm^{-1}	12 ± 3	5 ± 1
Butene HYD		
SSQ/DF[a] x 10^6	5.5	5.6
k_B, $cm^3/min\ g\ atm^2$	94 ± 2	94 ± 2
K_B, atm^{-1}	7 ± 5	4 ± 3
K_S, atm^{-1}	-2.3 ± 0.4	-1.2 ± 0.2
k_1[b], $cm^3/min\ g\ atm^2$	98 ± 7	

[a]Sums of squares/degrees of freedom (11).
[b]First-order rate constant.

Table 2. Kinetic parameters for hexene runs with Cyanamid catalyst.

	n=1	n=2
SSQ/DF[a] x 10^4	54	55
k_{Hx}, $cm^3/min\ g\ atm^2$	92 ± 12	92 ± 12
K_{Hx}, atm^{-1}	3.0 ± 6.6	1.4 ± 2.9
K_S, atm^{-1}	4.6 ± 4.4	2.1 ± 2.0
k_1[b], $cm^3/min\ g\ atm^2$	79 ± 12	

[a]Sums of squares/degrees of freedom.
[b]First-order rate constant.

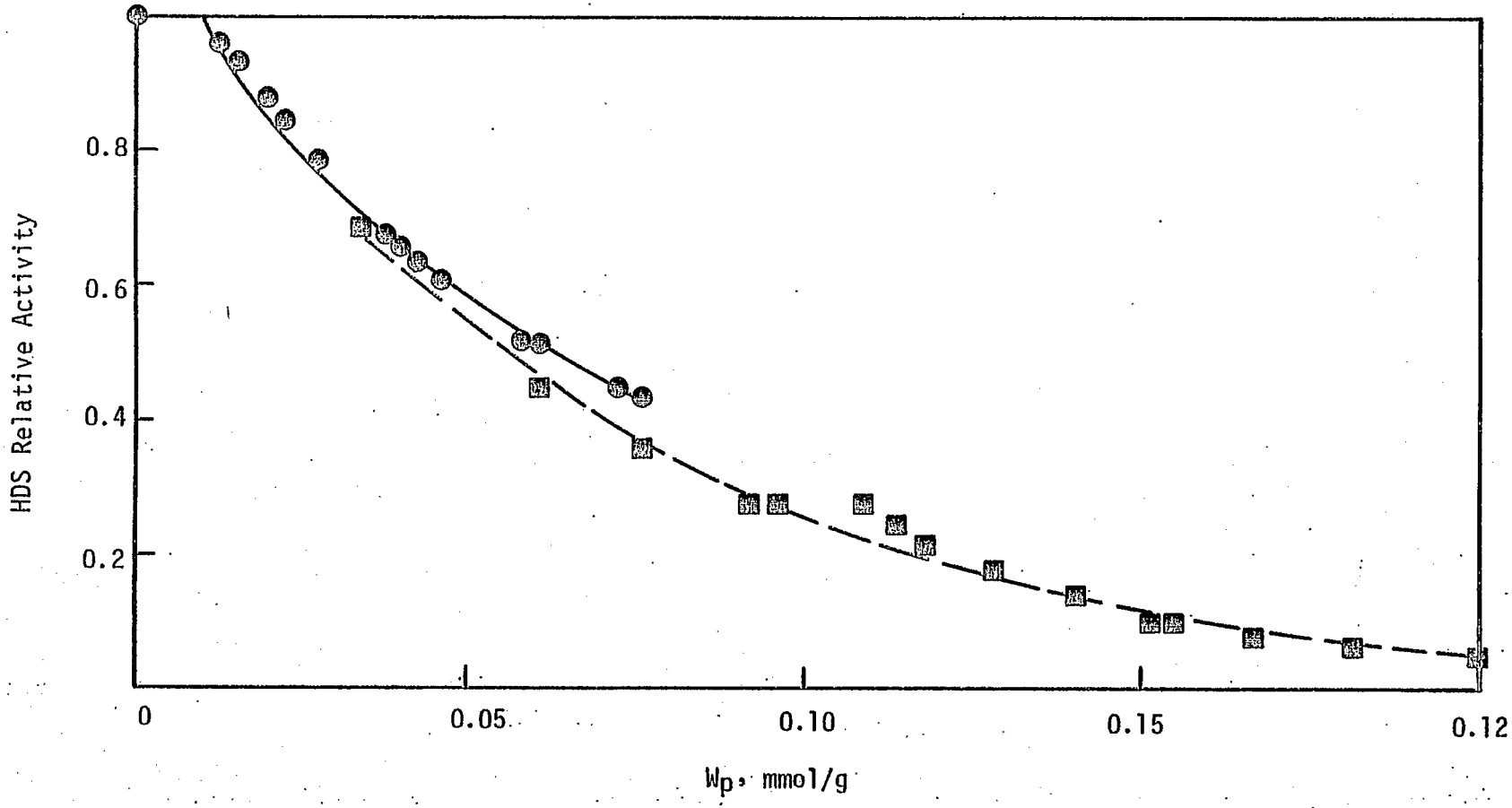

Figure 1. Relative HDS activity vs. amount of N-poison on laboratory-prepared $CoMo/Al_2O_3$ catalyst. ● 2,6-lutidine, ■ 3,5-lutidine.

Task 12

Diffusion of Polyaromatic Compounds in Amorphous Catalysts Supports

Faculty Advisor: F.E. Massoth
Post-Doctoral Fellow: G. Seo

Introduction

This project involves accessing diffusional resistance within amorphous-type catalysts. Of primary concern is the question of whether the larger multiring hydroaromatics found in coal-derived liquids will have adequate accessibility to the active sites within the pores of typical processing catalysts. When molecular dimensions approach pore size diameters, the effectiveness of a particular catalyst is reduced owing to significant mass transfer resistance. An extreme case occurs when molecular and pore size are equivalent and pores below this size are physically inaccessible.

The project objective can be achieved through a systematic study of the effect of molecular size on sorptive diffusion rates relative to pore geometry. Conceptually, the diffusion of model aromatic compounds is carried out using a stirred batch reactor. The preferential uptake of the aromatic from the aliphatic solvent is measured using a UV spectrometer. Adsorption isotherms are determined to supplement the diffusion studies.

Four aromatic solutes ranging from 7 to 19 Å and four aluminas (representative of catalyst supports) having average pore sizes of 50 to 150 Å have been studied. The solutes were dissolved in cyclohexane solvent for ambient temperature studies. n-Dodecane was employed as solvent for high temperature studies because of its lower vapor pressure. Uptake experiments demonstrate that the slow step in the adsorption process was intraparticle diffusion. Equilibrium adsorption isotherms of the various solutes for the different aluminas in cyclohexane solvent were all nonlinear and well represented by Freundlich equations. Effective diffusivities were determined from the uptake data by applying a pore diffusion model incorporating a Freundlich isotherm. At higher temperature, reproducible adsorption isotherms were not obtained due to impurities in the dodecane. Effective diffusivities were calculated from the uptake data assuming a linear isotherm.

The effective diffusivities were found to be less than those for free pore diffusion, the ratio giving a measure of the restrictive effect due to pores. This restrictive factor was shown to decrease with increasing ratio of solute molecular diameter to alumina pore diameter. At ambient conditions, empirical correlations between the restrictive factor and the ratio of molecular to pore diameter were obtained, which agreed well with literature results for other systems.

No significant effect of pressure on effective diffusivities of solute was observed up to 70 atm of hydrogen or helium. But the effect of temperature on effective diffusivities was significant. The increase in effective diffusivity was appreciably greater than predicted by the increase in bulk diffusivity for this temperature range. This difference indicates that pore diffusion is an activated process. Even at elevated temperature, the effective diffusivities to the free-solution diffusivities of the same cross-sectional area ($D_e/D_b\varepsilon$) were all less than unity, indicating that the mobility of the solutes in alumina is less than their mobility in free solution of same cross-sectional area.

Project Status

Additional data were obtained during this period to confirm previous findings[1] relative to the effect of temperature on the restrictive diffusion factor and to obtain a quantitative correlation. The restrictive factor, $F(\lambda)$ is defined by the equation,

$$F(\lambda) = \tau_0\left(\frac{D_e}{D_b\varepsilon}\right) \qquad (1)$$

where λ is the ratio of molecular diameter of the diffusing solute to the pore diameter of the alumina, τ_0 is the tortuosity at $\lambda=0$, D_e is the measured effective diffusivity, D_b is the bulk diffusivity and ε is the porosity of the alumina. Casting equation (1) in logarithimic form gives,

$$\ln\left(\frac{D_e}{D_b\varepsilon}\right) = \ln F(\lambda) - \ln \tau_0 \qquad (2)$$

A plot of $\ln (D_e/D_b\varepsilon)$ versus λ then allows determination of the relationship between $F(\lambda)$ and λ. Figure 1 presents such a plot for all the data obtained for the three solutes (coronene, octa-ethylporphine, tetra-phenylporphine) and the three aluminas (C, M, L) in dodecane solvent at three temperatures.

Since the aluminas used were the same as in previous studies,[2] a value of τ_0 of 1.3 was assumed. The logarithms of the group parameter $D_e/D_b\varepsilon$ decrease approximately linearly with increasing λ at each temperature. The slopes, α, determined from least-squares analyses are 5.7 at 25°C, 4.6 at 40°C and 3.6 at 60°C. Thus, the slopes decrease with increasing temperature, confirming that the restrictive effect becomes less prominent as temperature increases. Hence, pore restriction is not only a function of λ, but also of temperature. The relationship between the restrictive factor and λ can be expressed as

$$F(\lambda) = e^{-\alpha\lambda} \qquad (3)$$

The restrictive coefficient, α, is introduced for expressing the degree of restriction in pore diffusion. When the restrictive coefficient is zero, the restrictive factor equals unity for all values of λ, and Equation (1) can be written as $D_e = D_b\varepsilon/\tau_0$, indicating that there is no restriction in pore diffusion, except for the tortuosity effect. When the values of α are higher, restrictive diffusion becomes important.

The relative standard deviation of duplicate runs was 22%. The relative standard error of deviation of the slopes of Figure 1 are 20%, 20%, and 27% at 25°C, 40°C and 60°C, respectively. Since the error in the slopes are close to the experimental error of repeat runs, the correlation of Equations (2) and (3) are reasonable.

Steric hindrance at the entrance to the pores and frictional resistance (hydrodynamic drag) within the pores were thought as possible causes of restriction in the diffusion into porous cellulose membranes.[3] The first factor expresses the condition that for entrance into a pore, a molecule must pass through the opening without striking the edge. The second factor denotes the friction between a molecule moving within a pore and its walls. For diffusion in alumina, the above-mentioned causes were discussed as possible mechanisms of restriction.[2]

From the effective diffusivities at elevated temperature, the pore diffusion was supposed as an activated process. The steric hindrance factor should not be affected by temperature since it is related to the ratio of molecular diameter to pore opening. So, the energy barrier in pore diffusion depends on the hydrodynamic drag. As the diffusing molecule has a larger kinetic energy at elevated temperature, it becomes easier to pass the energy barrier.

A plot of logarithm of the restriction coefficient versus inverse temperature is linear, as shown in Figure 2. The equation relating the restrictive coefficient with temperature is,

$$\ln\left(\frac{\alpha}{5.7}\right) = 1300\left(\frac{1}{T} - \frac{1}{298}\right) \qquad (4)$$

Using this relationship and Equation (3), it is possible to estimate the temperature above which restriction in diffusion can be neglected ($F(\lambda)>0.9$). For example, if λ is 0.2, the restrictive factor is 0.9 at 383°C, and if λ is 0.5, the temperature would be 944°C for the same restrictive factor. This shows a steep increase in temperature for the same restrictive factor with the ratio of diameter of diffusing molecule to pore opening. Conversely, the restrictive factor can be estimated at a given temperature for different λ values. For example, at a temperature of 350°C, a typical reaction temperature for hydrodesulfurization,[4] a restrictive factor of 0.89 is predicted for $\lambda = 0.2$ and a value of 0.75 for $\lambda = 0.5$. Hence, restrictive diffusion may be important under hydroprocessing conditions when the molecular size of the reactants are sufficiently large compared to the catalyst pore size. The restrictive factor would contribute to an additional lowering of the effectiveness factor of the catalyst calculated by conventional methods.[5] However, it should be cautioned that the restrictive factors were obtained over a limited temperature range and extrapolation to higher temperatures is uncertain.

Future Work

Work on this project has been completed and a paper on the significant results obtained is being prepared.

References

1. W.H. Wiser et al., DOE Contract No. DE-AC01-79ET 14700, Quarterly Progress Report, Salt Lake City, Utah, Oct-Dec 1982.

2. A. Chantong, Ph.D. Dissertation, University of Utah, Salt Lake City, Utah, 1982.

3. E.M. Renkin, J. Gen. Physiol., 38, 225(1944).

4. B.C. Gates, J.R. Katzer and G.C.A. Schuit, "Chemistry of Catalytic Processes," McGraw-Hill, 1979, p. 34.

5. C.N. Satterfield and T.K. Sherwood, "The Role of Diffusion in Catalysis," Addison-Wesley, Massachusetts, 1963.

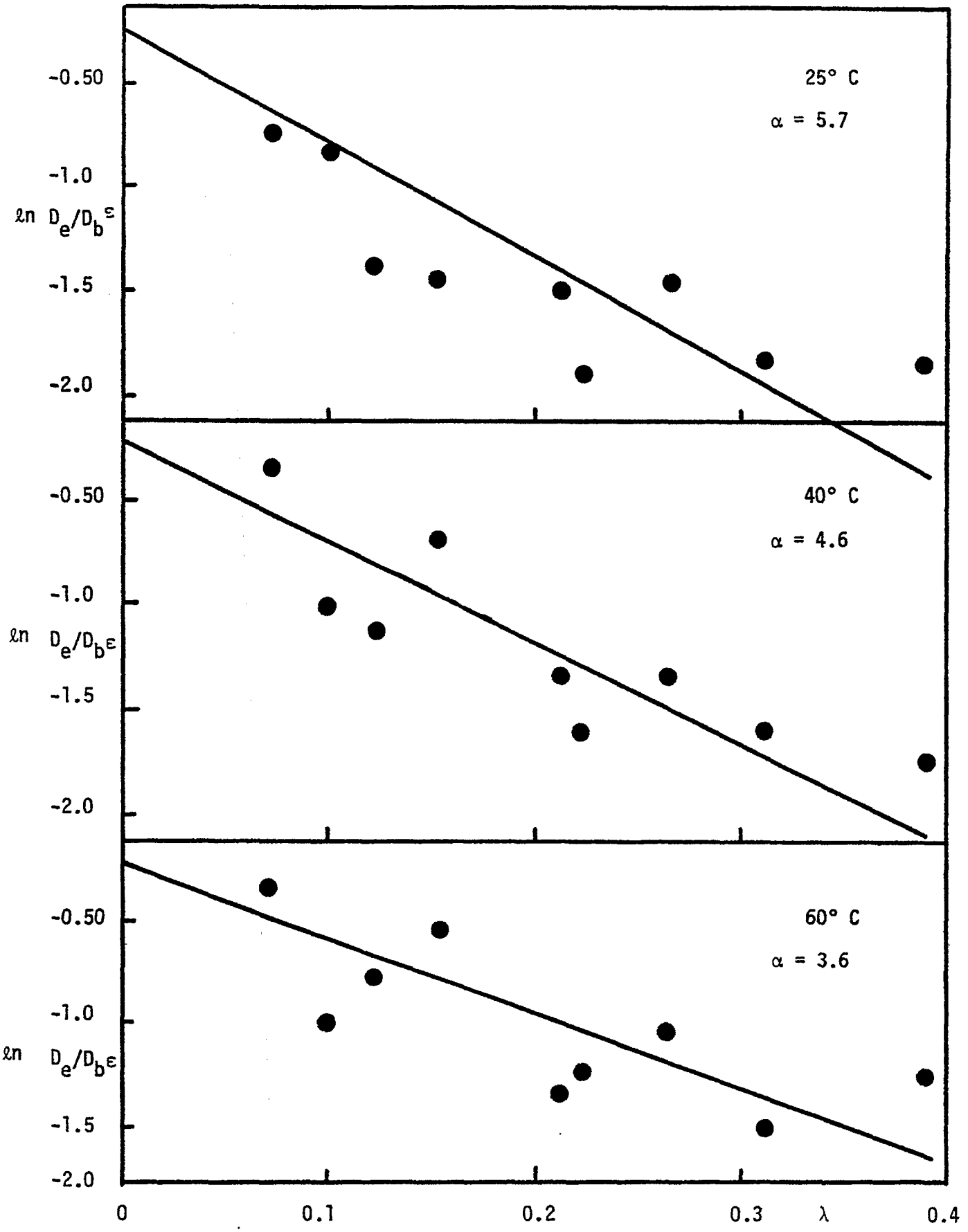

Figure 1. Plot of $\ell n\ D_e/D_b\varepsilon$ versus λ at different temperatures.

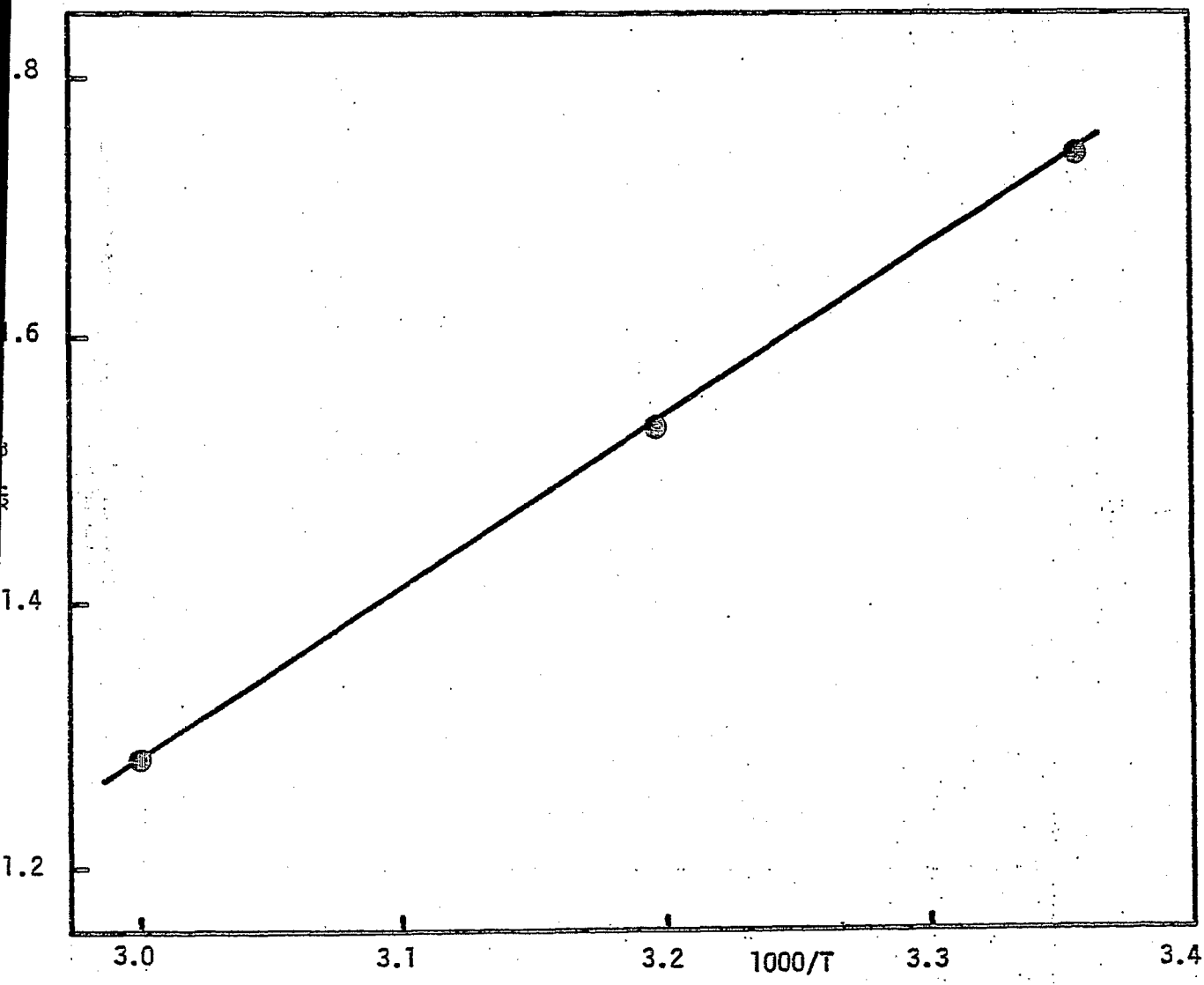

Figure 2. - Plot of logarithm of restrictive coefficient, α, versus inverse of temperature.

Task 13

Catalyst Research and Development

Synthesis of Light Hydrocarbons from CO and H_2

Faculty Advisor: F.V. Hanson
Graduate Student: Y.S. Tsai

Introduction

The production of low molecular weight olefins (C_2-C_4) from the hydrogenation of carbon monoxide has been investigated over unsupported iron-manganese catalysts. The results from the preliminary tests which were performed in a bench-scale fixed-bed reactor system showed that the unsupported Fe-Mn catalysts were very selective in the production of C_2-C_4 olefins. Data from the screening tests of the sixteen iron-manganese catalysts indicated that a catalyst composed of 2 parts of Mn per 100 parts of Fe was the most selective. The effects of the process variables were also studied. The results mostly were in agreement with those found in the literature.

The in-situ reduction of the catalyst by flowing hydrogen at ambient pressure and 400°C for 20 hours has been employed to activate the Fe-Mn catalyst. The CO pretreatment is another catalyst activation method commonly used in CO hydrogenation research. The influence of the CO reduction on the product yield and selectivity may be different from that of the H_2 activation, and it is an interesting subject to be explored. In the previous study a volumetric catalyst dilution ratio of 4/1 (Denstone 57/catalyst) was effective in maintaining a uniform temperature profile in the catalyst bed. Therefore, an investigation on the effects of the catalyst pretreatment has been initiated to determine the best catalyst activation method that would result in a high production of C_2-C_4 olefins with a dilution ratio of 4/1.

Project Status

The YST-2 coprecipitated Fe-Mn catalyst (3.0 Mn/100 Fe) was pretreated with carbon monoxide at ambient pressure and 400°C for 20 hours. The operating conditions for the tests on the catalyst performance were H_2/CO= 2/1, 200 psig and 1.0 cc $g^{-1}sec^{-1}$ space velocity. Each experiment ran for 11 hours to allow the catalyst to reach a steady state of activity and selectivity.

Data on the product yield and selectivity for the YST-2 Fe-Mn catalyst reduced by hydrogen as a function of temperature and time are presented in Table 1. Initially, the catalyst activity was higher, e.g., 9.7% CO conversion at 227°C and 2 hours on stream. However, it leveled off after 6 hours on stream, e.g. 6.4% CO conversion at 225°C. The selectivities also indicated that the catalyst was stabilized after 6 hours. As the reaction time increased, the production of CO_2, C_2-C_4 and C_5^+ increased, while the selectivities of CH_4 and ROH decreased. However, both the activity and selectivity reached a steady state after 10 hours.

Table 2 lists the data on the product yield and the distribution for the YST-2 catalyst activated by the CO pretreatment. The CO conversion was initially much higher, e.g., 30% at 226°C and 1.5 hours on stream, than that of the catalyst reduced by hydrogen, e.g., 9.7% conversion at 227°C and 2 hours on stream. After 10 hours activation time, the CO conversion was still 8.7% at 210°C, however, the activity and selectivity indicated a constant level of production. The CO pretreated catalyst had relatively higher activity than the hydrogen reduced catalyst. The O/P ratio of the C_2-C_4 hydrocarbons for the hydrogen reduced catalyst reached a value of 2.82 at about 10 hours. The O/P ratio for the CO reduced catalyst only increased to 1.39. The hydrogen reduced catalyst seemed more selective in the production of C_2-C_4 olefins than the CO pretreated catalyst. Though the long-term effects have not been explored, the speculation is that the hydrogen reduced catalyst may show a more stable total yield and a higher selectivity of C_2-C_4 olefins than the CO reduced catalyst.

The catalyst bed temperature profiles for four distinct conversion levels are presented in Figures 1 and 2. Generally, all the profiles did not indicate any sharp rise in temperature in the catalyst zone even at a CO conversion of 30%. A small increase of about 3-5°C was expected and it obviously did not cause any shift in catalyst activity and selectivity.

The hydrogen reduction for the Fe-Mn catalyst will be applied to future CO hydrogenation experiments, since it resulted in a higher selectivity of C_2-C_4 olefins and a more stable catalyst that reduced the heat and mass transfer problem in the fixed-bed reactor. The catalyst dilution also was effective in maintaining a uniform temperature distribution in the reactor.

Future Work

The catalyst characterization studies will be initiated. A literature survey concerning the CO hydrogenation as well as the heat and mass transfer for the fixed-bed reactor will be continued.

Table 1. Product yield and selectivity versus time for YST-2 catalyst; H_2 reduction; H_2/CO= 2/1; 200 psig; 1.0 $ccg^{-1}sec^{-1}$.

Time on stream(hr.)		0.6	2.0	3.5	4.6	6	9.5	10.6
Temp.(°C)		220	227	225	225	225	225	226
CO Conv.(%)		6.4	9.7	7.7	7.0	6.4	6.4	6.7
Selectivity(%)	CO_2	8.0	9.3	9.7	10.2	10.8	11.4	11.6
	C_1	33.3	24.7	21.1	19.1	18.4	18.0	18.2
	C_2-C_4	41.7	44.9	46.3	46.5	47.1	47.3	47.4
	C_5^+	10.8	16.9	18.9	18.9	18.6	18.3	19.1
	ROH	6.2	4.2	4.0	5.3	5.1	4.5	3.7
O/P in C_2-C_4		0.82	1.51	2.12	2.52	2.73	2.86	2.82

Table 2. Product yield and selectivity versus time for YST-2 catalyst; CO reduction; $H_2/CO=2/1$; 200 psig; 1.0 cc g^{-1} sec^{-1}.

Time on stream(hr.)	0.3	1.5	3.0	4.5	5.6	6.7	10.3
Temp.(°C)	225	226	215	215	215	215	210
CO Conv.(%)	30.2	30.0	14.8	12.4	11.2	11.7	8.7
Selectivity(%) CO_2	8.8	10.8	7.1	7.7	7.9	7.8	6.8
Selectivity(%) C_1	31.1	26.6	25.5	24.7	23.9	24.3	24.1
Selectivity(%) C_2-C_4	41.9	42.7	43.7	44.3	44.5	44.6	45.1
Selectivity(%) C_5^+	16.9	18.5	19.9	20.4	21.3	20.9	21.5
Selectivity(%) ROH	1.3	1.4	3.8	2.9	2.4	2.3	2.5
O/P in C_2-C_4	0.40	0.72	0.98	1.15	1.27	1.27	1.39

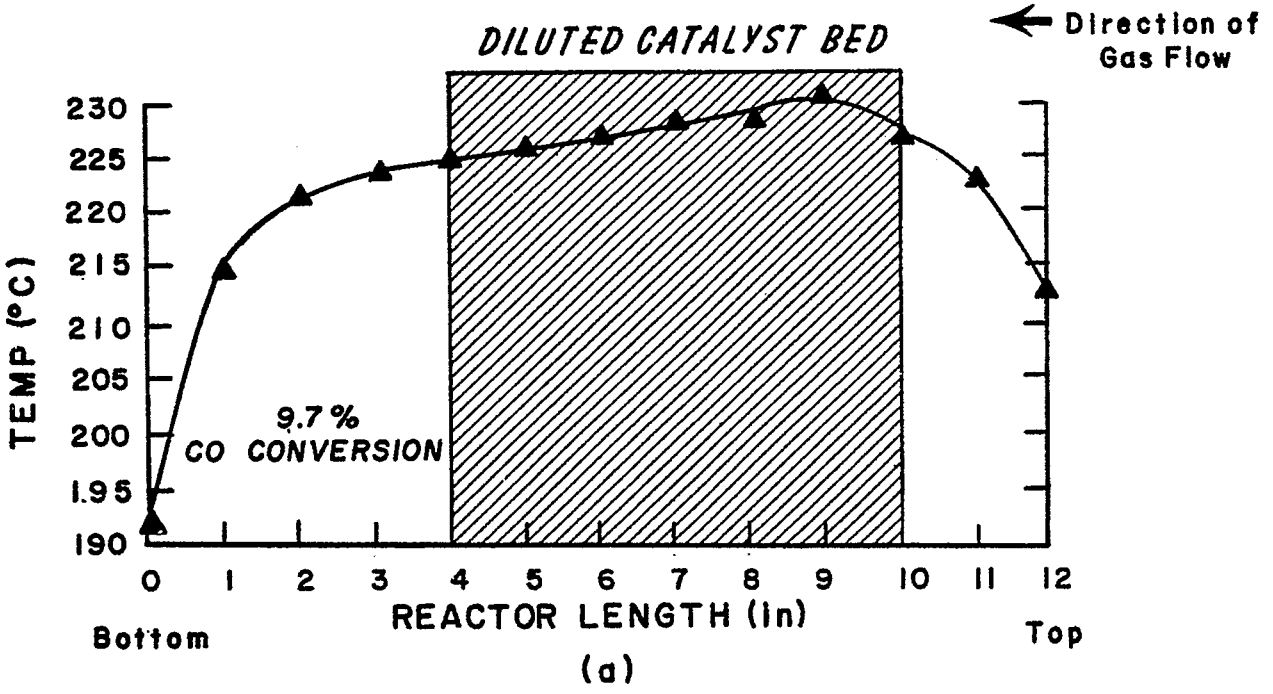

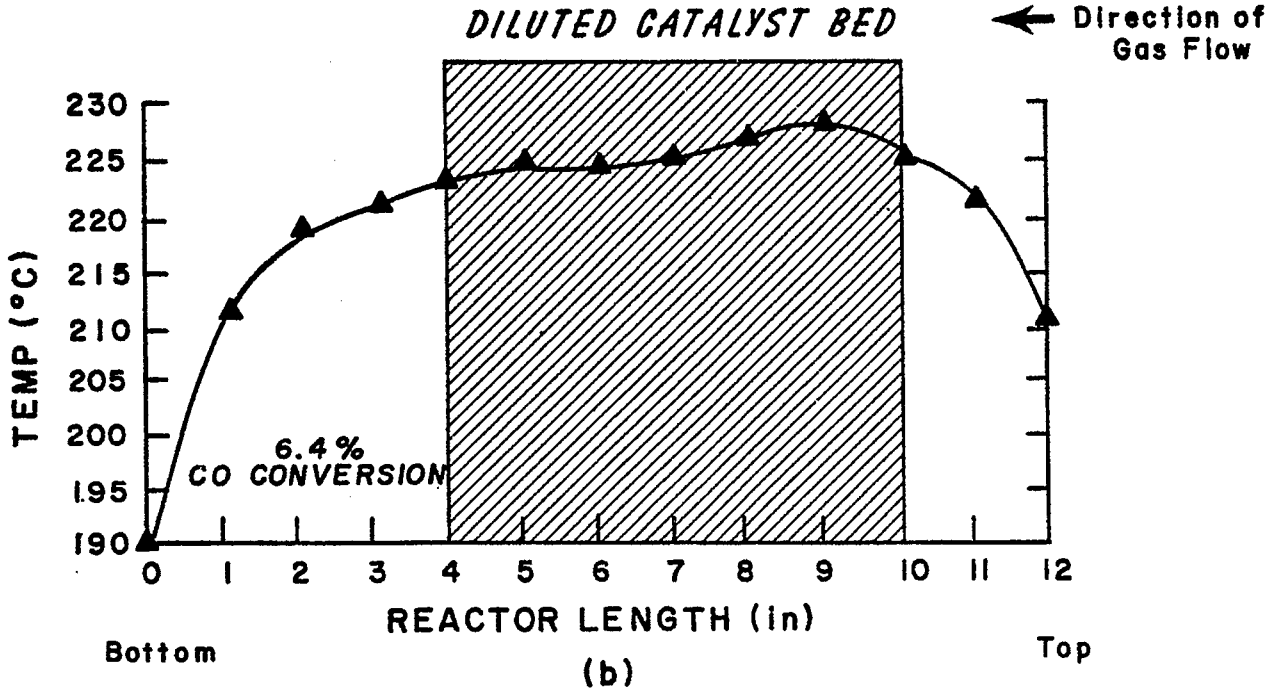

Figure 1. Temperature distribution in the fixed-bed reactor for YST-2 catalyst; (a) 9.7% CO conversion; (b) 6.4% CO conversion (Dilution ratio 4/1, 4.8 g used, H_2 reduction).

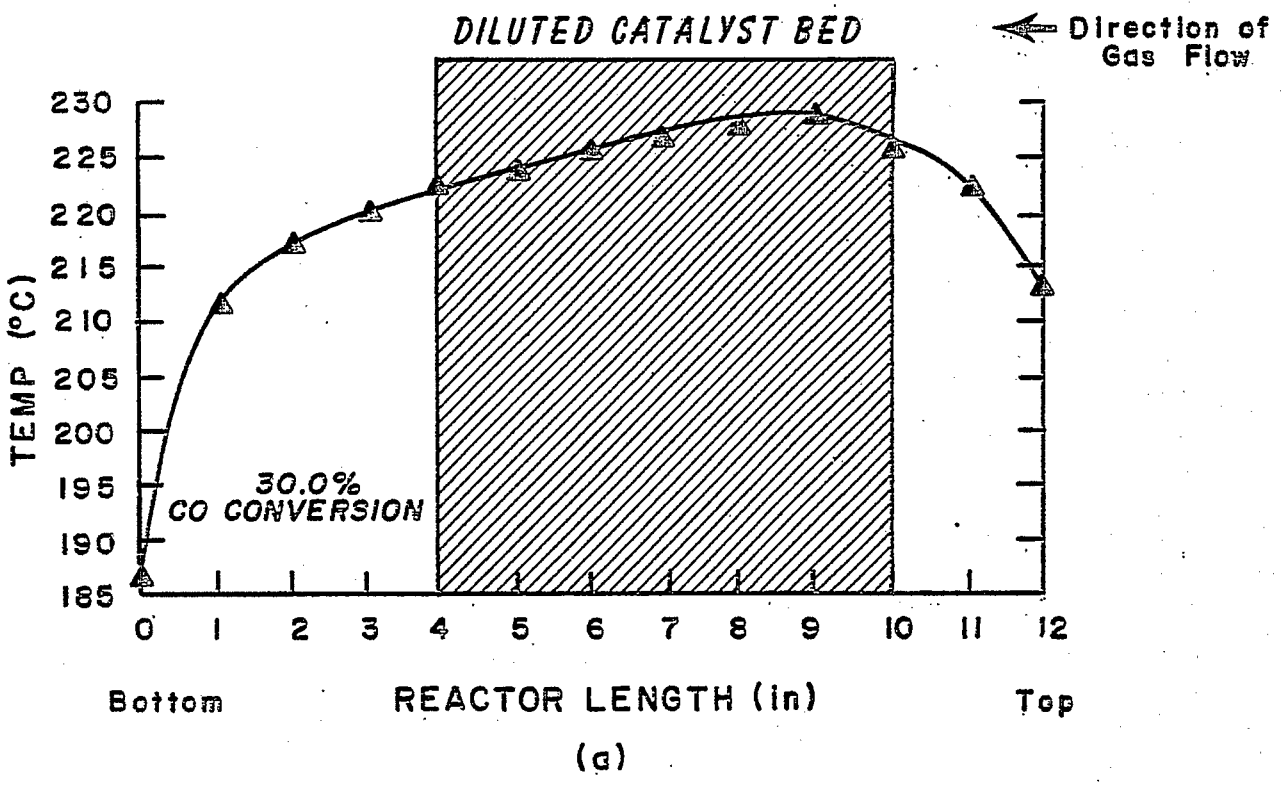

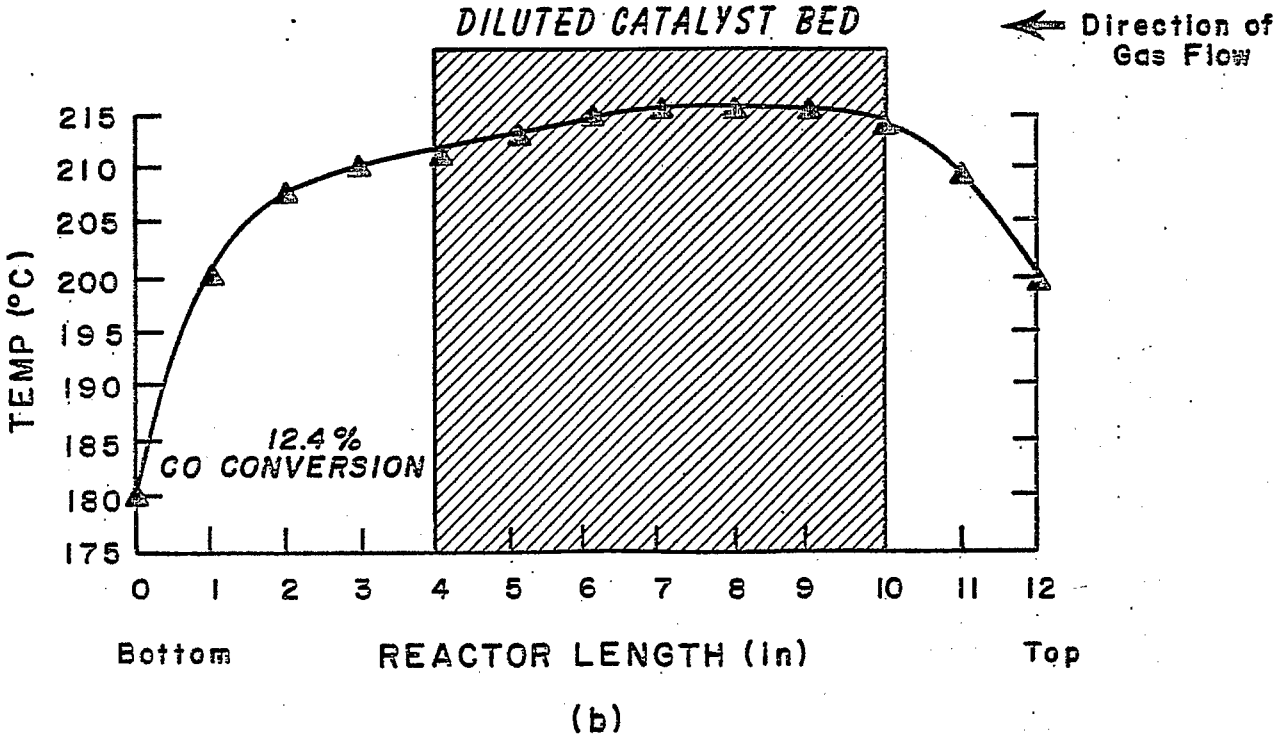

Figure 2. Temperature distribution in the fixed-bed reactor for YST-2 catalyst: (2) 30.0% CO conversion; (b) 12.4% CO conversion (Dilution ratio 4/1, 4.8 g used, CO reduction).

Task 13

Catalyst Research and Development

Hydrogenation of Carbon Monoxide Over Raney Fe-Mn Catalyst

Faculty Advisor: F. V. Hanson
Graduate Student: K. R. Chen

Introduction

The objectives of this project are to determine the kinetics of the caustic leaching of aluminum from iron-aluminum alloys and to determine the optimum process operating conditions for the production of low molecular weight olefins from hydrogen and carbon monoxide over Raney iron-manganese catalysts.

A single phase Al-Fe (53/47, wt%) alloy was prepared for the leaching kinetic study. The leaching conditions were: leaching temperature 303-353 K, alloy granule particle size 30-325 mesh, 5% NaOH solution and alloy sample size 5 grams. The volumetric flow rate of the hydrogen evolved was determined with a wet test meter.

A Raney iron-manganese catalyst, prepared from an Al-Fe-Mn (59/38/3) alloy, was used to evaluate the activity and selectivity of the catalyst. Catalyst loading and stability tests were conducted prior to the process variable study.

Project Status

A schematic of the apparatus in which the aluminum leaching study was conducted is presented in Figure 1. The data obtained in the leaching experiments is presented in Table 1. The aluminum in the iron-aluminum and iron-manganese-aluminum alloys is leached according to the following reaction

$$2Al + 6NaOH \rightarrow 2Na_3AlO_3 + 3H_2$$

The aluminum leaching curves are presented in Figures 2 through 4. As the leaching temperature increased the rate of aluminum leaching increased; however, above 343 K the terminal extent of aluminum leaching was approximately constant. At a fixed temperature the extent of aluminum leaching was greater for smaller alloy particles and the rate of leaching was greater. Analysis of the aluminum leaching data indicated that a chemical reaction control model fit the data better than a diffusion control model. The catalyst loading tests were conducted to determine the appropriate inert particle/catalyst ratio required to minimize heat transfer limitations in the catalyst bed. The catalyst stability tests were conducted to determine the stability with regard to the activity (i.e., carbon monoxide conversion) and the selectivity (i.e., olefin/paraffin ratio) of the Raney catalysts. The loading and selectivity studies were conducted at a standard set of operating variables, that is, a reactor

pressure of 200 psig, a reactor temperature of 443 K, a reactant space velocity of 4.2 and a hydrogen to carbon monoxide ratio of 2. The experimental data from the stability tests are presented in Tables 3 through 5. The comparisons of the selectivity for the dense and diluted bed reactor modes are presented in Figures 5 through 7. The catalyst stability tests indicated that the diluted bed gave a more uniform temperature profile and the product distribution exhibited less variation relative to the dense bed. At three different inert/catalyst ratios; 0/1, 2/1, 4/1; the activity and selectivity of the catalyst were stable up to 40 hours on stream. The preferred inert/catalyst ratio was 4/1. The conversion of carbon monoxide versus time on stream for different inert/catalyst ratios is presented in Figure 8. The induction period required to stabilize the catalyst with regard to carbon monoxide conversion was 15 hours. In previous experiments[1] at a reactor temperature of 353 K, the induction period was 6 hours. The effect of reactor temperature on selectivity at different inert/catalyst ratios is presented in Figures 9 through 12. As the reactant space velocity increased from 4.2 to 10 hr^{-1} the selectivity for CO_2 decreased, that is, at 453 K, the yield of CO_2 was 20 weight % and a space velocity of 4.2 hr^{-1} whereas at 453 K and a space velocity of 10 hr^{-1} the yield of CO_2 was 14 weight %. The maximum permitted temperature at which the heat released in the reaction can be effectively controlled for the dense bed catalyst loading was 453 K whereas with the diluted bed the maximum temperature was 473 K.

Anderson proposed the following equation for the hydrogenation of carbon monoxide over iron catalysts

$$-\ln (1-X) = K/S$$

where X is the fractional conversion of carbon monoxide, K is the first order rate constant (hr^{-1}) and S is the space velocity (hr^{-1}). A Raney iron-manganese catalyst was evaluated at a reactor pressure of 200 psig, a reactor temperature of 453 K, a hydrogen to carbon monoxide ratio of 2/1 and an inert to catalyst ratio of 4/1 to determine the fit to the empirical equation of Anderson. The space velocity ranged from 2 to 10 hr^{-1} in this series of experiments. The data are presented in Table 6 and Figure 13. The slope of the straight line obtained when plotting -ln (1-X) versus S^{-1} (Figure 13) was determined and the rate constant was calculated to be 0.197 hr^{-1}.

Future Work

A process variable study employing the statistical method for the design of experiments will be conducted to determine the optimum conditions for maximizing the production of low molecular weight olefin.

References

1. C.S. Kim, Ph.D. Thesis, University of Utah, Salt Lake City, Utah, 1983.
2. Y.S. Tsai, M.S. Thesis, University of Utah, Salt Lake City, Utah, 1980.
3. T. Freel, W.J. Pieters, and R.B. Anderson, J. Catal., 14, 247 (1969).
4. G.E.P. Box and K.B.T. Wilson, Royal Statistical Society (Series B), 13, No. 1, 1 (1951).

Table 1. Aluminum Leaching Data.

Run No.	1	2	3	4	5	6	7	8
Mesh	25 50	200 270	270 325	25 50	200 270	270 325	25 50	200 270
Temp K	323	323	323	343	343	343	353	353
NaOH %	5	5	5	5	5	5	5	5
Time Min	Conversion %							
1	2.6	10.0	6.2	4.5	18.3	41.1	8.8	30.8
2	4.3	18.8	13.3	11.2	31.8	64.3	20.7	51.6
3	6.3	25.5	18.6	17.9	48.9	79.4	34.8	76.1
4	8.4	33.7	25.2	25.5	56.0	86.8	46.7	88.8
5	10.3	36.9	33.1	37.0	61.5		55.3	94.0
6	12.2	42.1	39.3	43.7	62.8		67.2	94.5
7	14.3	47.1	45.5	49.6			75.1	94.8
8	16.7	49.0	50.5	55.8			80.3	
9	19.6	56.0	55.7	62.5				
10	22.2	60.0	61.0	67.8			85.6	
12	27.2	66.0	70.2	75.9			87.3	
14	33.4	66.8	76.7	81.9			87.7	
16	-			84.5				
20	47.0			85.9				
22	51.8							
24	55.1							
26	58.5							
28	61.3							
30	63.2							
32	65.4							
36	66.6							
36								

Table 2. Catalyst Loading and Stability Test

Dense Bed Loading — Reactant Space Velocity = 4.2
Inert/Catalyst Ratio = 0/1 — H_2/CO Ratio = 2
Reactor Pressure = 200 psig — Reactor Temperature = 343 K

Sample No.	Time (hr)	CO Conv (%)	O/P (-)	CO_2 (%)	C_1 (%)	C_2-C_4 (%)	C_5 (%)
1	3.00	3.6	2.4	14.9	20.2	50.7	28.5
2	5.00	5.3	2.6	21.6	18.3	52.3	29.0
3	6.00	3.7	2.6	14.4	18.7	49.2	28.5
4	7.00	3.8	2.6	16.3	19.5	52.2	28.2
5	11.00	3.5	2.6	17.7	19.5	53.3	27.2
6	15.00	3.3	2.5	17.8	19.6	52.6	27.8
7	19.00	2.4	2.3	19.7	19.7	52.7	27.7
8	20.00	2.5	2.3	20.3	19.7	52.3	25.6
9	23.00	3.5	2.5	18.7	18.7	52.4	28.6
10	25.00	3.0	2.4	19.0	18.7	49.3	28.4
11	27.00	2.7	2.2	18.5	23.5	51.7	25.7
12	33.00	2.4	2.3	20.3	21.9	52.5	26.4
13	39.00	2.5	2.3	20.0	20.6		26.8

Table 3. Catalyst Loading and Stability Test

Diluted Bed Loading — Reactant Space Velocity = 4.2
Inert/Catalyst Ratio = 2/1 — H_2/CO Ratio = 2
Reactor Pressure = 200 psig — Reactor Temperature = 343 K

Sample No.	Time (hr)	CO conv (%)	O/P (-)	CO_2 (%)	C_1 (%)	C_2-C_4 (%)	C_5 (%)
1	3.00	3.5	2.2	14.7	27.7	46.7	24.5
2	6.00	3.0	2.3	13.5	25.0	48.3	25.5
3	10.00	3.0	2.4	13.8	23.0	48.7	27.8
4	15.00	2.7	2.4	13.7	23.2	49.3	26.8
5	24.00	2.9	2.3	16.2	23.0	50.8	25.8
6	30.50	2.8	2.3	16.2	21.9	50.1	28.4
7	32.00	2.7	2.3	16.0	20.9	50.0	28.6

Table 4. Catalyst Loading and Stability Test.

Diluted Bed Loading — Reactant Space Velocity = 4.2
Inert/Catalyst Loading = 4/1 — H_2/CO Ratio = 2
Reactor Pressure = 200 psig — Reactor Temperature = 343 K

Sample No.	Time (hr)	CO Conv (%)	O/P (-)	CO_2 (%)	C_1 (%)	C_2-C_4 (%)	C_5 (%)
1	3.00	3.2	2.2	14.2	22.7	49.4	26.0
2	6.00	3.2	2.3	13.6	26.1	48.0	25.3
3	9.00	2.8	2.4	13.1	24.6	49.4	25.4
4	12.50	2.7	2.5	13.4	23.0	51.5	25.0
5	16.00	3.1	2.4	12.9	22.1	48.1	25.3
6	28.00	2.6	2.5	13.9	21.8	52.7	25.0

Figure 1. Reactor for Leaching

A: Cooling Water Inlet
B: Alloy Inlet
C: Stirrer
D: Thermocouple
E: Hydrogen Outlet
F: Cooling Water Outlet
G: Wet Test Meter
H: Liquid Collector
I: Condenser
J: Temperature Controller

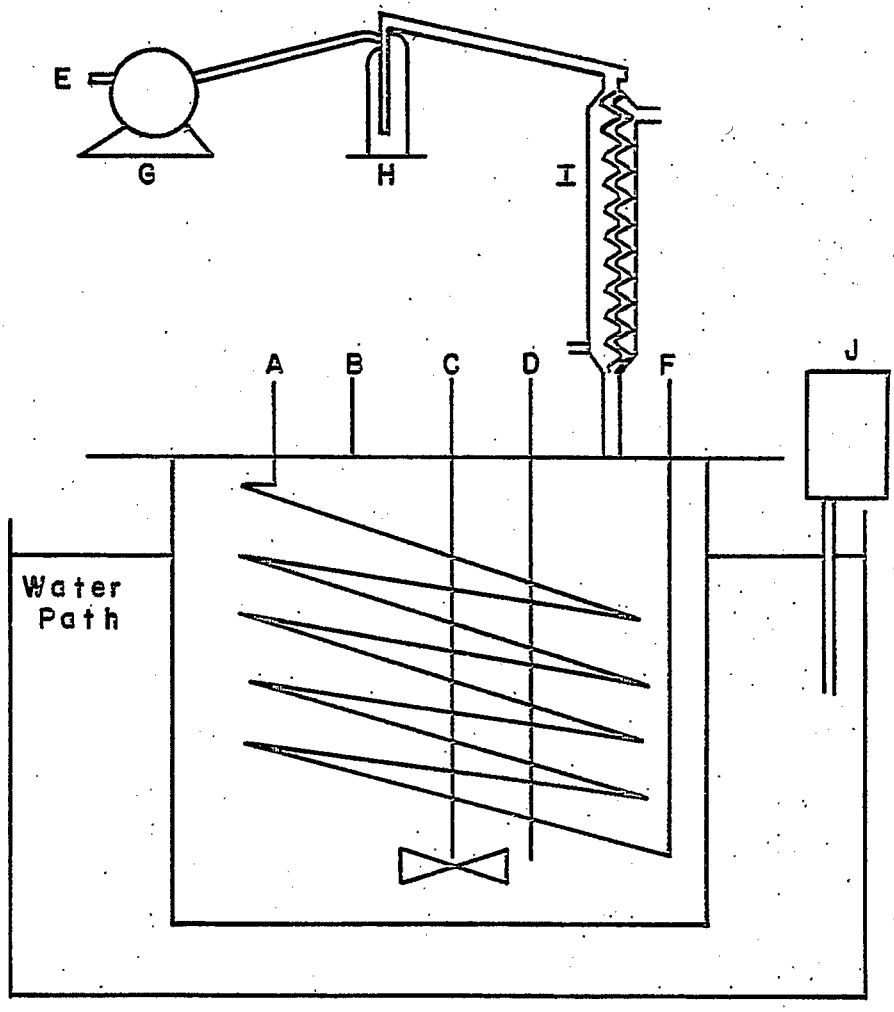

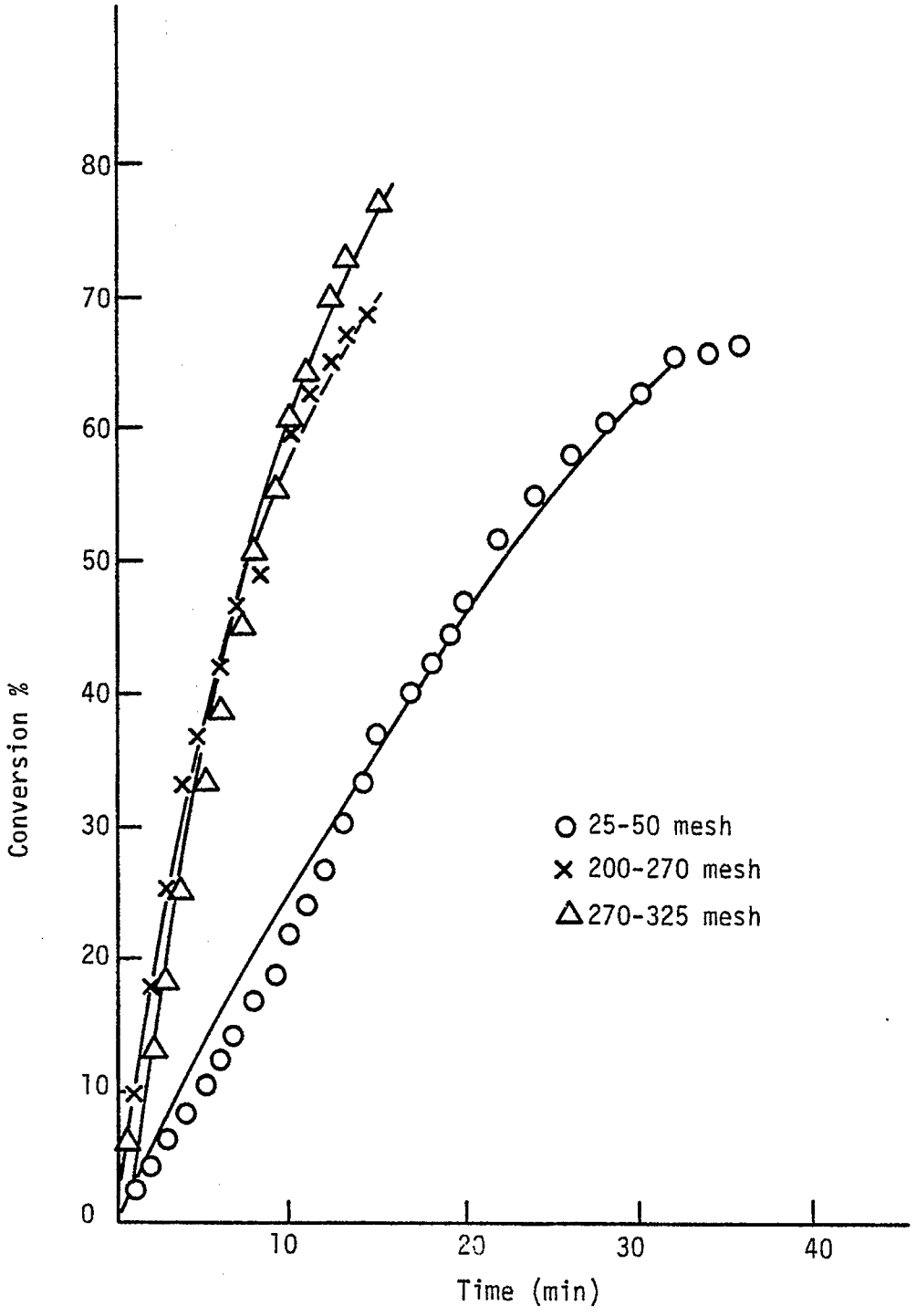

Figure 2. Aluminum Leaching Curves
T-323 K, 5% NaOH Solution

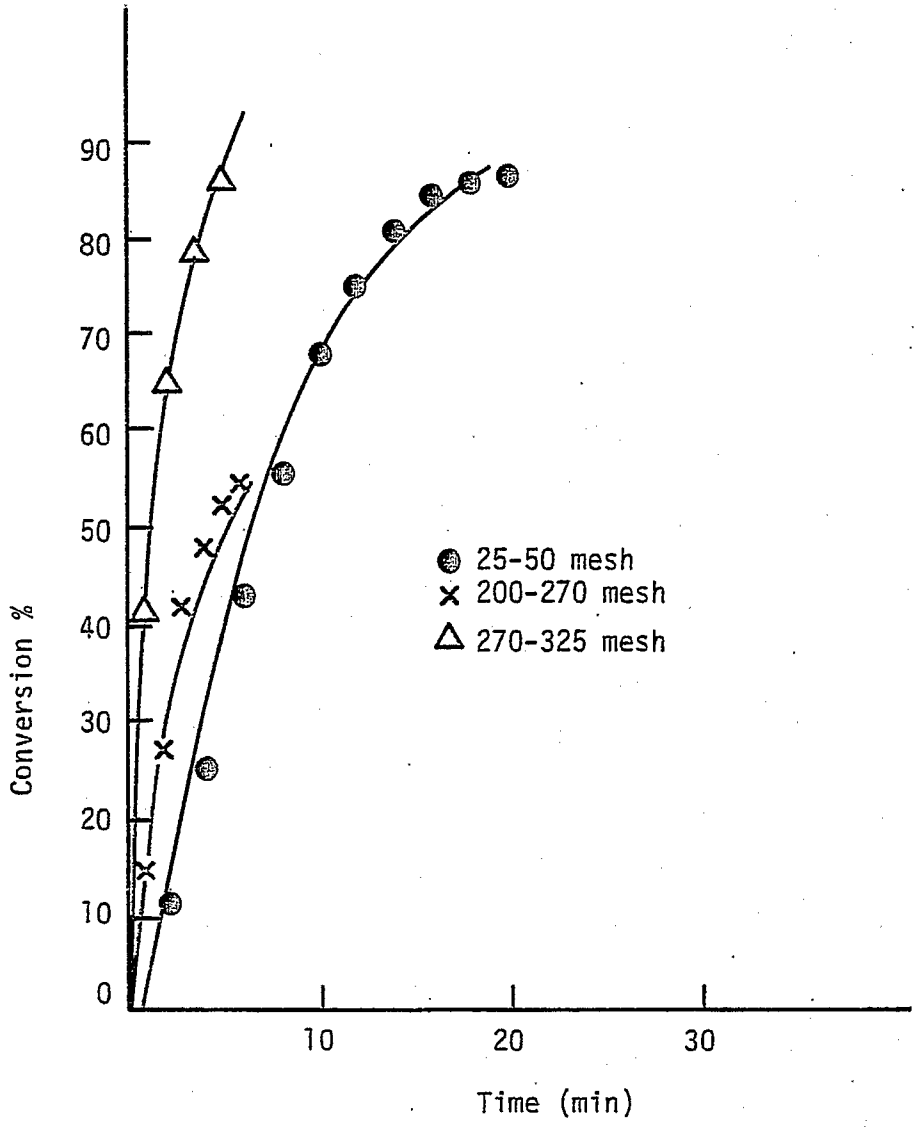

Figure 3. Aluminum Leaching Curves
T-343 K, 5% NaOH Solution

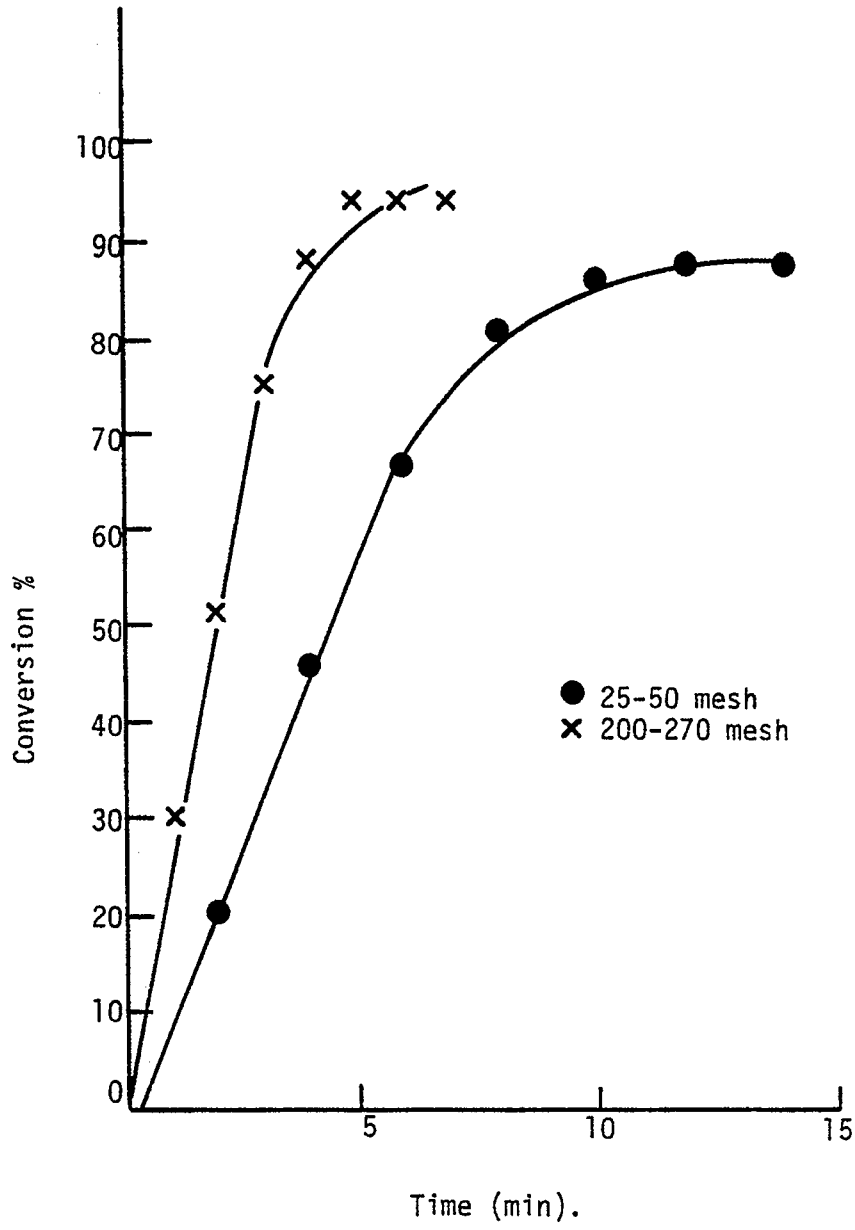

Figure 4. Aluminum Leaching Curves
T-353 K, 5% NaOH Solution

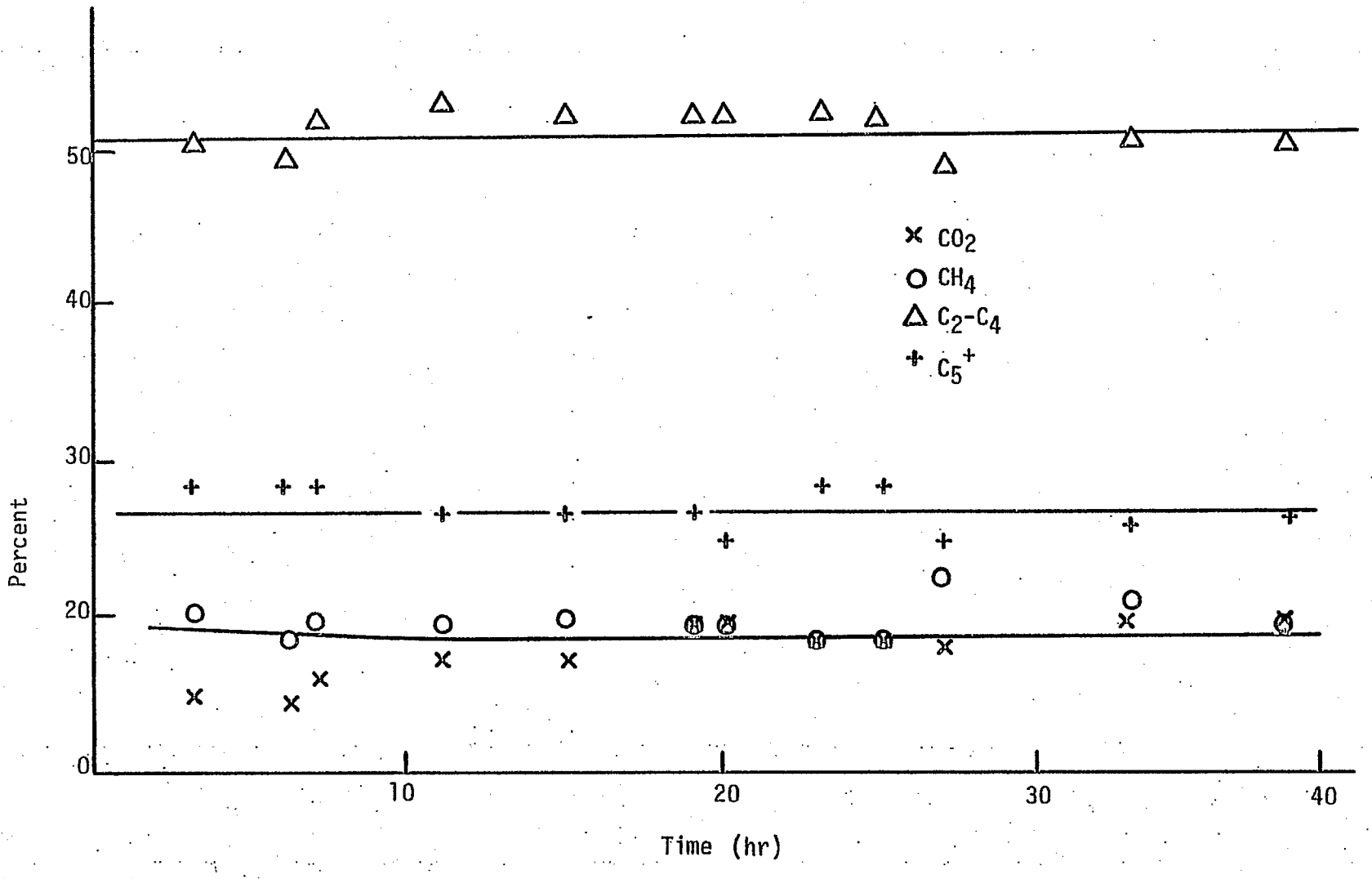

Figure 5. Catalyst Stability Test. Dense Bed.

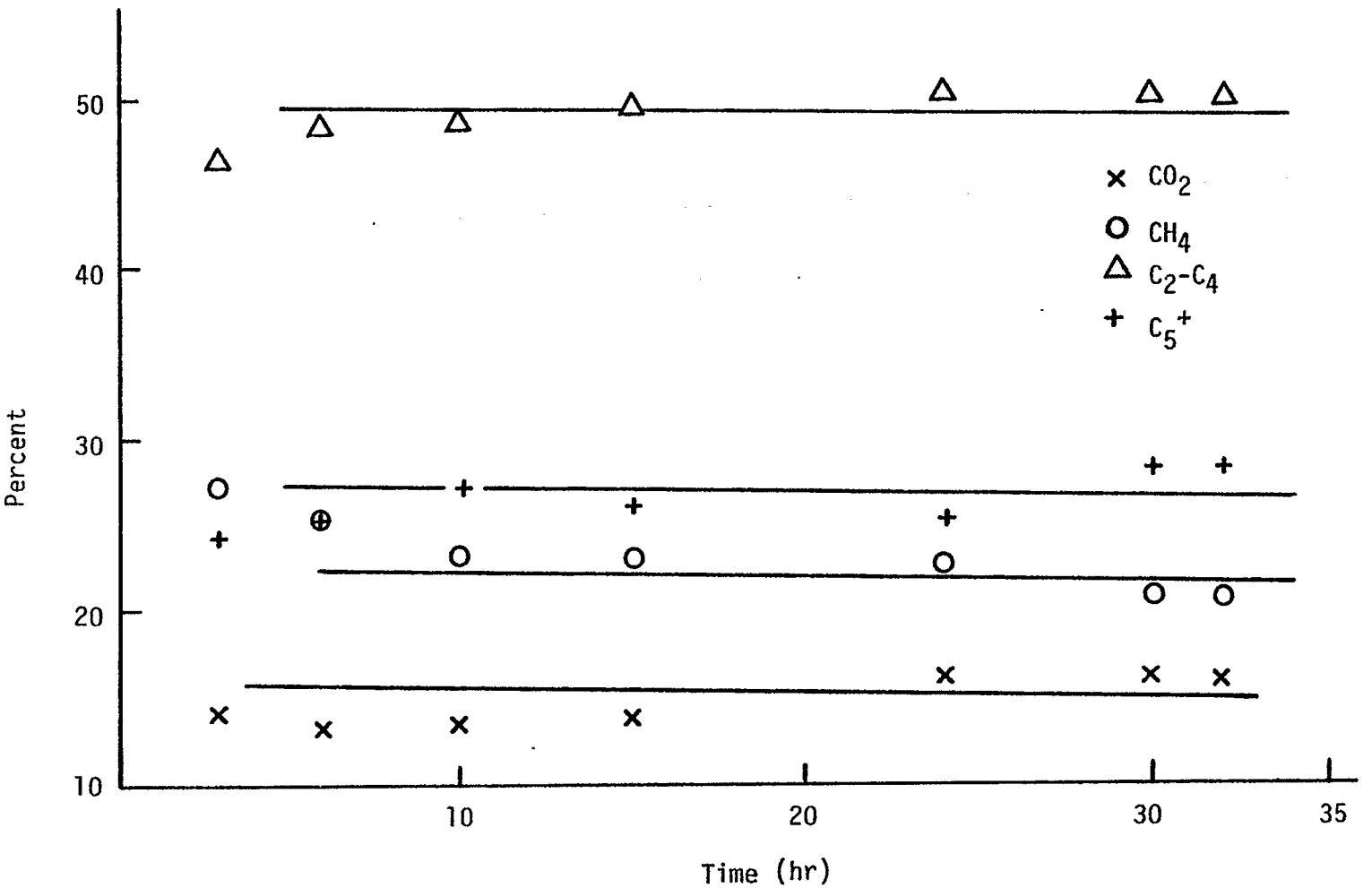

Figure 6. Catalyst Stability Test. Diluted Bed. Inert/Catalyst Ratio 2/1.

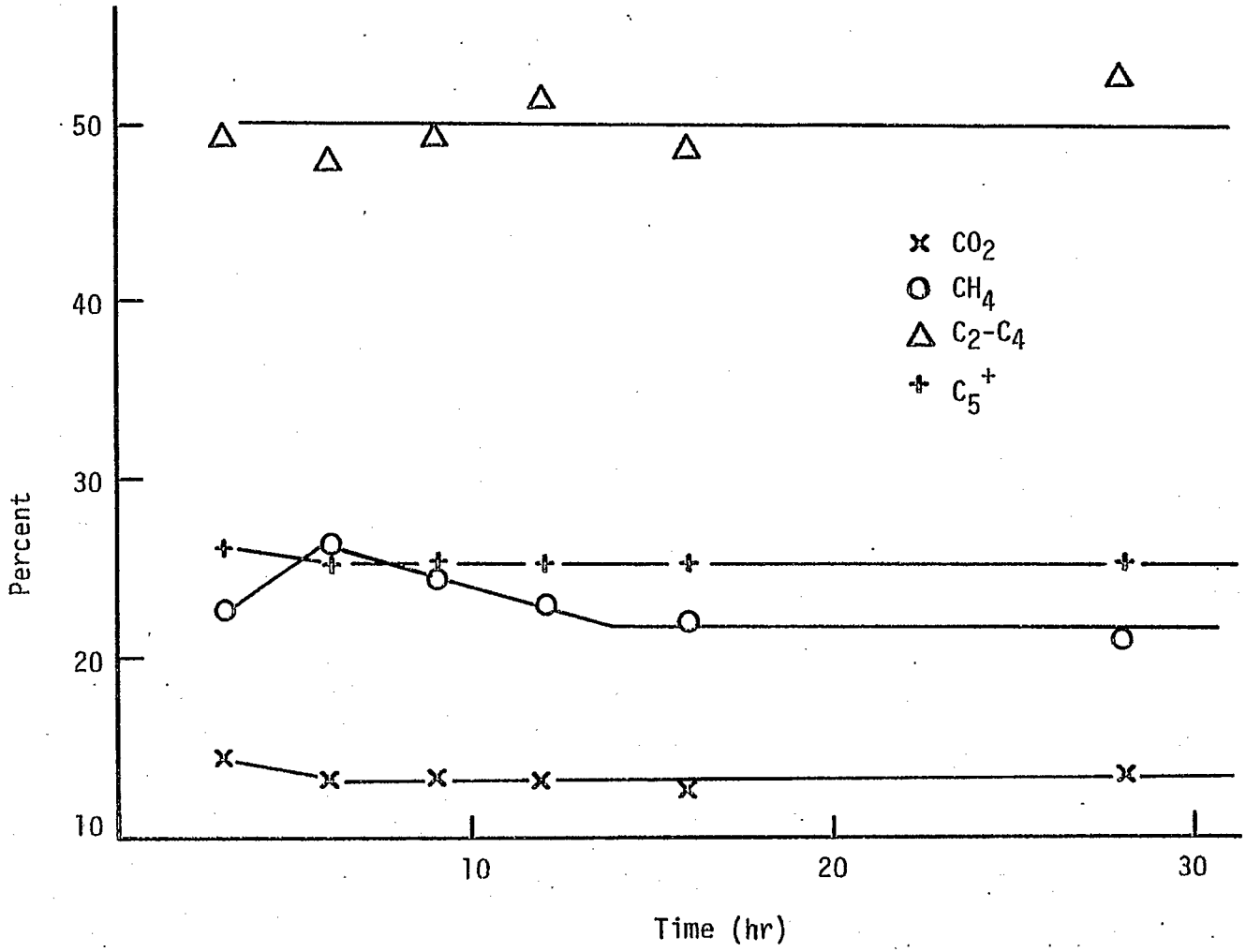

Figure 7. Catalyst Stability Test. Diluted Bed. Inert/Catalyst Ratio 4/1.

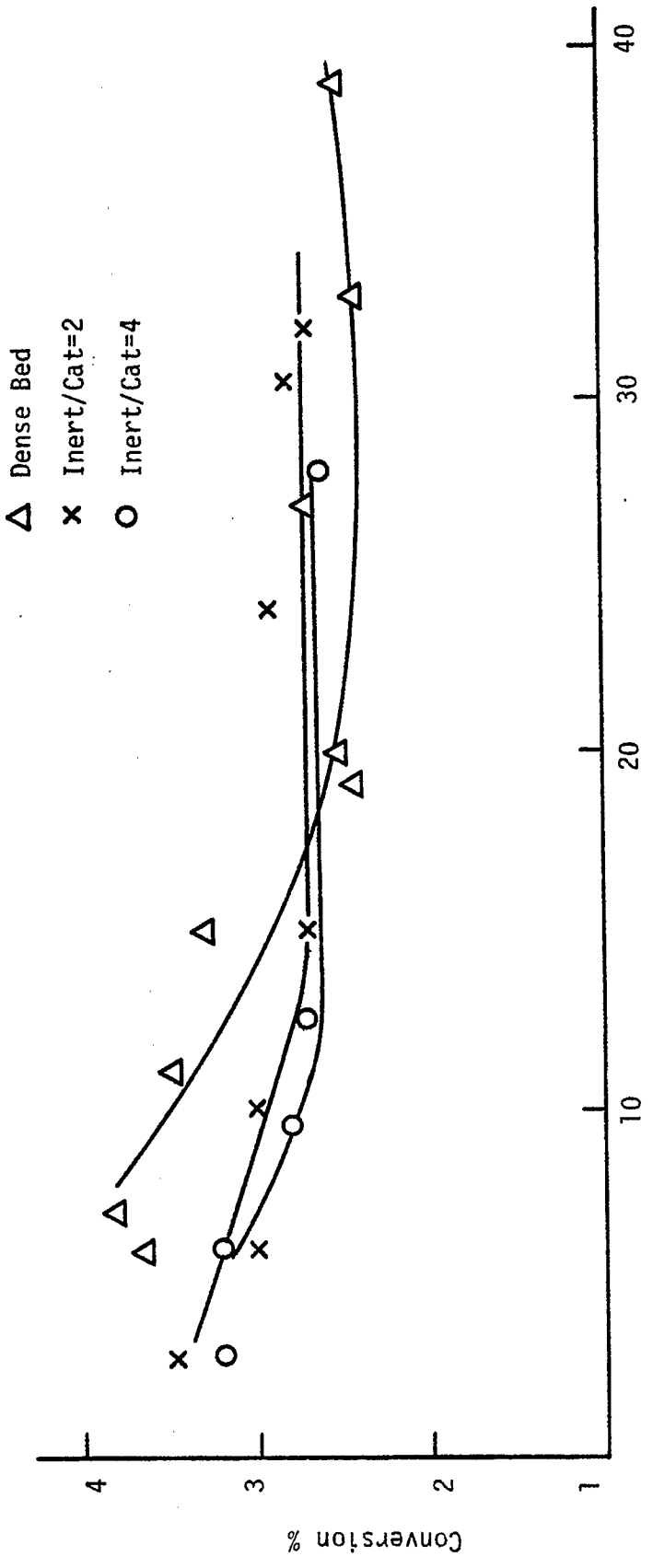

Figure 8. Carbon Monoxide Conversion. Dense versus Diluted Bed.

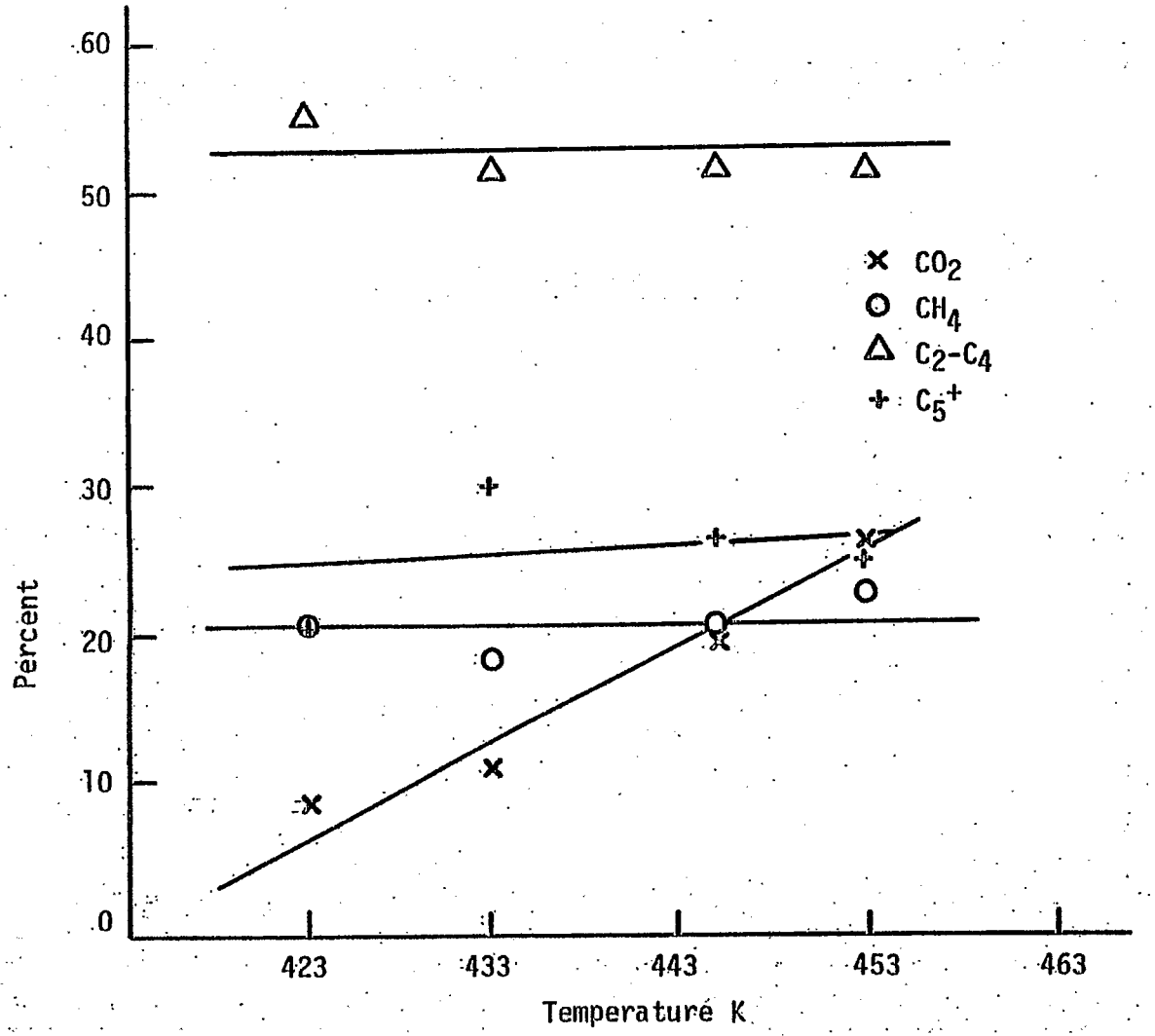

Figure 9. Effect of Reactor Temperature of Selectivity. Dense Bed.

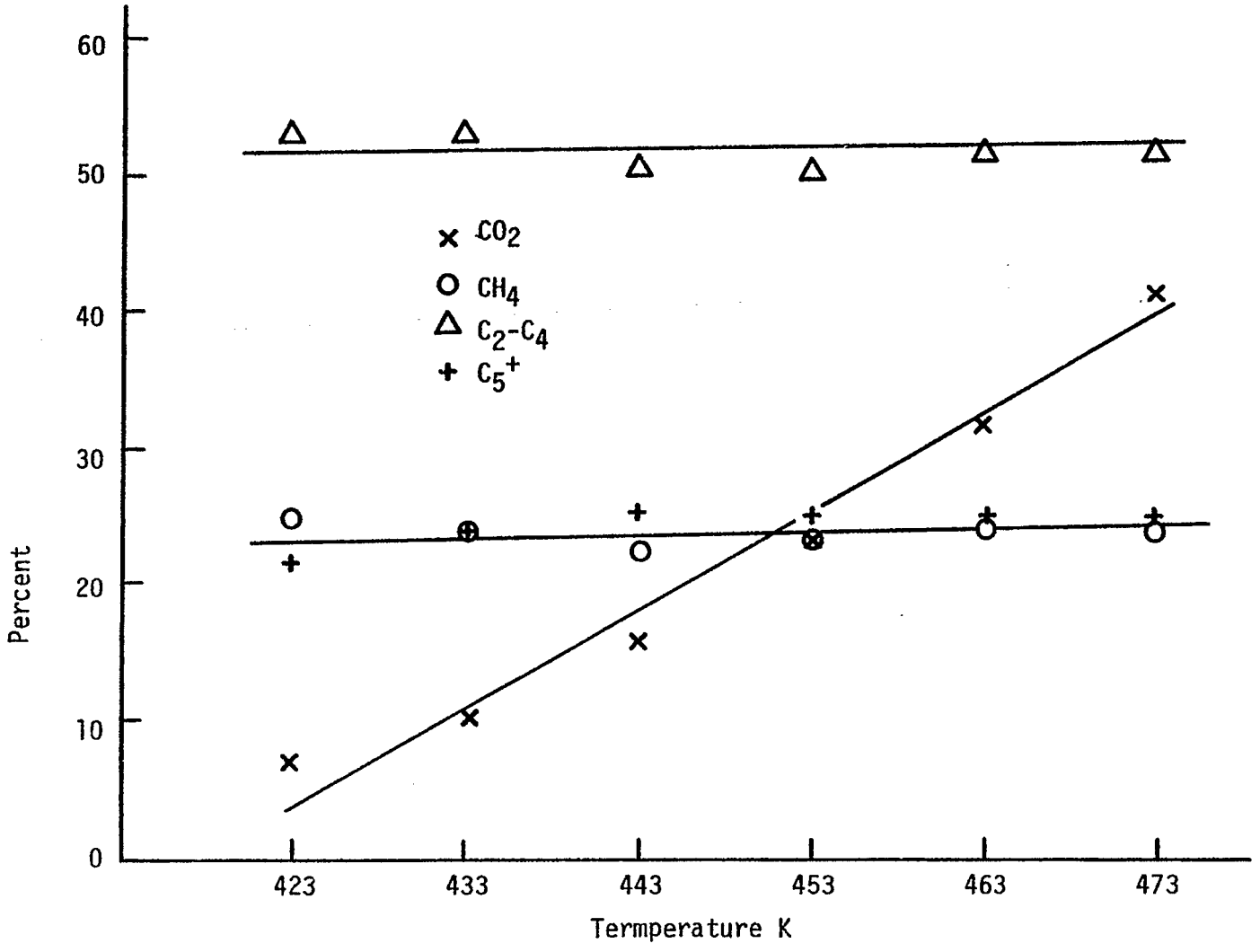

Figure 10. Effect of Reactor Temperature of Selectivity. Diluted Bed. Inert/Catalyst Ratio 2/1.

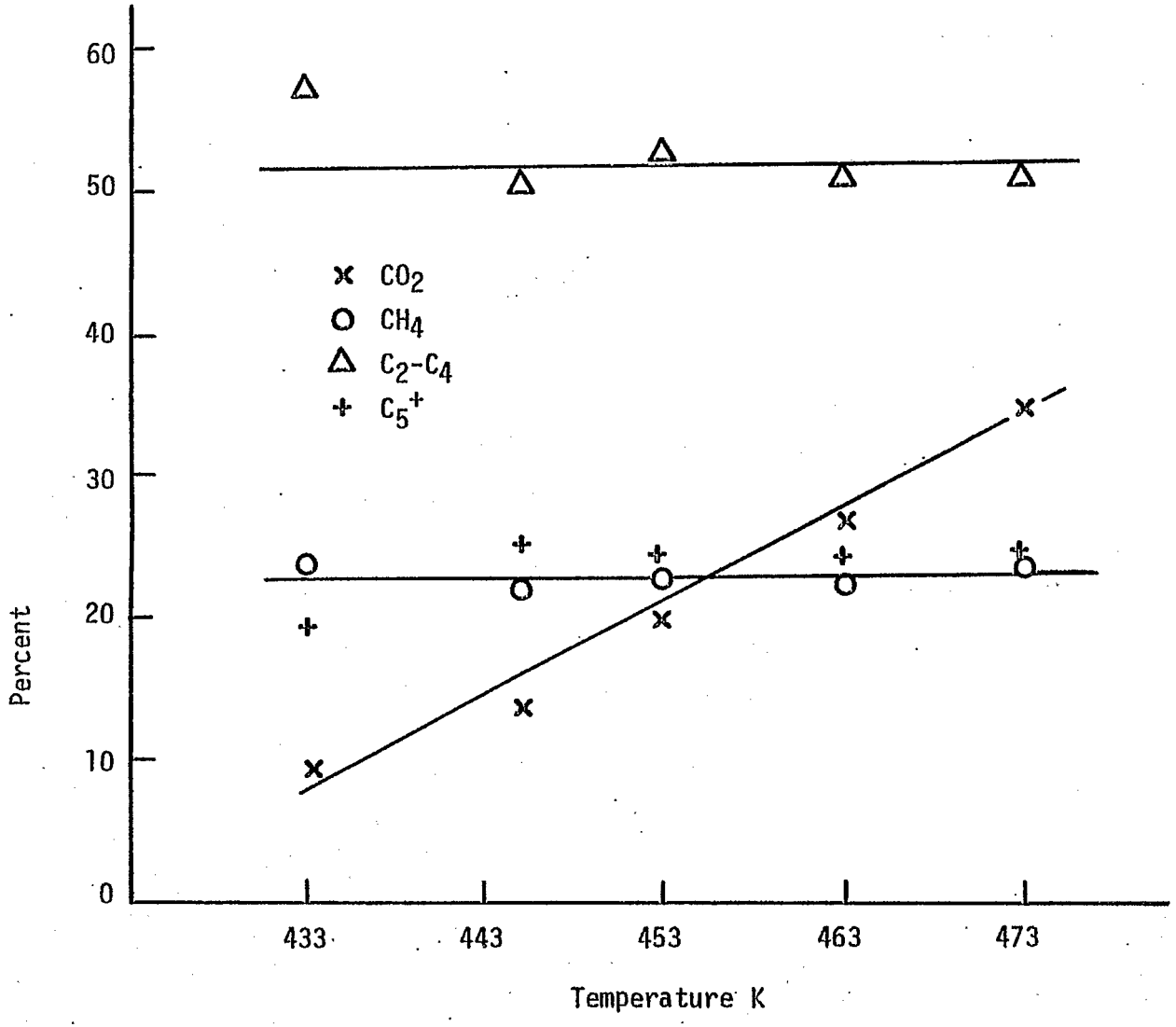

Figure 11. Effect of Reactor Temperature of Selectivity. Diluted Bed. Inert/Catalyst Ratio 4/1. Space Velocity 4.2 hr^{-1}.

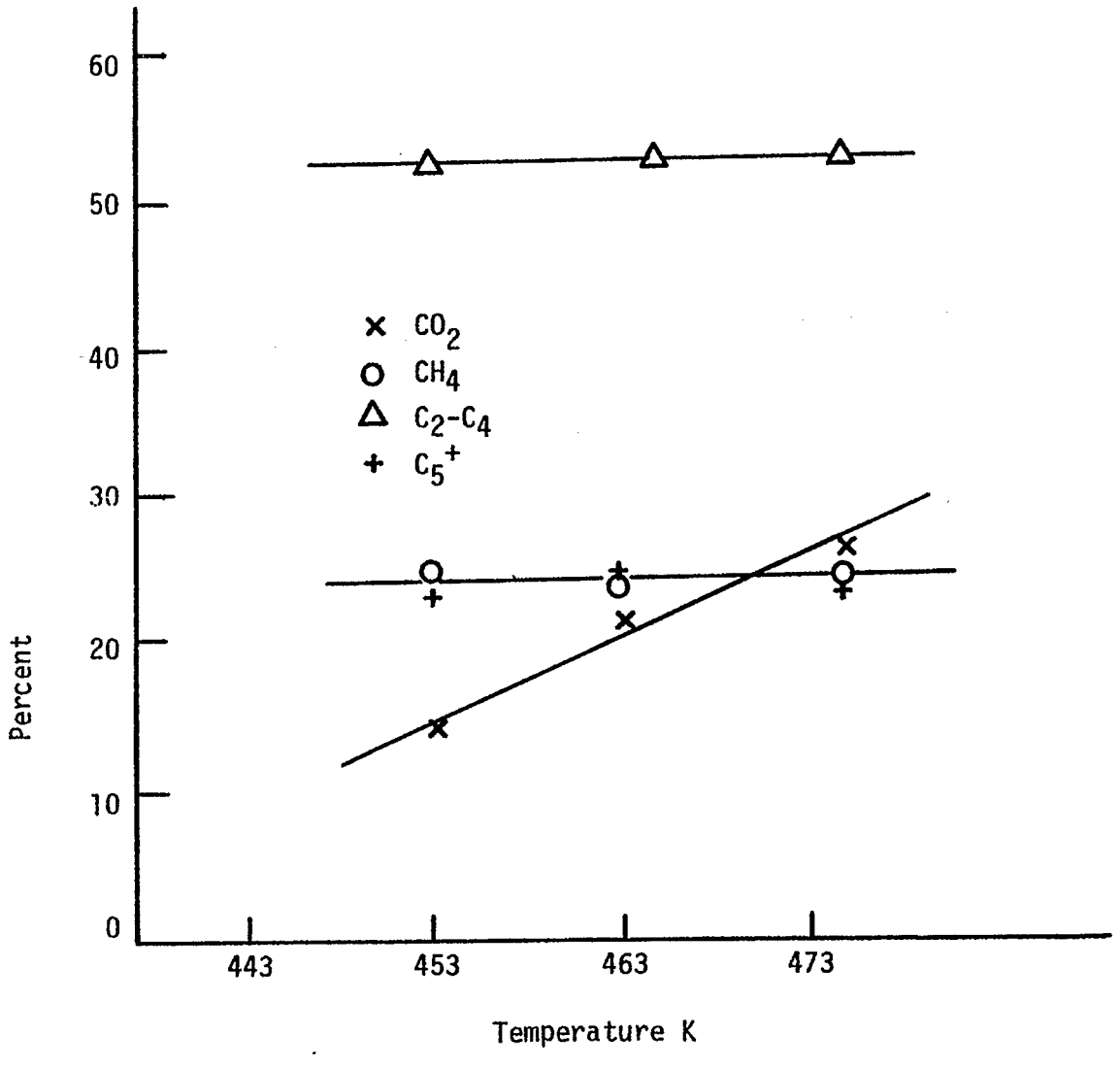

Figure 12. Effect of Reactor Temperature of Selectivity. Diluted Bed. Inert/Catalyst Ratio 4/1. Space Velocity 10 hr^{-1}.

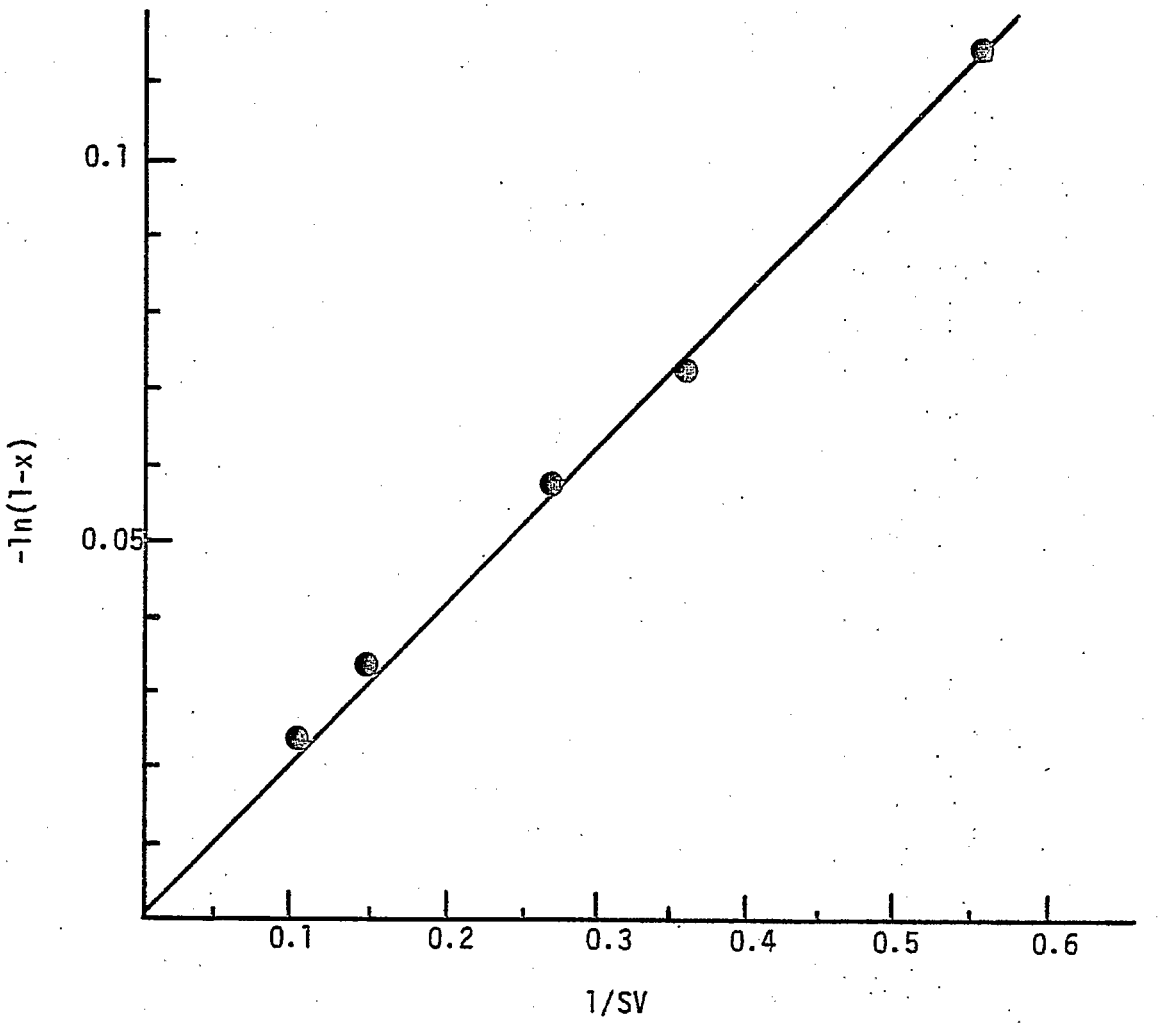

Figure 13. -ln(1-x) vs. 1/SV with Raney catalyst (FeMn 90°C leaching).

V. Conclusions

Detailed conclusions are included in the reports for each task. Task 4 is no longer funded and has been discontinued. Task 14 is inactive. No work was done under Task 15.

☆ U.S. GOVERNMENT PRINTING OFFICE: 1983-646-069/842